In Cylinder Liquid Fuel Visualization during Cold Start

by

Mark A. Dawson

BE, Mechanical Engineering
University College Dublin, Ireland
1996

Submitted to the Department of Mechanical Engineering in Partial Fulfillment of the Requirements for the Degree of

MASTER OF SCIENCE IN MECHANICAL ENGINEERING
AT THE
MASSACHUSETTS INSTITUTE OF TECHNOLOGY

September 1998

Signature of Author _____
Department of Mechanical Engineering
December 14, 1998

Certified by _____
Simone Hochgreb
Associate Professor of Mechanical Engineering
Thesis Supervisor

Accepted by _____
Ain A. Sonin
Chairman, Departmental Graduate Committee

In Cylinder Liquid Fuel Visualization during Cold Start

by

Mark A. Dawson

Submitted to the Department of Mechanical Engineering
on August 7, 1998 in partial fulfillment of the
requirements for the Degree of

Master of Science in Mechanical Engineering.

ABSTRACT

In recent years carburetor injection systems in spark ignited (SI) engines have been replaced with port-fuel injection systems, and as a result there has been a significant increase in the levels of hydrocarbon (HC) emissions from SI engines during their cold start period. The presence of liquid fuel in the combustion chamber, during a cold start, is believed to contribute significantly to the increased levels.

This work uses planar laser induced fluorescence to visualize the development of liquid fuel in the cylinder of a firing SI engine. A closed valve injection strategy was used, as this is the strategy most commonly found in practice. Fluorescence from indolene and iso-octane doped with acetone and 3-pentanone was used to examine volatility effects. Images were taken on three planes through the cylinder and a number of post-processing techniques were used to analyze the results. The results were analyzed on both a time and crank-angle (CA) basis.

Analysis on a crank-angle basis relates the location of liquid fuel entering the cylinder to engine events, and shows a maximum in the quantity of liquid fuel coming from the back of the intake valve at the crank angle position closest to the position of maximum valve lift. A semi-quantitative analysis based on the integration of the image intensities shows the time development of liquid fuel in the cylinder, and highlights the volatility effects.

Thesis Advisor: Professor Simone Hochgreb
Title: Associate Professor of Mechanical Engineering

ACKNOWLEDGEMENTS

Where to begin?

This is possibly the hardest page to write in any document and I apologize in advance to anyone I forget to include. First and foremost, I want to thank Professor Simone Hochgreb for her support in all aspects of my life during my time at MIT. Her hard work and commitment to her students may sometimes go unappreciated, but, in my experience, there are few other professors as committed to the education of her students and the success of their research.

Professor's Heywood and Cheng also provided me invaluable support through their advice and suggestions, and they contributed in no small way to my educational experience.

The trio of Nancy Cook, Brian Corkum and Peter Menard were not only an excellent resource for all my technical and administrative needs, but also became good friends, who often brightened my day, and reminded me how to smile when needed.

Another body of people that must be thanked not only for supporting me at times when even I found myself unbearable, but also for the wealth of memories they gave me, are my fellow students. In particular I would like to mention Micha Wiegel, Helen Liu, Brad VanDerWege, Chris O'Brien, Jim Cowart, Matt Rublewski, Kelly Baker, Robert Meyer, Ertan Yilmaz, Cornelius O'Sullivan and Carlos Herrera. They are just a few from a vast number. Some other non-MIT people that deserve my sincerest thanks are Gareth Brannigan, Katrina Harris and Natasha Winters.

My family mean more to me than anything and I owe them so much for supporting and encouraging me in my studies even during difficult times in their own lives.

The MIT Engine & Fuels Research Consortium (General Motors R&D, Ford Motor Co., Chrysler Motor Corp., Mobil Corp., Volvo Car Co., Shell Ltd./Equilon Enterprises Ltd., Renault SA and Peugeot SA) have funded this work.

TABLE OF CONTENTS

LIST OF FIGURES

LIST OF TABLES

1 INTRODUCTION

1.1 Background

With the advent of catalytic converters and the subsequent replacement of carburetor injection systems with port-fuel injected (PFI) systems for better air-fuel ratio control, engine out hydrocarbon (HC) emissions from spark-ignited (SI) engines were found to increase during the cold start process. Although of great interest, the relative contributions of the different mechanisms of formation of HC emissions during cold start are not well quantified. However, it is believed that the presence of liquid fuel in the cylinder of the engine is one of the main contributors [1].

Catalytic converters require a tight tolerance of the air to fuel equivalence ratio about a value of 1.0 so that they can achieve acceptable efficiency levels. This level of control is not possible with carburetors, because of the fuel's long residence time in the intake system with respect to the duration of one engine cycle. In order to eliminate the control problem, multi-point fuel injection systems were introduced. These systems are located in the intake port of modern engines, and because of their close proximity to the cylinder they achieve the close tolerances required by catalytic converters to realize acceptable catalyst efficiencies.

Excess liquid fuel is injected during start-up to ensure prompt starting. A consequence of the reduced residence time is that more of this excess liquid fuel enters the cylinder during the cold-start and warm-up periods of the engine. It is believed that much of this fuel does not burn during the combustion process and that it is exhausted out as unburned hydrocarbons (UHCs). During these cold-start and warm-up periods the catalytic converter has not reached its activation temperature and therefore cannot reduce the levels of these emissions. A third problem is that the oxygen sensor used as the source of a feedback signal for the fuel metering system does not work when cold and so the system is operating in an open loop. These compounded effects during the first few minutes of engine operation mean that almost ninety percent of the HC emissions occur during the engines first few minutes of running.

1.2 Previous Work

In order to eliminate the source of HC emissions, a good understanding of the fundamental processes involved is necessary. Cheng et al. [1] performed a review of research on HC emissions mechanisms under warmed-up conditions in SI engines, summarizes the processes by which gasoline compounds escape burning during normal combustion as:

1. Gasoline vapor-air mixture compressed into the combustion chamber crevice volumes.
2. Gasoline compounds absorbed in oil layers on the cylinder liner.
3. Gasoline absorbed by, and/or contained within, deposits on the cylinder head and piston crown.
4. Quench layers on the combustion chamber wall left as the flame extinguishes close to the walls.
5. Gasoline vapor-air mixture left unburned when the flame extinguishes prior to reaching the walls.
6. Liquid gasoline within the cylinder that does not evaporate and mix with sufficient air to burn prior to the end of combustion.
7. Leakage of unburned mixture through the (nominally) closed exhaust valve.

The processes by which these unburned hydrocarbons can oxidize or exit the cylinder were also estimated:

1. Outflow of unburned fuel-air mixture from crevice volumes and mixing with burned gases.
2. Diffusion of hydrocarbon vapor out of oil layers and deposits into the burned gases.
3. Mixing of wall and bulk quench gases with burned gases.
4. Oxidation in the exhaust pipe

The final outcome of these estimates is an attribution of the fractional contribution of each mechanism to the total HC emissions during warmed-up conditions. Table 1.1 shows the results.

Table 1.1: HC Sources: Magnitudes, and Percent of Total Engine-out HC Emissions [1]

Source	% Fuel Escaping Normal Combustion	% HC Emissions
Crevices	5.2	38*
Quench	0.5	5
Oil Layers	1.0	16
Deposits	1.0	16
Liquid Fuel	1.2	20
Exhaust Valve Leakage	0.1	5
TOTAL	9.0	100

*Blowby (0.6%) subtracted

Since the publication of this paper an extensive amount of research has been performed on each of these mechanisms, and a revision of these values is necessary. The focus of the current work is the liquid fuel entering the cylinder, particularly during cold start.

A recent review of combustion related emissions in SI engines [2], detailed how the relative contributions of HC sources are quite different during cold start than at warmed up conditions. Significant mixture enrichment and poor mixture vaporization are the main sources of HC during cold start. In this work, a

comprehensive discussion is given of the effects of liquid fuel and mixture preparation during both cold start and steady state operation. As mentioned in this work, typically 8-15 times the stoichiometric amount of fuel is injected during the first few cycles.

A number of techniques have been used to quantify the liquid fuel present in the intake port and cylinder of a firing SI engine during the cold start and warm up periods. Takeda, et al. [3] used a specially designed engine with hydraulically controlled valves to measure wall wetting during a cold start. To determine the extent of "cylinder wall-wetting", the specially designed engine was started and the valves were operated normally. The engine was shut off suddenly and the intake and exhaust valves were kept closed. The fuel was then vaporized and analyzed through a FID and its total mass was calculated by integration. A similar procedure was used for analyzing the intake port wall wetting. One interesting result from this work was that the liquid fuel in the intake port peaks at about 30 seconds, whereas the cylinder wall wetting decreases gradually with time from the first cycle on. Schurov and Collings [4] developed this technique further. A disadvantage of this method is that there is no information on where in the cylinder or intake port the liquid fuel originates.

A significant amount of research has been devoted to optical techniques for visualizing and quantifying the liquid fuel present in both the intake port and the cylinder [5-17]. The advantage of optical techniques is that they are in general non-intrusive and therefore can be used during normal operation. Laser Induced Fluorescence (LIF) is currently the most commonly used optical technique for fuel visualization. Other optical techniques include Phase Doppler Particle Anemometry (PDPA), which gives information on both droplet size and velocity. The disadvantage of PDPA is that it is a point measurement, whereas LIF is a planar technique. Another optical technique used for droplet sizing is Interferometric Laser Imaging for Droplet Sizing (ILIDS). ILIDS is a wide-field, time-resolved droplet sizing technique for sparse polydisperse sprays. ILIDS is most suited to lean burn engines where the sprays are more disperse.

The technique of laser induced fluorescence is based on exciting molecules to a gigher energy state, then collecting the ligth emitted by the excited molecules. The light collected may be at the same frequency as the laser light (resonance fluorescence) or, more frequently, shifted to a lower frequency [18].

Johnen and Haug [6] used Planar Laser Induced Fluorescence (PLIF) to measure the fuel film thickness inside a specially built intake manifold. Felton et al. [7] used PLIF to study the fluorescence, in the intake manifold, from a dye contained in Unocal RF-A gasoline. Laser Induced Exciplex Fluorescence (LIEF) was used [8] to qualitatively visualize the mixture preparation in a firing SI engine using different fuel injection strategies. Witze and Green [9] used a wide beam laser induced fluorescence technique, in conjunction with high speed imaging, to visualize liquid fuel films on the combustion chamber walls of a firing SI engine with both Open Valve Injection (OVI) and Closed Valve Injection (CVI). Kelly-Zion et al.

[10] performed high-speed imaging of liquid fuel entering the combustion chamber of a single cylinder optical engine illuminated through a window in the piston crown in a motored engine. This work investigated the effect of operating conditions such as swirl, number of injections, and fuel type, on the wall impingement, amount of liquid entry, droplet size and duration of liquid entry.

Other optical techniques use lasers for velocimetry and droplet/particle sizing. Schünemann, et al. [11] used Laser Doppler Velocimetry (LDV) to investigate crank angle resolved air velocities and fuel droplet velocities inside the intake port of a six cylinder four valve production engine, as well as PDPA to characterize the injector by measuring both droplet sizes and velocities. Posylkin et al. [12], Cousyn et al. [13], Hardalupas et al. [14] and Meyer et al. [15], have measured in-cylinder liquid fuel droplet size and velocities using PDPA. Meyer et al. [16] used PDPA to investigate the liquid fuel transport mechanisms in the vicinity of the intake valve of a firing spark ignition engine, estimating the liquid fuel inflow into the cylinder with crank angle (CA) resolution for both OVI and CVI strategies. That study also used LIF information acquired jointly with the present study for guidance on the location of the droplets.

Work by Whelan et al. [17] looked at back-flow atomization in the intake port of spark ignition engines. This work used a laser diffraction particle sizing technique to measure drop sizes in the intake port of a motoring engine. The effects of number of injections, start of injection timing, engine speed and manifold pressure, on the distribution of liquid fuel in the intake port were investigated. The results of this work indicate that the back-flow process provides significant dispersion of the fuel in the intake manifold prior to induction into the cylinder. The Sauter Mean Diameters (SMDs) for the droplets produced by back-flow atomization were found to be between 20 and 80 μm, which, as noted by the authors, is significantly smaller than the drop sizes produced by many production fuel injectors.

Research into mixture preparation during cold start is a relatively recent, but rapidly developing area of investigation. Previous work has been done to visualize the liquid fuel present in the cylinder and intake port. However, most of the previous investigations involved visualization of liquid fuel in motored engines. Further, due to the pent roof geometry, optical access to the valve region in most of the studies is difficult, so that visualization is only possible across the cylinder cross section rather than the plane of the intake valves. The advantage of the current work is that it creates a map of liquid fuel in the cylinder of a firing engine. This allows a relative analysis of the concentration of liquid fuel in the cylinder as well as the identification of how the liquid fuel enters the cylinder. The disadvantage of the LIF technique and facility, as described in the next chapters, are that the geometry is somewhat different from a real engine, and that the technique does not allow separate visualization of liquid and vapor streams.

The objective is to investigate the process of liquid fuel entrainment in the cylinder of a firing SI engine by PLIF visualization of the liquid fuel present in the cylinder of an engine during the warm-up period.

Different fuel mixtures have been used to investigate the effects of fuel volatility. In the present investigation, the process of liquid fuel entrainment is investigated by PLIF visualization of the liquid fuel present in the cylinder of an engine during the warm-up period. Different fuel mixtures have been used to investigate the effects of fuel volatility. A recent paper [14] uses a combination of PLIF and PDPA to quantify the liquid fuel entering the cylinder. The results are analyzed by integrating image signals, as a tool for assessing the relative amounts of liquid fuel entering the cylinder.

2 EXPERIMENTAL SETUP

2.1 The Engine

This work was carried out in the square piston engine test cell at the Sloan Automotive Laboratory. A schematic of the optical engine used in this work is shown in Figure 2.1. This engine consists of a flatroof combustion chamber, one intake valve, one exhaust valve, an elongated square piston, one steel back wall, two quartz side walls and a front steel wall with a cutout for a third quartz window. There are also two holes on the top of the combustion chamber for spark plugs and a third hole on the steel back wall for a pressure transducer. For this work the spark plug was positioned between the intake and exhaust valves The large quartz side walls are held in place by easily removable metal frames. The third quartz window is held in place by a small metal frame. This small metal frame is easily removable for cleaning of the quartz pieces.

The compression ratio of the engine is 8.0. The combustion chamber is sealed by spring-loaded graphite bars, which press against the engine walls and overlap one another in each corner. The engine is not cooled and can only be run for at most 5 minutes. The engine is coupled to a Powrmastr® motor, made by IDM Controls Inc. The nature of the square piston engine is such that it never produces power at the conditions run here. The motor provides the engine with the extra power it needs to stay at a constant, user defined, speed, and for the rare occasions when the engine is run at conditions where it will produce power, the motor is connected to a large resistance to dissipate the extra power. The details of the engine are in Table 2.1. A more detailed description of the engine can be found in [19]

Table 2.1: Engine Specifications

Cross Section	82.9 mm x 82.9 mm
Stroke	114.3 mm
Displacement	0.785 liters
Compression Ratio	8.0
Number of Valves	2
Intake Valve Open	5 CAD bTDC
Intake Valve Close	55 CAD aTDC
Exhaust Valve Open	48 CAD bTDC
Exhaust Valve Close	12 CAD aTDC

2.2 *PLIF System*

For the purposes of visualization a planar laser induced fluorescence (PLIF) system was used. The PLIF system consists of a Lambda Physik Compex 102 laser and a Princeton Instruments Intensified Charge Coupled Device (ICCD) camera system, consisting of a Princeton Instruments ST138 camera controller, a Princeton Instruments PG200 pulse generator, a Princeton Instruments 576SE ICCD detector, and a personal computer. The CCD array has 384 rows and 576 columns of pixels and is coupled with a Nikkor 60mm camera lens.

This system is described in detail in [20]. Figure 2.2 shows a schematic of the system. The laser beam was shaped by a pair of lenses and a slit, producing a sheet 0.5 mm thick and 20 mm high. The beam was then directed along one of three different planes through the combustion chamber, a plane through the valve centerline, one 8-mm offset and one 18-mm offset from the valve centerline.

An intensified CCD camera placed in front of the quartz window captured the fluorescence and transfered the image to a personal computer for post processing. The data transfer process from the camera array to the camera controller was the time limiting factor and it limited the number of images, which could be taken, to approximately one image every two seconds. Figure 2.3 shows a typical image with a schematic of the piston top, intake valve and cylinder walls superimposed. This image can also be depicted as a negative, which gives better clarity when reproduced. An inverted image is shown in Figure 2.4. A summary of the specifications of the optical system is given in Table 2.2.

Table 2.2: Optical System Setup

Laser Type	XeCl Excimer
Laser Dimensions	22 mm x 7 mm
Laser Wavelength	308 nm
Maximum Repetition Rate	20 Hz
Maximum Pulse Energy	240 mJ
Lens A Focal Length	157.1 mm
Lens B Focal Length	52.3 mm
Slit Dimensions	30 x 0.5 mm
Minimum Camera Exposure Time	50 ns
CCD Array	384 rows x 576 columns
Camera Dynamic Range	16 bit, 65536 gray levels
Camera Lens	60 mm

The pulse is generated at the desired CA using a DCI counter box. When it receives a DCI box pulse the PG200 pulse generator sends a triggering pulse to the laser and after a short delay sends a gate pulse to the camera.

2.3 Dopants

Only certain compounds fluoresce when excited by laser light at 308 nm. Gasoline, for example is a mixture that contains both fluorescing and non-fluorescing compounds. A fluorescent dopant is typically added to fuels so that a particular volatility compound can be investigated and so that quantification is possible. In the case of indolene it is not necessary to add a dopant, as there are already fluorescing compounds present, such as naphthalene. According to an analysis performed by Le Coz et al. [21], fluorescence from standard gasoline is generated mostly by naphthalene. Naphthalene has a boiling point of 217^0C [972832] and is not representative of gasoline, which has a 50% evaporation point of 109^0C (this is the temperature at which 50 % of the gasoline will have evaporated on a mass basis). When indolene evaporates, the low boiling point, high volatility components evaporate first, and this leads to an enrichment of the low volatility compounds in the remaining liquid. This uncertainty in the concentration of the fluorescing compounds in the fuel, coupled with some uncertainty in what compounds are fluorescing makes it very difficult to use indolene for the purposes of quantifying the liquid fuel present. However, indolene is still a useful fuel for qualitative analysis, and undoped indolene was used in this study to visualize the behavior of low volatility compounds present in regular fuel.

In order to analyze the high and medium volatility compounds present in gasoline, iso-octane fuel was doped with either acetone or 3-pentanone. Iso-octane was chosen as a fuel because it is a pure single component fuel known to have very little fluorescence response. Acetone (52^0C) was used to represent the high volatility components in gasoline, and 3-pentanone (b.p. 102^0C) was chosen to represent the medium volatility components. In these cases the mixture proportions were 10 parts fuel to 1 part dopant by volume. It has been shown in the literature that this mixture strength gives an adequate signal from liquid fuel and a relatively low signal from the vapor phase [20]. Fujikawa et al. [5] investigated the suitability of fluorescence tracers and excitation wavelength for quantitative 2-D fuel distribution measurements. The temperature and pressure dependencies of the LIF signal from both acetone and 3-pentanone are shown in Table 2.3 for excitation wavelengths of 248, 266, 308 nm. It was also found that the LIF intensity of 3-pentanone saturated near TDC because of the increase of its temperature dependence in the high temperature region. Consequently, Fujikawa et al. conclude that 3-pentanone is not suitable for the quantitative fuel concentration measurements in engines, especially near top dead center in fired operation. In the current study, only the intake stroke is analyzed, so the error due to the temperature dependence is small [5]. Absorption and emission spectra for acetone, 3-pentanone, and many other ketones can be found in the literature [22.].

Table 2.3: Pressure and temperature effects of LIF Intensity [5]

Tracer	Excitation Wavelength (nm)	Pressure (%/MPa)	Temperature (%/100K)
Acetone	248	60	-25
	266	5	-7
	308	12	13
3-pentanone	248	70	-28
	266	3	-11
	308	0	30

2.4 Data Acquisition (DAQ)

Pressure, head temperature, equivalence ratio, spark timing and injection timing data were acquired using a National Instruments Lab-PC-1200 data acquisition board with a 50 pin I/O connector block. The Lab PC 1200 consists of 8 analog I/O channels, with 12 bit resolution and 3 external use counters/timers. The details of both the DAQ board and the LabVIEW® program are given in detail in appendix 2.

2.5 Port Fuel Injection System

The injector used in this work was a standard Bosch EV1.1A with a sauter mean diameter of approximately 130μm. The square piston optical engine is often criticized for its unrealistic in-cylinder charge motion, due to its unique square geometry. The injector targeting in the intake port is, however, very similar to that used in a real engine as shown in Figure 2.6. The injector was aimed at 45 degrees to the horizontal axis, such that the maximum amount of injected fuel hit the back of the intake valve. The intake valve heats up faster than the walls of the intake port and therefore gives faster vaporization during warm up.

The engine controller described in the next section generates the injection signal used to control the injector. In order to ensure prompt starting this injection pulse is passed through a first pulse enrichment box. This box passes no signal when switched off. When it is switched on, the enrichment box passes each pulse with the width of the first pulse scaled by some multiple determined by a rheostat. In this work the first pulse was six times the width of the subsequent pulses. This first pulse enrichment is a simple version of more complicated enrichment sequences used in a real engine to ensure prompt starting.

2.6 The Engine Controller

A LabVIEW ® program controlling a National Instruments® PC-TIO-10 timing input/output board generates Spark and fuel injection timing pulses. The system takes bottom dead center (BDC) compression and crank angle degree (CAD) signals as inputs. The spark signal is set high at BDC, which starts the spark coil charging, and is then set low, which discharges the coil, at a crank angle position defined by the user. The fuel injection signal, a TTL low signal, begins at a crank angle defined by the user, and its duration is for a specific number of milliseconds, defined on the program's user interface. The injection signal is timed in real time so that changes in speed do not affect the fuel to air ratio. In the current work the coil discharged at 25 CAD bTDC of compression, the fuel injection started at 60 CAD aBDC of the compression stroke and lasted for 10 milliseconds. Again more information can be found on the engine controller in reference [20].

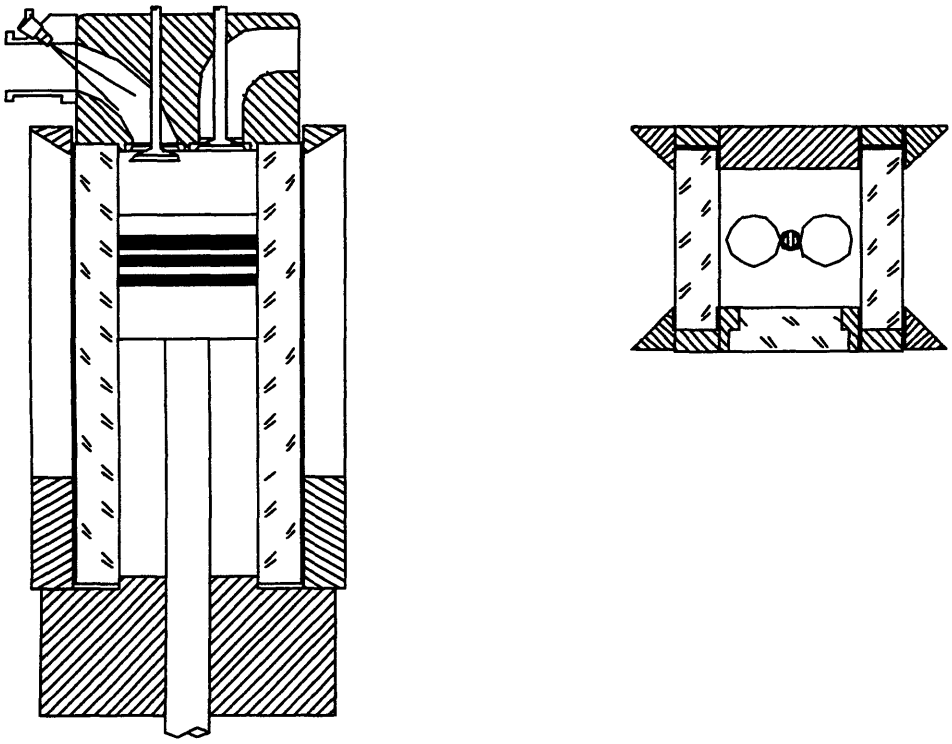

Figure 2.1: Optical engine schematic

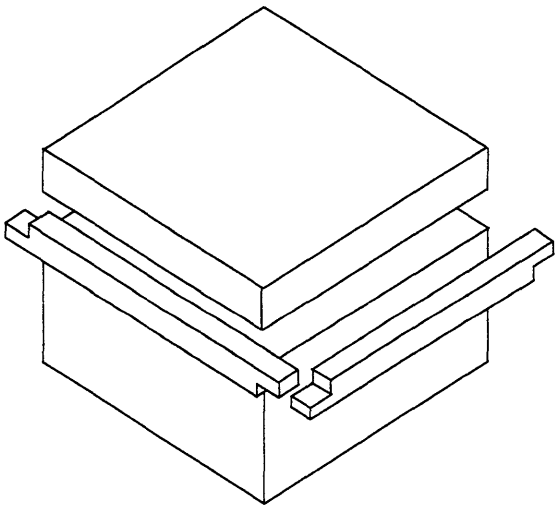

Figure 2.2: Piston bar layout

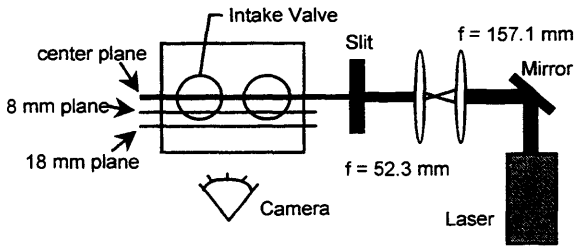

Figure 2.3: Schematic of the PLIF system

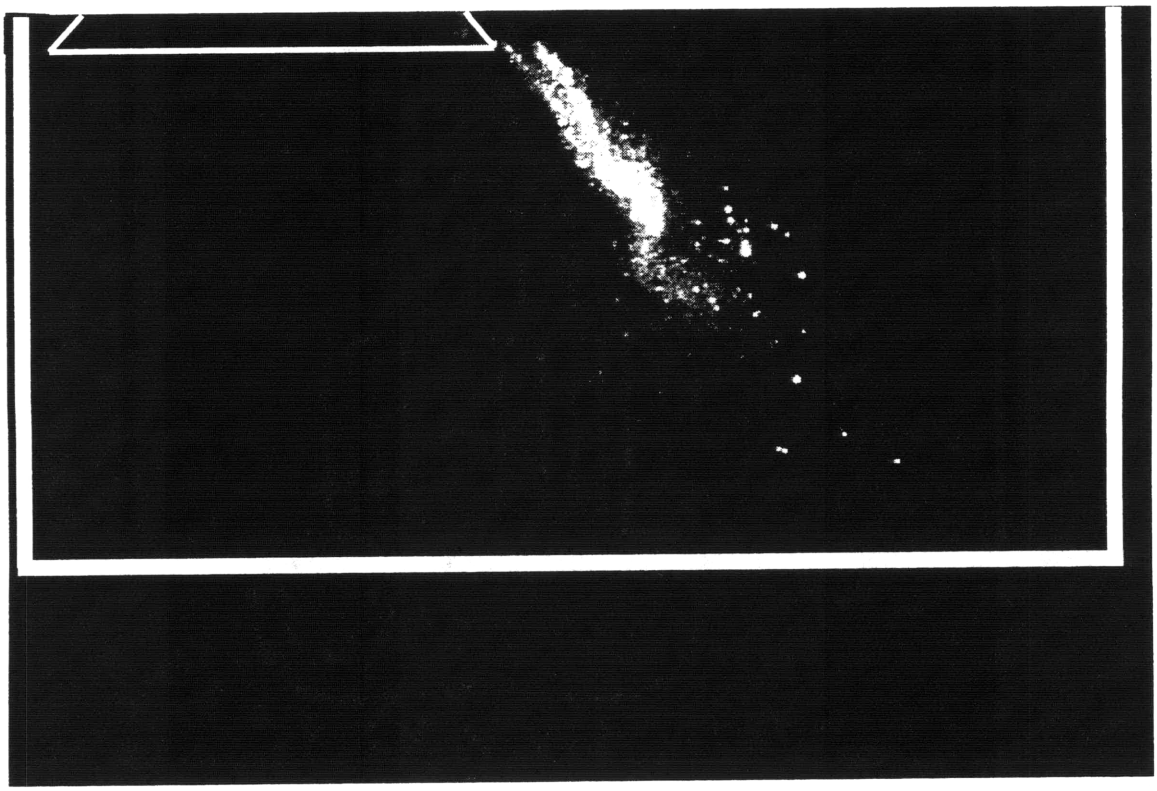

Figure 2.4: Sample image with mask of piston top, intake valve and cylinder walls superimposed.

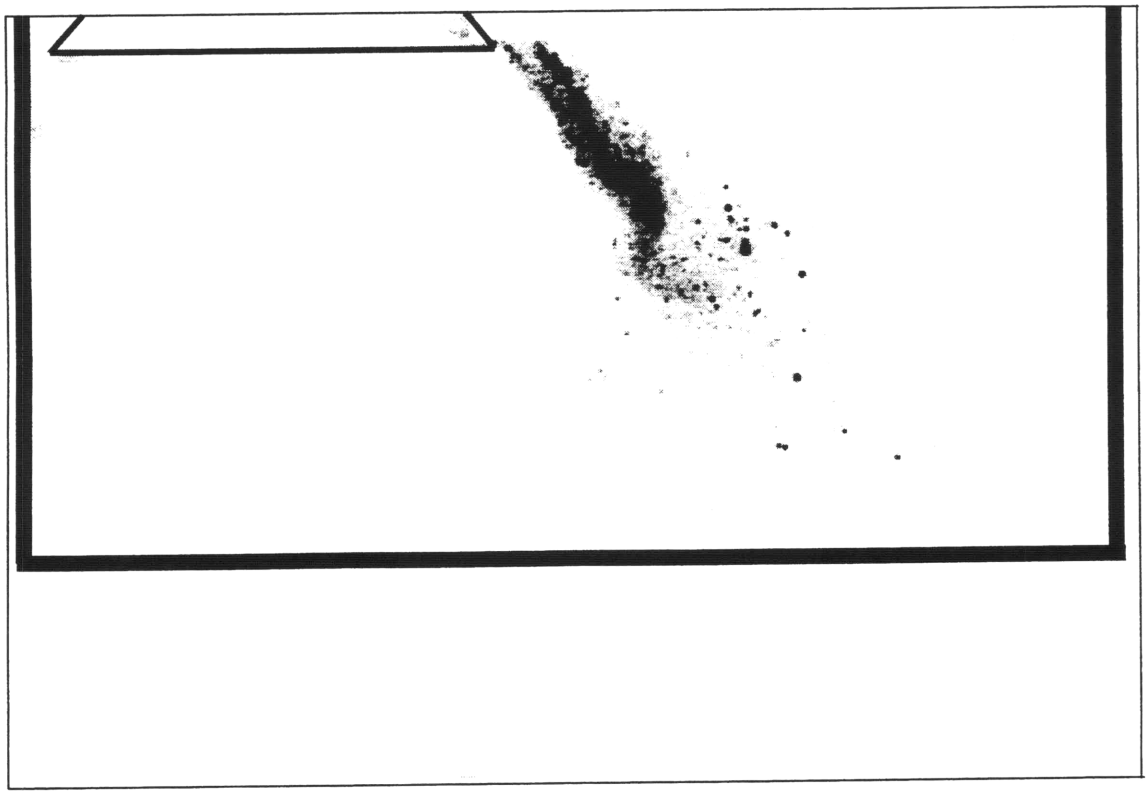

Figure 2.5: Inverted sample smage with mask of piston top, intake valve and cylinder walls superimposed.

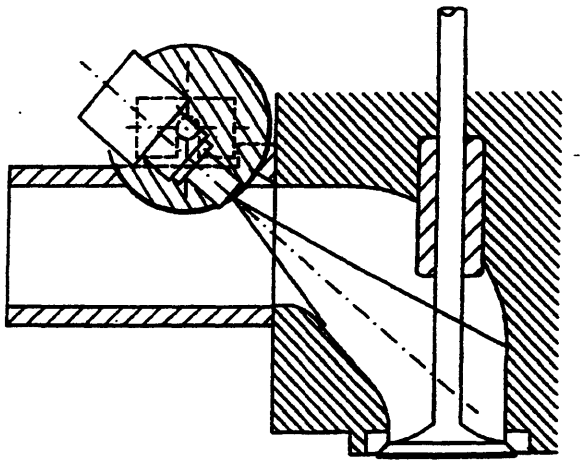

Figure 2.6: Injector targeting and intake port geometry

3 EXPERIMENTAL PROCEDURES

3.1 Test Procedures

When performing a test run a specific procedure was followed. Correct procedures are very important for the success of the experiment: something as simple as failure to remember a lens cap can waste a number of hours in engine cooling. This experimental procedure is presented briefly and given as a checklist in Appendix 3.

The engine is motored from rest until the desired speed for the testis reached. At this time spark and injection are enabled. Image acquisition is then started and the engine is allowed to fire for 60 seconds while a set of 30 images is acquired. At this time the engine is stopped.

Once a test is complete, the engine must be cooled before another cold start experiment can be performed. To speed up this cooling process the engine walls were removed and bags of ice were placed on both the piston and the engine head. A fan was also used to aid cooling.

3.2 Test Conditions and Matrix

All test runs were performed at an intake pressure of approximately 0.5 bar. The injection strategy used was closed valve injection (CVI), as shown in Figure 3.1. Closed valve injection was chosen because it is the strategy used in most production engines. Injection occurred at 60 CAD aBDC and lasted 10 milliseconds. Tests were performed over a range of crank angle positions for each of the fuel/fuel-dopant mixtures. Table 3.1 shows the test matrix, where each CA position represents one experiment.

Table 3.1: Test Matrix for Experiments

Fuel/Fuel Dopant Mixture	**Beam Location**	**CA Positions**
Indolene	Center	45, 60, 75, 90, 105, 120, 135, 150
	8 mm	45, 60, 75, 90, 105, 120, 135, 150
	18 mm	45, 60, 75, 90, 105, 120, 135, 150
Iso-octane + Acetone	Center	45, 60, 75, 90, 105, 120, 135, 150
	8 mm	45, 60, 75, 90, 105, 120, 135, 150
	18 mm	45, 60, 75, 90, 105, 120, 135, 150
Iso-octane + 3-pentanone	center	45, 60, 75, 90, 105, 120, 135, 150
	8 mm	45, 60, 75, 90, 105, 120, 135, 150
	18 mm	45, 60, 75, 90, 105, 120, 135, 150

3.3 Image Post-Processing

The experiments above resulted in approximately 2160 individual images. In order to relate the image intensity to the volume of liquid fuel present, it was necessary to condense the data into meaningful values. This was accomplished through the use of Winview®, which allows for custom programmed macros. The analysis techniques described below were implemented through the use of these macros which are described in detail in Appendix 1.

Each test produced a raw data set, consisting of 30 images taken at two-second intervals during a run. This data was processed in two different manners to yield information about liquid fuel volume in time as well as liquid fuel volume dependence on CA.

The first analysis procedure examined how the volume of liquid fuel changed throughout the starting period at a given CA. An average pixel intensity was found for each image and was taken as a measure of the liquid fuel in the chamber. By looking at the consecutive images temporal information could be extracted.

In order to find an average pixel intensity certain areas of the raw image had to be excluded because they saturated the CCD array. These areas are the intake valve and intake valve side wall regions where liquid fuel accumulated. These areas could either be masked out before subsequent analysis of the entire frame, or a region of interest (ROI) could be chosen for analysis that did not include the saturated areas. An ROI is defined as (x, y) = (x1, y1) to (x, y) = (x2, y2), i.e. in terms of the upper left and lower right vertices of a rectangle. The latter method was chosen because its implementation into computer code was more straightforward. After finding an average pixel intensity for the chosen ROI, the background average pixel intensity value for that same ROI was subtracted to yield the actual average pixel intensity due to the fuel.

The second analysis procedure examined how the liquid fuel volume varied at different crank angles. Since each test produced a data set associated with a given crank angle, the analysis procedure found an average image for each data set. The averaging process involved constructing a single image by taking the 30 images and finding an average value for each pixel. The application of this technique to a transient time, like the warm up period has both advantages and disadvantages. On the negative side, any information about the time development of the fuel stream is lost. However, the temporal aspect of the data was addressed with the first data analysis technique. On the other hand, the advantage of this technique is that it eliminates cycle to cycle variability reasonably well, and it therefore allows for accurate analysis of the spatial development of the fuel stream as a function of crank angle position. This technique is summarized in Figure 3.2.

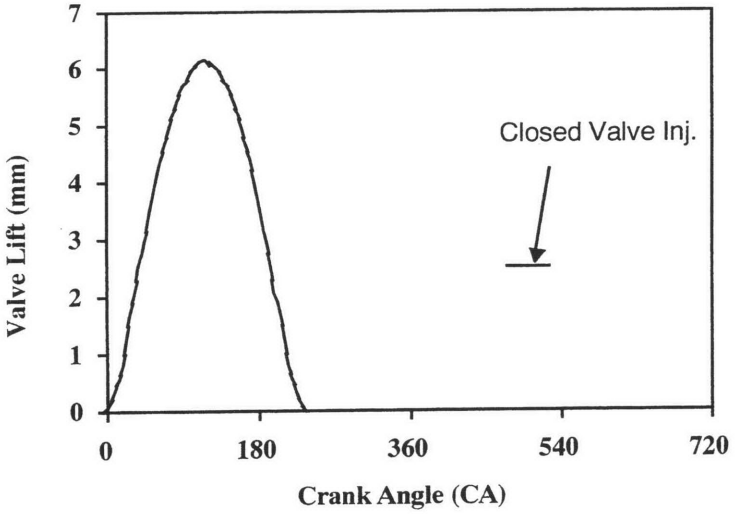

Figure 3.1: Injection timing related to intake valve lift

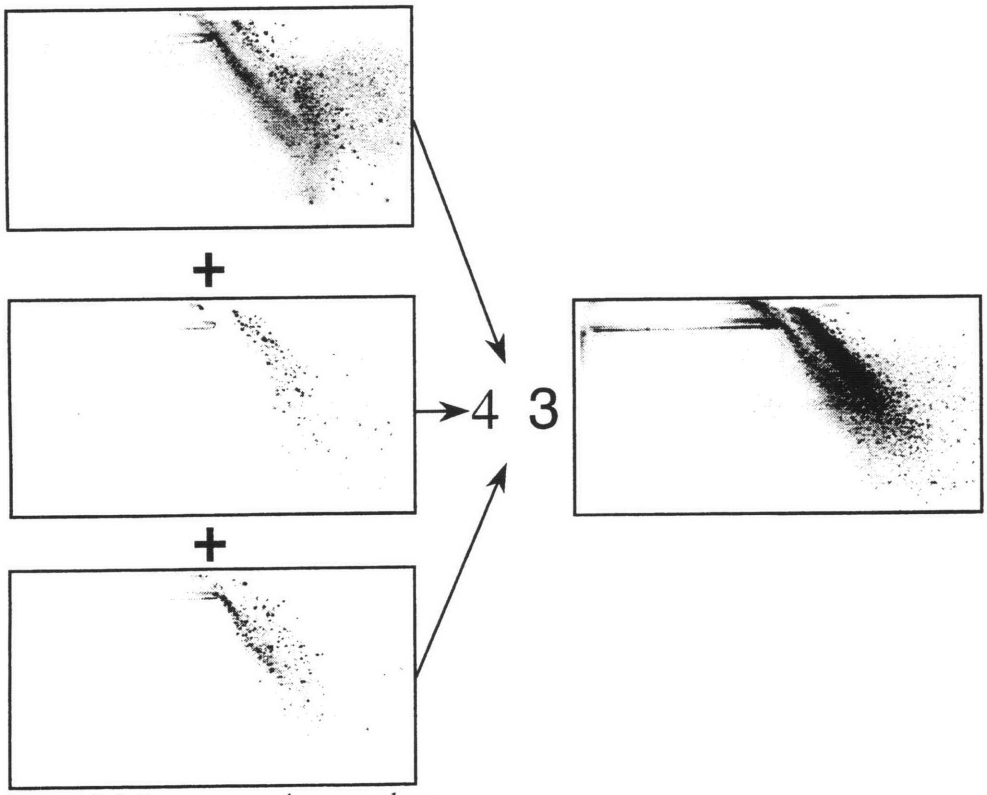

Figure 3.2: Image averaging procedure

4 EXPERIMENTAL RESULTS – ANALYSIS OF TRANSIENT BEHAVIOR

This chapter presents the results from the first analysis method that was used to examine the transient behavior of the liquid fuel. Each fuel/fuel-dopant mixture is presented separately by showing the results of each of the planes (centerline, 8 mm offset, 18 mm offset) at the different crank angles. The different planes are compared for each fuel as well.

4.1 Results for Indolene

As discussed in the Dopant section of the Experimental Setup chapter, the indolene fluorescence results are most useful for qualitative analysis.

4.1.1 Centerline Plane

Figure 4.1 shows the consecutive raw images for the position 45 CA after Top Dead Center Intake (aTDCI). Initial, visual observations about the liquid fuel volume present can be made by inspecting these raw data images. In the zero-second image, the liquid fuel fluorescence is weak, followed by an image with strong fluorescence most likely as a result of the six times enrichment of the first injection pulse. The fluorescence from the liquid fuel in the next twelve seconds is slightly weaker than that in the two-second image. The fluorescence in the sixteen- and twenty-second images is noticeably stronger than in any of the other images in this series. This corresponds to the peak in mass of liquid fuel entering the cylinder as droplets as shown previously to be the case for a closed valve injection strategy [15] in the same engine setup. This is shown in Figure 4.2. The signal in the eighteen-second image is not particularly strong. One possible explanation for this weaker image is cycle-to-cycle variations in the amount of liquid fuel entering the cylinder, caused by non-uniform fuel streams, or "rivulets" on the back of the intake valve as seen by Witze and Green [23]. After the twenty-second image the signal intensity gets steadily weaker until it seems to reach a steady state at about 34 seconds.

The following section describes results obtained through the image processing. It is important to remember that for each given image or ROI, it is only after the average pixel intensity has been computed that the background pixel intensity can be subtracted.

Figure 4.3 (a) shows the average pixel intensities for the 45 CA aTDC case depicted as unprocessed images in Figure 4.1. No region of interest was chosen, but, as is the case for all analysis in this chapter, the average background intensity was subtracted. As can be seen from the Figure 4.1, there is a large percentage of the area in each image that does not contain the fluorescence signal from the liquid fuel. By including the pixels from this void are in the average, the changes in intensity due to changes in the volume

of liquid fuel are less pronounced. Therefore it is desired that the ROI chosen for analysis not only excludes the areas where the CCD camera signal is saturated but is also as small as possible to eliminate attenuation of the intensity values. However, care must be exercised in choosing the size of the ROI because if the region is too small it will no longer accurately reflect all the changes in the liquid fuel volume in the cylinder. This is demonstrated in Figure 4.3 (b) which shows average pixel intensities after background subtraction calculated using an ROI [x,y = (276, 9) – x,y = (296, 117)] that was too small. This ROI is also shown graphically in Figure 4.4. This ROI is narrow in the x-direction and wide in the y-direction. The result is that much of the liquid fuel that entered the cylinder earlier and has passed by this region is not represented in the average pixel intensities. Comparing figures 4.3 (a) and (b) we can see that the smaller ROI does not capture the large average pixel intensity present in the two-second image compared to the other images in the set. Figure 4.5 shows the ROI (x, y) = (276, 9) to (x, y) = (296, 117) superimposed on the two-second image where it can be clearly seen that the ROI is not adequate.

Figure 4.3 (c) shows average pixel intensities for the ROI [(x, y) = (264, 29) to (x, y) = (430, 252)] and is also graphically shown in Figure 4.4. This larger ROI preserves the changes in average pixel intensity values and the 16- and 20-second values are approximately twice the steady state values. The conclusion is that for analysis of images taken along the center plane, this larger ROI is effective in capturing the behavior of the liquid fuel volume while still reducing the attenuating effect of using the entire image. Using this image processing technique, it is only necessary to look at a single plot of average pixel intensities rather than 30 individual images to discern relative liquid fuel volumes; although, if an interesting feature is noticed in the intensity plots, it is useful to return to the raw images for a closer analysis. The ROI [(x, y) = (264, 29) to (x, y) = (430, 252)] shown in Figure 4.3 (b) was chosen for processing all of the data files acquired from the centerline plane experiments and are presented below.

Figure 4.6 shows plots of average pixel intensity versus time for the valve centerline, using the ROI (x, y) = (264, 29) to (x, y) = (430, 252), at crank positions between 60 and 150 CAD in 15 CAD intervals. Figure 4.6 (a) shows results from 60 CAD. The plot exhibits an initial peak, caused by first pulse enrichment, and then a second set of peaks at approximately 10 –14 seconds which is similar to the 45 CAD case for which the peak liquid fuel inflow in droplet form occurs at 10 – 20 seconds. An interesting feature is the peak in average pixel intensity values that occurs at about 40 seconds. This 40-second peak appears in a number of the plots shown in Figure 4.6, and will be addressed later in this Chapter. Figure 4.6 (b) for 75 CAD shows a more erratic behavior, with a number of initial peaks, followed closely by the second set of peaks at 14 – 22 seconds and a particularly large peak at 40 seconds. Similarly, Figures 4.6 (c) and (d) are erratic in their values. Figure 4.6 (c) has an initial peak occuring later than in most runs, appearing at about 6 seconds, with more peaks occurring for the next 45 seconds. Figure 4.6 (d) again shows a large initial intensity, which drops with time until about 20 seconds where it increases to another peak. The intensity continues to decrease to steady state levels with smaller peaks occurring at 30 and 40 seconds. Figure 4.6 (e) shows an

initial peak followed by small peaks at 18 and 20 seconds and a larger peak at 40 seconds. Both Figure 4.6 (e) and (f) show very little variation in average pixel intensity levels. Figure 4.6 (f) has a large initial value and then drops to a baseline level. In the case of 4.6 (g) there is no variation, just a baseline level. Both of these cases are very late in the cycle and most of the fuel will have entered at this time.

To further investigate the peaks that occur at 40 seconds, the raw images were examined more closely. Figure 4.7 shows images around this time for each of the cases plotted in Figure 4.6 at 60 CAD. As mentioned above, the fluorescence from the 42-second image is particularly strong in the 60 CAD aTDC position, as shown in Figure 4.7 (a). In the 75 CAD aTDC case, Figure 4.7 (b), the fluorescence from the fuel stream in the 42-second image is again stronger than in the images around it. No single image in Figure 4.7 (c), the 90 CAD aTDC position, stands out as stronger than the other images in the series. In the 105 CAD position, Figure 4.7 (d), the 44-second image shows stronger fluorescence than surrounding times in this series. For the 120 CAD case, Figure 4.7 (e) it is once again the 42-second image which shows a stronger signal. In the last two series in this set, cases 135 and 150 CAD aTDC, the signal is low in every image except immediately after the initial pulse enrichment. This 40-second peak is also clearly evident in the PDPA data shown in Figure 4.2 [15]

A possible explanation for this 40-second peak is related to the peak in intake-port wall wetting, i.e. the liquid fuel present on the walls of the intake port. Takeda et al. [3] measured the extent of intake-port wall wetting as a function of time and found it to peak at approximately 30 seconds. The increased liquid fuel present in the cylinder at 40 seconds may be attributable to this liquid fuel in the intake port entering the cylinder. If this is the case, then it is interesting that the peak in liquid fuel inflow does not correspond to the peak in liquid fuel present in the intake port.

4.1.2 8 mm Plane

The 8 mm plane was chosen because it lies at the midpoint of the intake valve. Additionally, this plane was used in other work [15] that was useful in comparing data from this study. Figure 4.8 shows the raw images from the 45 CAD run in the 8-mm plane. Comparing these images to those from the centerline case (Fig 4.1), it is clear that the ROI that best captures the liquid fuel behavior is different from the ROI chosen for the centerline data. In order to analyze the images for the off center planes, it is necessary to redefine the ROI over which the average pixel intensity is calculated. This redefinition is necessary because the laser sheet is now intersecting the fuel stream and intake valve in a different plane, resulting in a different geometry. The ROI [(x, y) = (252, 15) to (x, y) = (481, 285)] chosen for the 8mm is shown against a typical image in Figure 4.9.

Average pixel intensity values for each CA position are plotted against time in Figure 4.10 (a) – (h). All values in Figure 4.10 are background subtracted. The results for this plane are similar to those for the

centerline plane, with a large initial value caused by first pulse enrichment, a second peak in fluorescence at between 12 and 20 seconds and a final peak occurring at about 40 seconds.

4.1.3 18 mm Plane

The 18 mm plane was chosen because it was near the edge of the intake valve (radius = 16 mm) and the raw images for the 45 CAD in this plane are shown in Figure 4.11. Once again a redefinition of the ROI is necessary, so that the changed geometry of the fluorescing section of the fuel stream can be accounted for. The most suitable ROI for analyzing the 18mm plane is (x, y) = (223, 44) to (x, y) – (534, 268). This ROI is shown in Figure 4.12. The results for this plane are plotted in Figure 4.13 (a) – (h). For this the third and final plane, the results are again mostly consistent with the centerline plane. The times of the peaks in fluorescence coincide well with the times of about 20 and 40 seconds seen in the other planes.

4.1.4 Comparison between Planes

In order to compare average pixel intensity values between planes it was necessary to compute them over the same number and location of pixels, i.e. the same ROI. For this purpose the most ROI was chosen as the entire image; however, it was then necessary to eliminate spurious sources of fluorescence by masking the side wall and intake valve regions as shown in Figure 4.14. Figure 4.15 shows plots of images processed in this way with background subtraction as well. With the exception of the 90 and 105 CAD aTDC positions the fluorescence in the 18-mm plane is larger than in the 8mm plane, which in turn is higher than in the centerline plane. In the 90 and 105 CAD positions the steady state fluorescence values for the three planes are all very close. In the 90 CAD position the 8mm plane initially has the largest intensity values, decaying back to the same level as the other planes.

The levels of the centerline plane are most probably lower than the other two planes, because of the shadowing effect the intake valve stem has on the fuel stream from the injector. Looking at the geometry of the fuel stream-laser sheet interaction provides a possible explanation for the stronger average pixel intensity in the 18mm plane. Two lines, as has been done for the averaged, centerline, image shown in Figure 4.16 (a), can bound the fuel streams of each plane. In Figure 4.16 (b) these lines have been mirrored about the centerline of the valve stem. Rotating these outlines about the valve stem in a direction out of the plane of the page, two hollow cones are formed. The laser sheet intersects these cones in a way similar to that shown in Figure 4.16 (c) [24] and in the case of the 18 mm plane two parabolas are formed as shown in Figure 4.16 (d). Comparing Figure 4.16 (b) and (d), it is seen that the laser sheet intersects approximately 50% more of the fuel stream in the 18-mm plane than the laser sheet in the centerline plane.

4.2 Results for Iso-octane, Acetone Fuel Mixture

As mentioned in the Dopant section of the Experimental Set-up Chapter acetone was used as a fluorescent tracer to represent the low boiling point components in gasoline. The results of the visualization are discussed here. The intensity values should not be compared with the indolene results.

4.2.1 Centerline Plane

Figure 4.17 shows a set of raw images for the iso-octane acetone mixture at 45 CAD aTDC along the centerline plane. The integrated intensity results for the centerline plane with the iso-octane, acetone fuel mixture are shown in Figure 4.18 (a)-(h). For each plane, both the iso-octane, acetone fuel mixture and the iso-octane, 3-pentanone fuel mixture were analyzed using the same ROIs used on the indolene fuel. As was the case for indolene, the signal is initially strong, due to first pulse enrichment. Again, there is a set of peaks between 15 and 20 seconds, related to the peak inflow of liquid fuel into the cylinder. In most cases there is a barely noticeable peak occurring around the 40-second point. The reason for the smaller peak at the 40-second point is thought to be due to preferential evaporation of acetone out of the fuel mixture, due to its lower boiling point. This preferential evaporation of high volatility components will reduce the concentration of acetone in the remaining liquid fuel. If the concentration of dopant is low in the liquid, then the overall signal for the plane will be lower, due to the significant density difference between vapor and liquid.

4.2.2 8 mm Plane

Raw images for the 8 mm off the valve centerline plane at 45 CAD aTDC are shown in Figure 4.19, and Figure 4.20 shows the results for this plane. The peak of signal intensity for the 8-mm plane occurs between 15 and 20 seconds although in this case the peaks are very small compared to the steady state levels and in some cases, for example the 60 CAD aTDC position, the peaks are barely noticeable. This difference in the size of the peaks between the centerline and 8-mm planes is believed to be attributable to the distribution of droplet sizes around the intake valve. As a droplet heats up the high volatility components will evaporate first, leaving a lower concentration of these high volatility components in the remaining droplet, and thus giving a lower LIF signal. Figure 4.21 (a) shows the droplet distribution around the circumference of the intake valve, obtained using PDPA [15]. It is evident from this that the droplets at the 135-degree valve angle position, corresponding to the 8mm plane, are considerably smaller than at the 180-degree valve angle position, corresponding to the centerline plane. Since the droplets in the 8-mm plane are smaller than the droplets in the 18-mm plane it is likely that more evaporation has occurred from the droplets in the 8-mm plane. This will give a lower concentration of the high volatility acetone in the droplets of the 8-mm plane, which would explain the weaker fluorescence signals in the 8-mm plane.

4.2.3 18 mm Plane

Figure 4.22 shows a set of raw images for the iso-octane acetone mixture at 45 CAD aTDC along the 18 mm off the valve centerline plane. Plots for the 18mm plane are shown in Figure 4.23. In this plane the peaks are, again, very small compared to the steady state levels. Once again these small peaks are most likely attributable to the distribution in droplet sizes around the intake valve, i.e. smaller droplets are present in the 90 degree valve angle position when compared with the droplet sizes at the 180 degree valve angle position of Figure 4.21 (a).

4.2.4 Comparisons between Planes

Plots comparing average pixel intensities for each plane at each crank angle position are shown in Figure 4.24. Unexpectedly, the trend seen for indolene fuel is reversed in this case. The strongest signal intensities are seen in the centerline plane, followed by the 8mm plane and then finally the 18mm plane has the lowest average pixel intensities. In considering the fluorescence of a liquid fuel droplet, it is important to consider the droplet size. Evaporation of dopant out of a droplet depends on droplet size. Figure 4.21 (a) shows plots of PDPA data [15] relating droplet diameter to position on the valve circumference as a function of CAD aTDC. It can be seen from this that droplet diameters are smaller at the position (135 degrees) closest to the 8mm plane than at the position (180 degrees) closest to the centerline plane. Since these droplets are smaller they would most likely contain a lower concentration of the high volatility fluorescent compound than the larger droplets near the valve centerline. This may provide an explanation for the lower signal intensities on the 8-mm plane as compared to the centerline plane, despite the fact that the 8-mm plane intersects more area of the fuel stream than the centerline plane.

Looking at Figure 4.21 (a) it is seen that the droplets at 90 degrees valve angle are larger than the droplets at the 135 degrees valve angle position, yet smaller than the droplets at the 180 degrees valve angle position. Based on this droplet distribution and remembering that the 18-mm plane intersects the largest area of the fuel stream, it could be expected that the signal intensities for the 18-mm plane would at least be higher than the intensities from the 8-mm plane. However, looking at Figure 4.24, it is obvious that this is not the case, the 18-mm plane has the lowest signal intensities of all the planes. There is definite explanation for this behavior, but one possibility is related to droplet travel time. When considering the droplets that are present in the different planes it is also important to consider not just the droplet diameters corresponding to the position where the plane intersects the valve circumference. It is also necessary to think about where the droplets originated from on the valve circumference. Assuming the droplets are travelling radially outwards from the valve then all the droplets present in the valve centerline plane will have originated from the 180 degrees valve angle position of figure 4.21 (b). In the 8-mm plane the droplets will originate from valve angle positions of 135 degrees to about 150 degrees. On the 18-mm plane a large number of the droplets will have a longer travel distance when compared with the droplets in the other

planes. This provides more time for the evaporation of these droplets. As explained earlier, this will give low concentrations of the high volatility acetone in the remaining droplet, resulting in low signal intensities.

4.3 Results for Iso-octane, 3-pentanone Fuel Mixture

Looking at the individual images of 3-pentanone, Figure 4.25, it is obvious that the images contain little or no fluorescence from liquid droplets. The average pixel intensity results for 3-pentanone, Figure 4.26 – 4.28 show very little variation at all, either as a function of crank angle or as a function of time. This is strange since 3-pentanone was chosen for its volatility, which lies between that of acetone and high boiling point fluorescing compounds of indolene. Other experiments performed on this engine using a similar iso-octane, 3-pentanone mixture fuel mixture, gave results with a fluorescence level similar to that of acetone [20]. The reason for the poor fluorescence of the iso-octane, 3-pentanone may have been due to a low concentration of 3-pentanone in the iso-octane, resulting from an inhomogeneous fuel mixture, oxygen quenching of the fluorescence, and/or the temperature dependence of the LIF signal from 3-pentanone. An exact cause is beyond the scope of this work, and since no verification of these experiments was able to be performed, conclusions could not be drawn from the 3-pentanone of images.

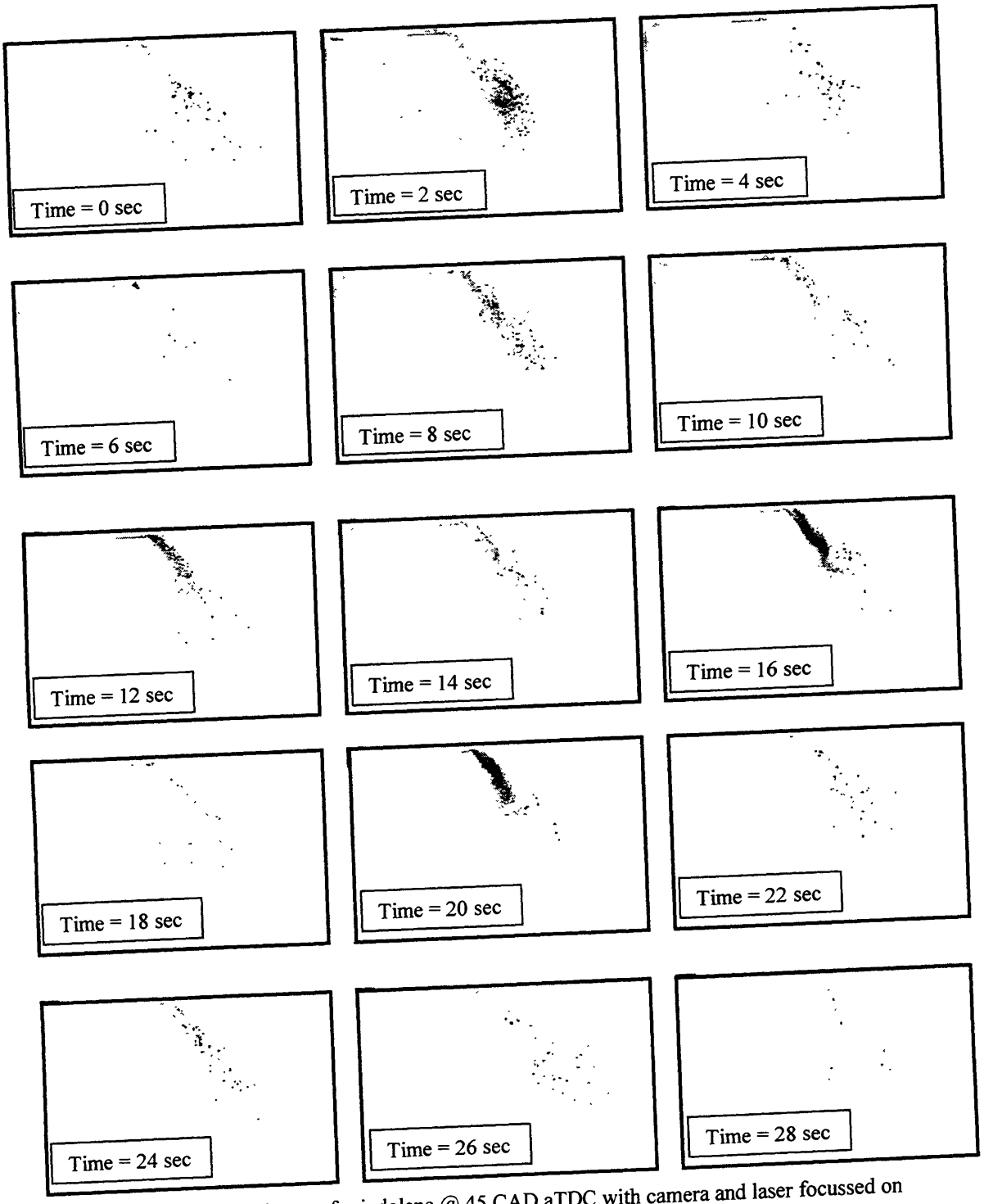

Figure 4.1: Consecutive images for indolene @ 45 CAD aTDC with camera and laser focussed on centerline plane

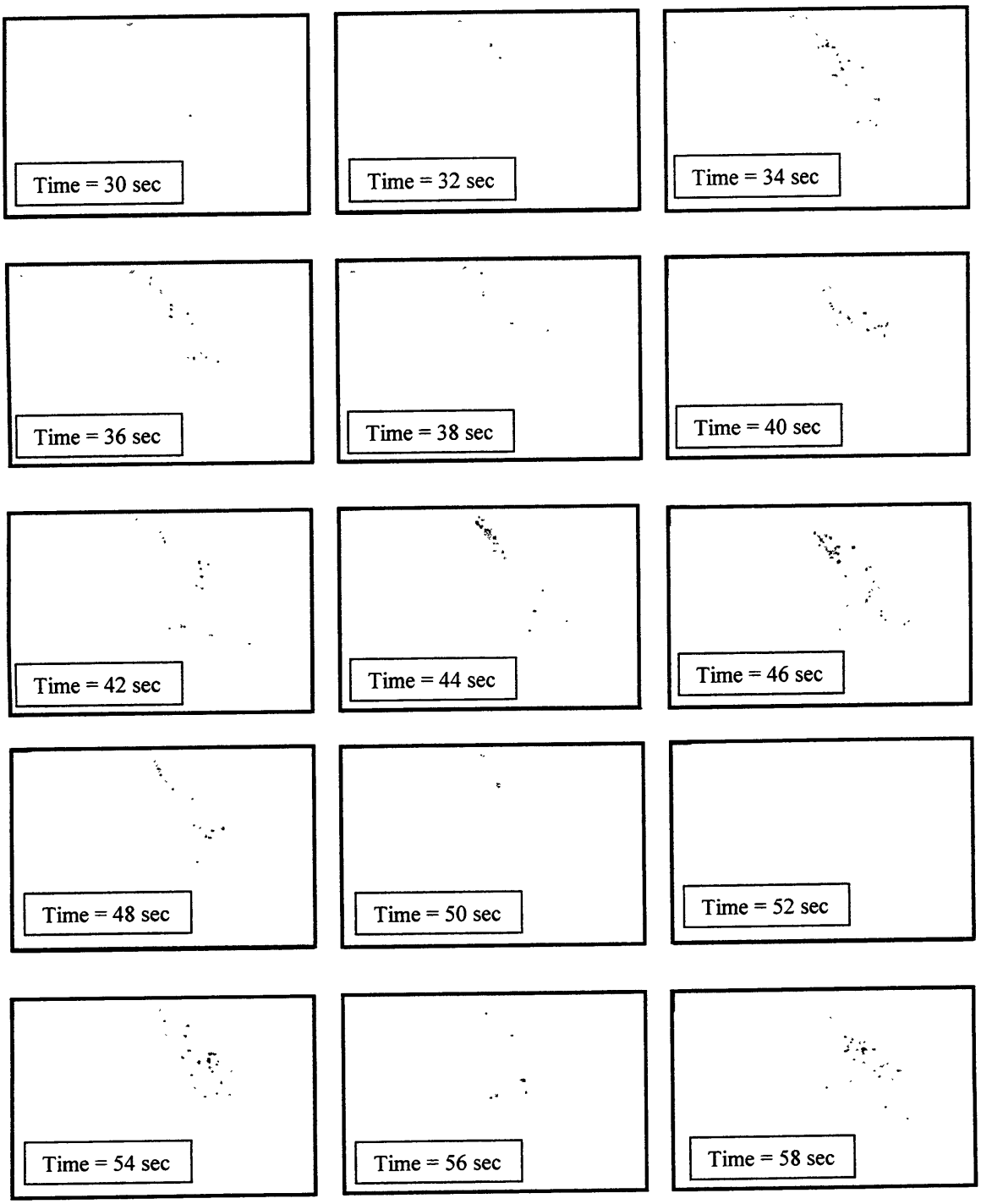

Figure 4.1 (continued): Consecutive images for indolene @ 45 CAD aTDC with camera and laser focussed on centerline plane

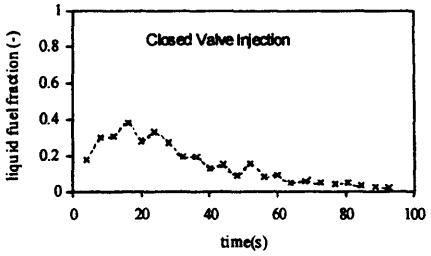

Figure 4.2: Integrated PDPA results for closed valve injection, indolene fuel

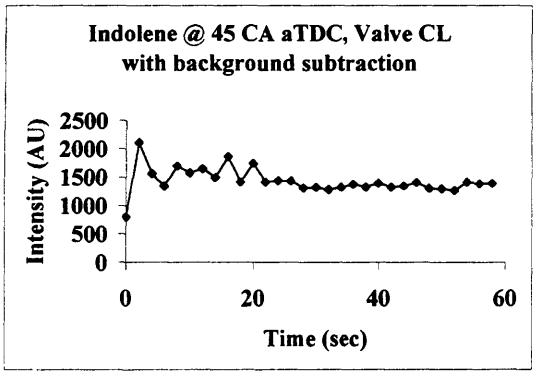

Figure 4.3 (a): Average Pixel Intensities on the Valve Centerline @ 45 CAD aTDC using Indolene Fuel

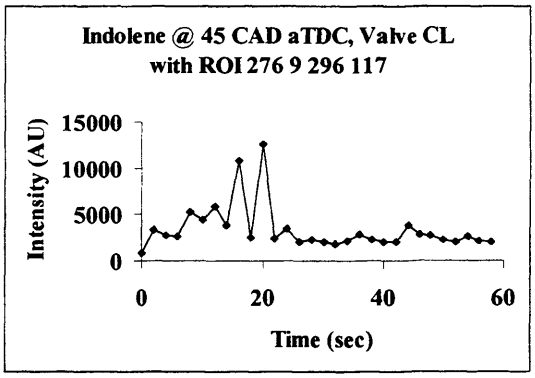

Figure 4.3 (b): Average Pixel Intensities with ROI (276, 9) – (296, 117) on the Valve Centerline @ 45 CAD aTDC using Indolene Fuel

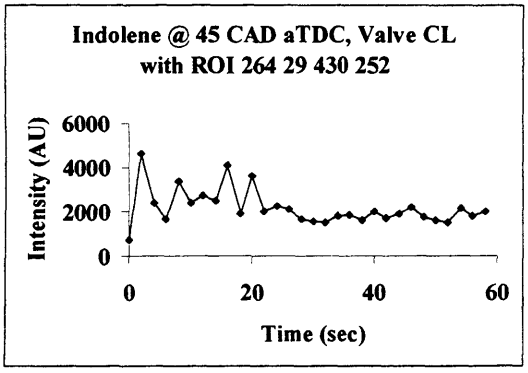

Figure 4.3 (c): Average Pixel Intensities with ROI (264, 29) – (430, 252) on the Valve Centerline @ 45 CAD aTDC using Indolene Fuel

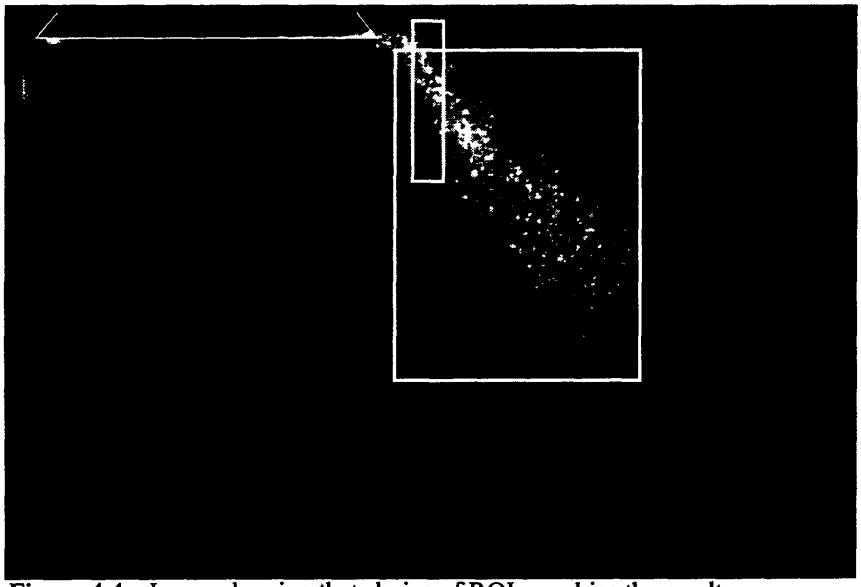

Figure 4.4 – Image showing that choice of ROIs can bias the result

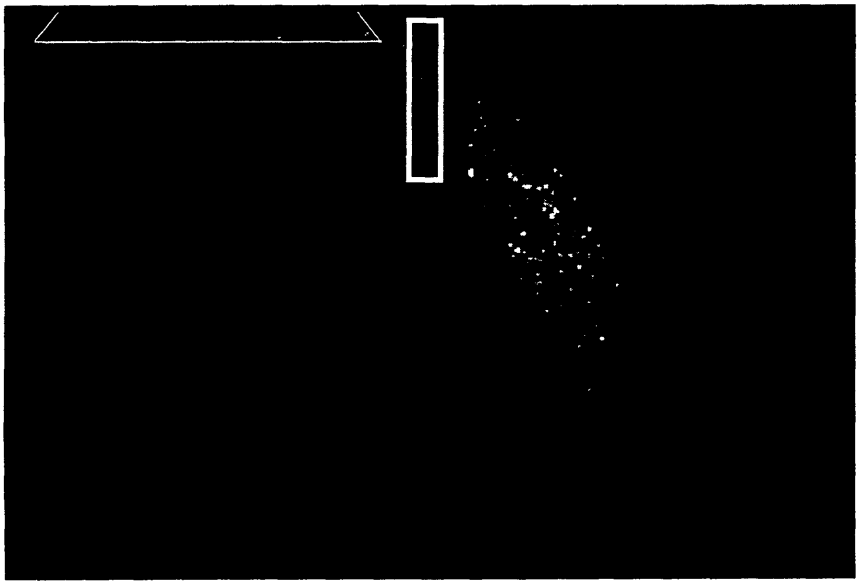

Figure 4.5: ROI (276, 9) – (296, 117) superimposed on two-second image of indolene fuel with camera triggered at 45 CA aTDC and focussed on valve centerline plane.

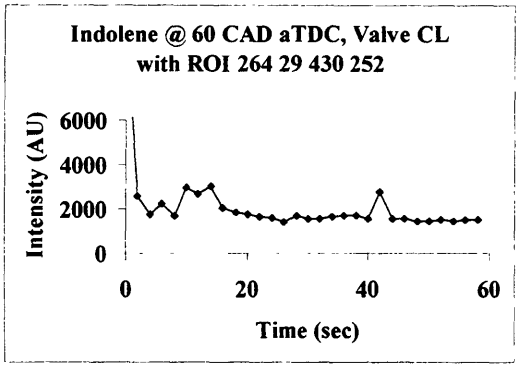

Figure 4.6 (a): Average pixel intensities with ROI (264, 29) – (430, 252) on the valve centerline @ 60 CAD aTDC using indolene fuel

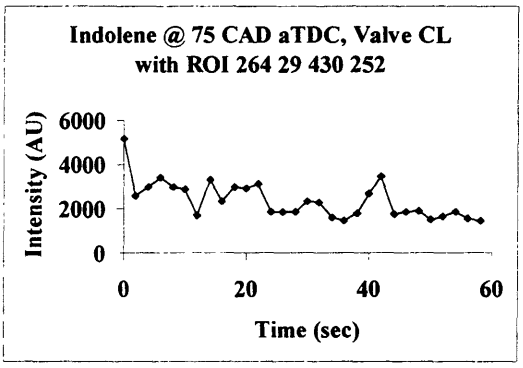

Figure 4.6 (b): Average pixel intensities with ROI (264, 29) – (430, 252) on the valve centerline @ 75 CAD aTDC using indolene fuel

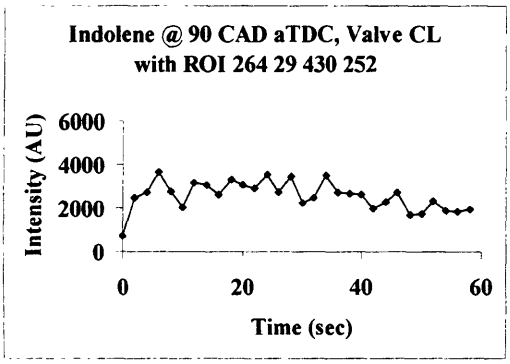

Figure 4.6 (c): Average pixel intensities with ROI (264, 29) – (430, 252) on the valve centerline @ 90 CAD aTDC using indolene fuel

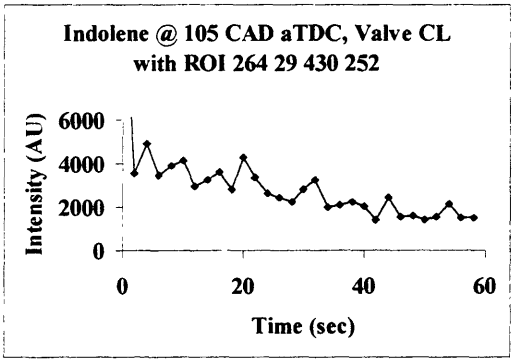

Figure 4.6 (d): Average pixel intensities with ROI (264, 29) – (430, 252) on the valve centerline @ 105 CAD aTDC using indolene fuel

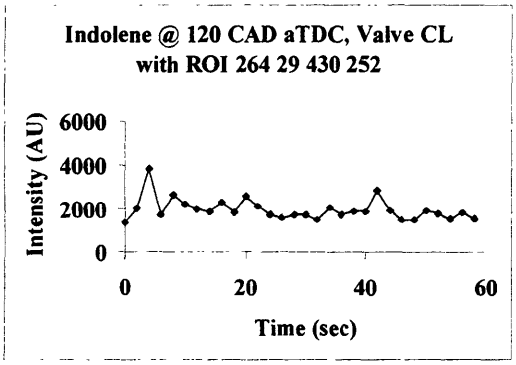

Figure 4.6 (e): Average pixel intensities with ROI (264, 29) – (430, 252) on the valve centerline @ 120 CAD aTDC using indolene fuel

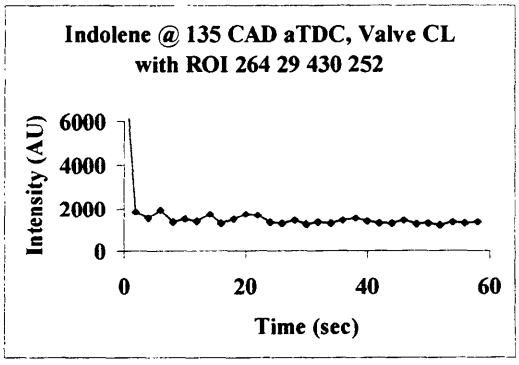

Figure 4.6 (f): Average pixel intensities with ROI (264, 29) – (430, 252) on the valve centerline @ 135 CAD aTDC using indolene fuel

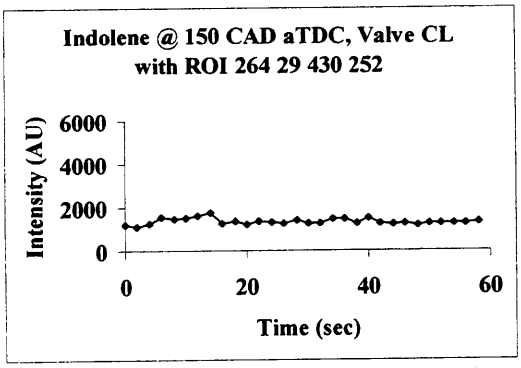

Figure 4.6 (g): Average pixel intensities with ROI (264, 29) – (430, 252) on the valve centerline @ 150 CAD aTDC using indolene fuel

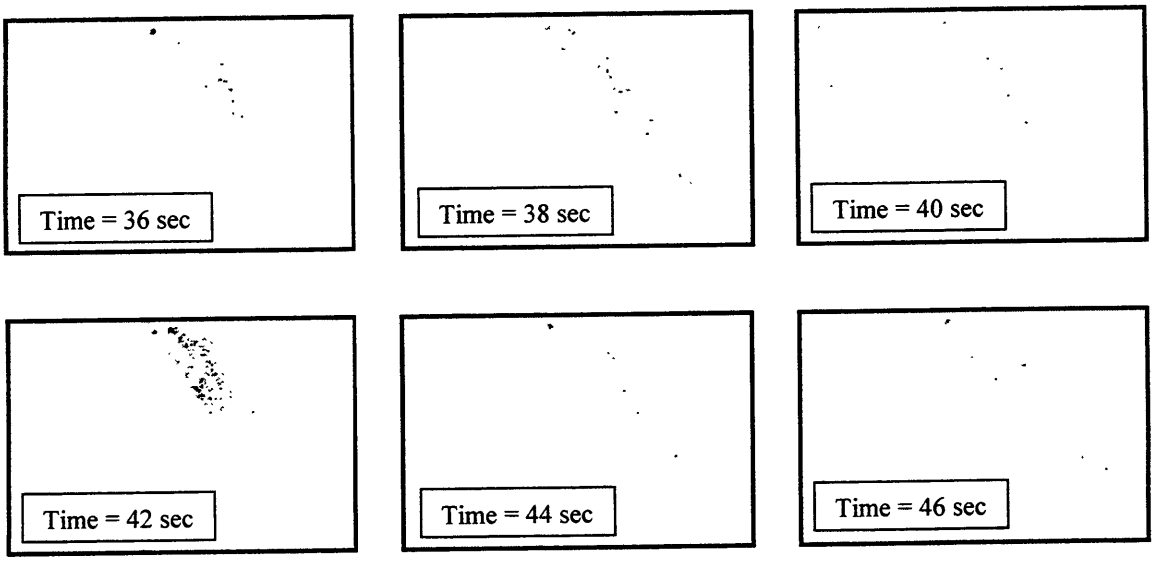

Figure 4.7 (a): Images for indolene @ 60 CAD aTDC with camera focussed on centerline plane

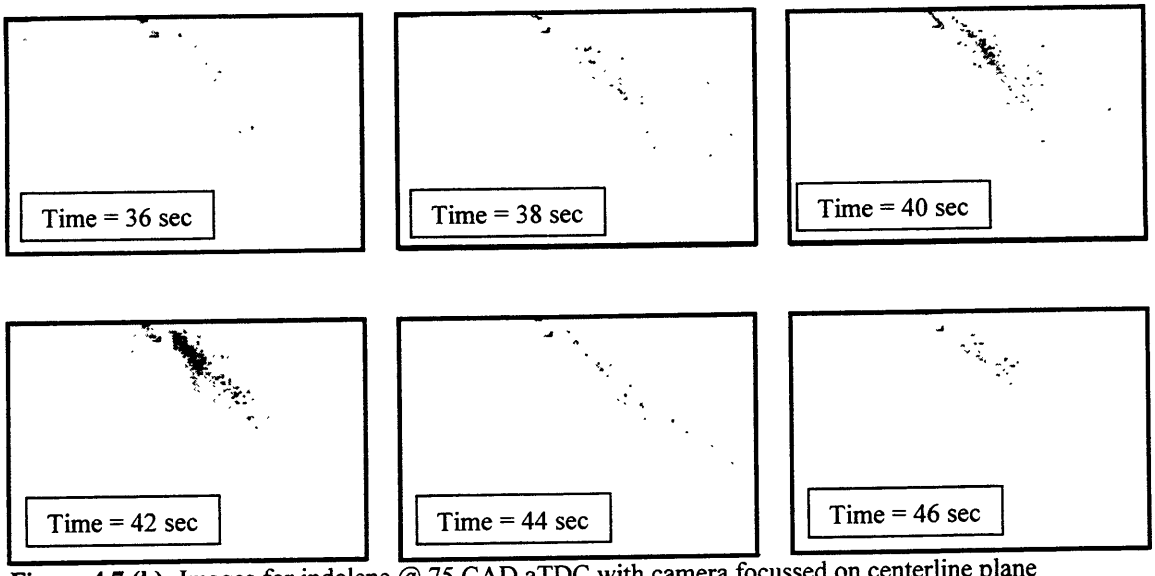

Figure 4.7 (b): Images for indolene @ 75 CAD aTDC with camera focussed on centerline plane

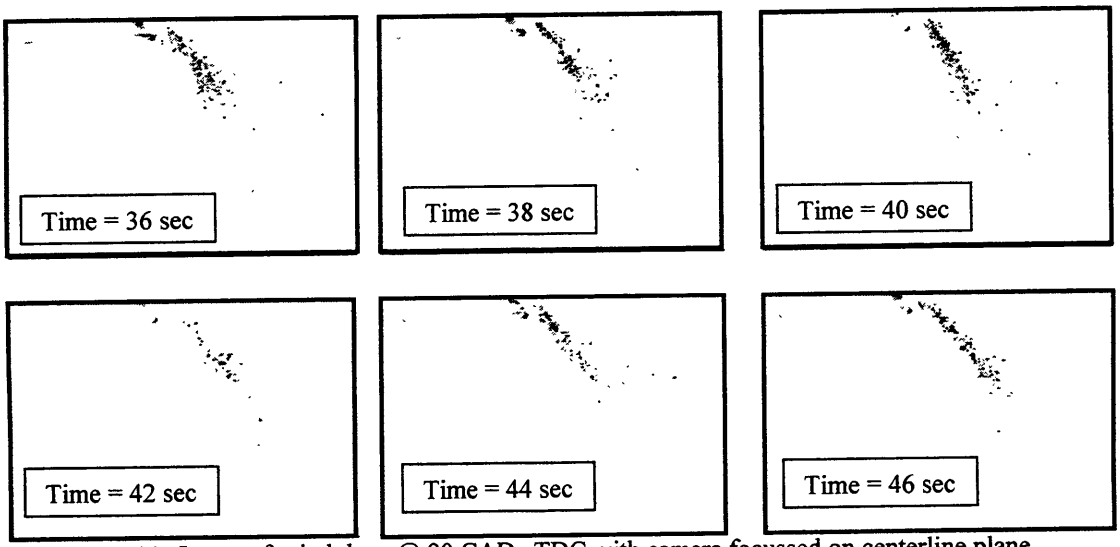

Figure 4.7 (c): Images for indolene @ 90 CAD aTDC with camera focussed on centerline plane

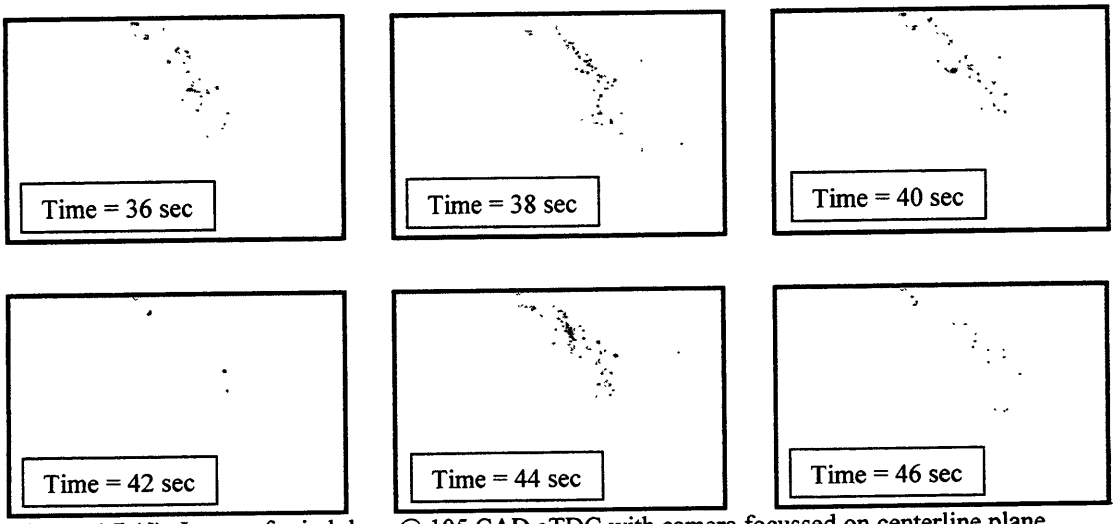

Figure 4.7 (d): Images for indolene @ 105 CAD aTDC with camera focussed on centerline plane

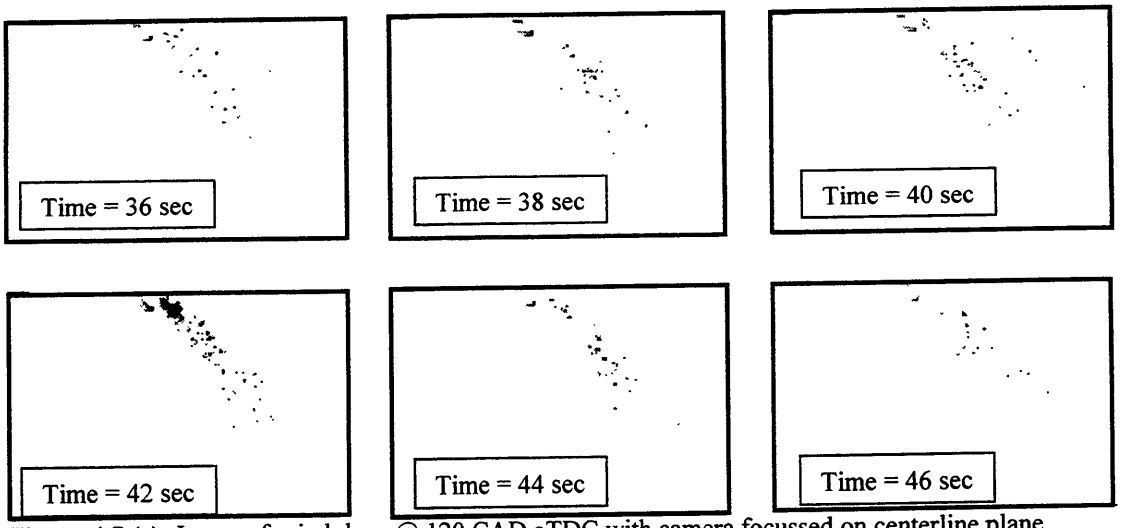

Figure 4.7 (e): Images for indolene @ 120 CAD aTDC with camera focussed on centerline plane

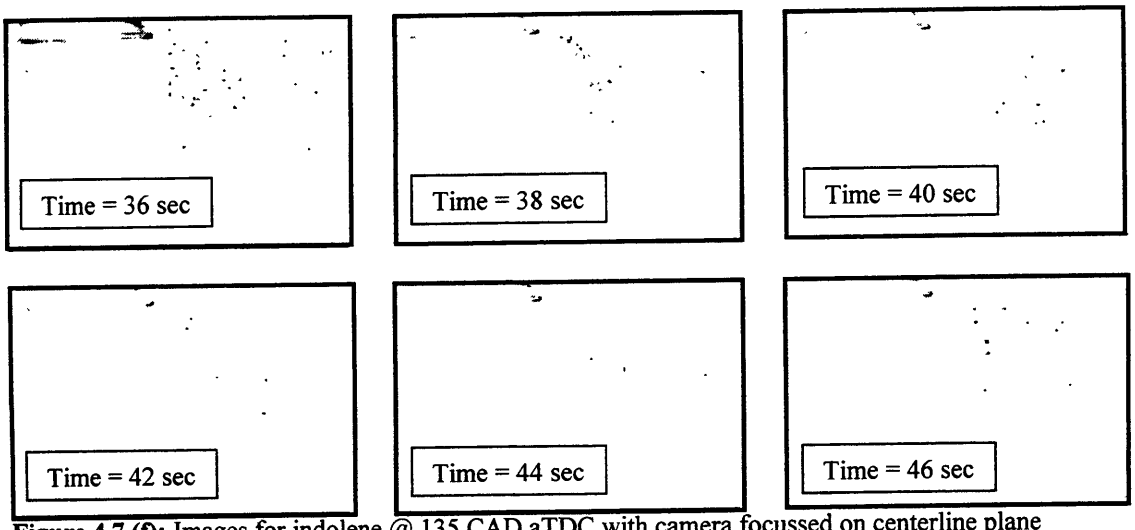

Figure 4.7 (f): Images for indolene @ 135 CAD aTDC with camera focussed on centerline plane

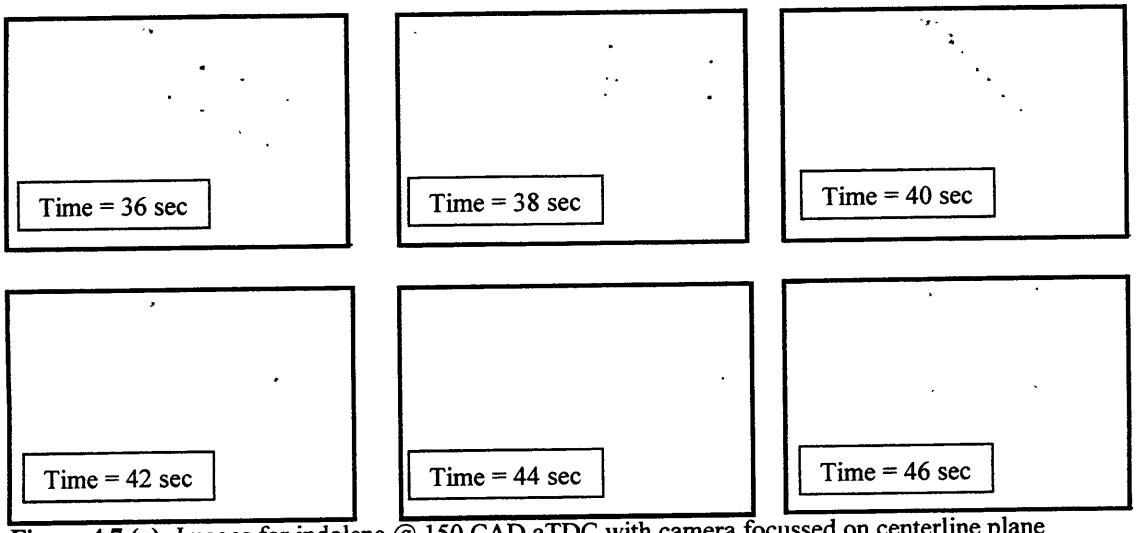

Figure 4.7 (g): Images for indolene @ 150 CAD aTDC with camera focussed on centerline plane

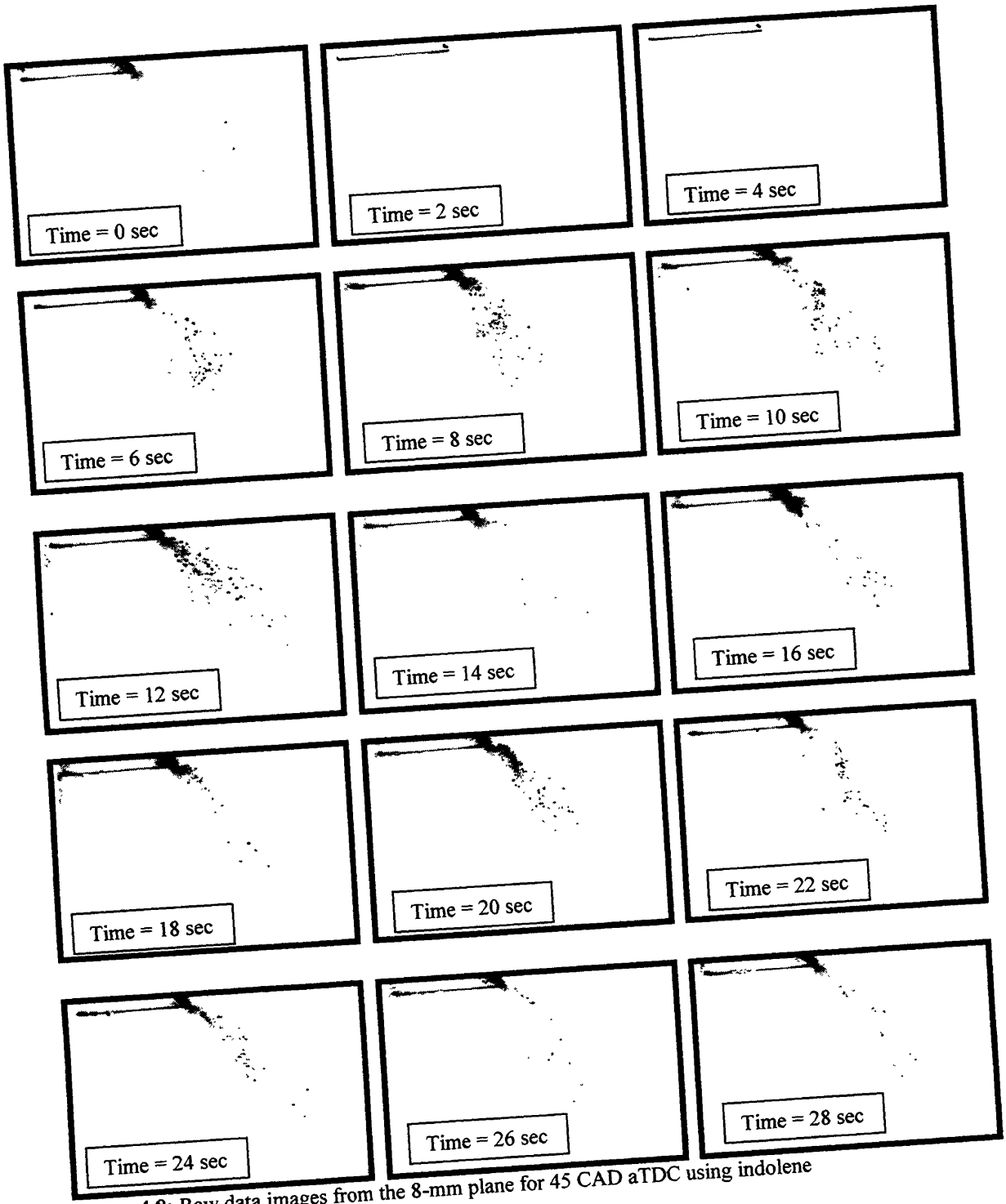

Figure 4.8: Raw data images from the 8-mm plane for 45 CAD aTDC using indolene

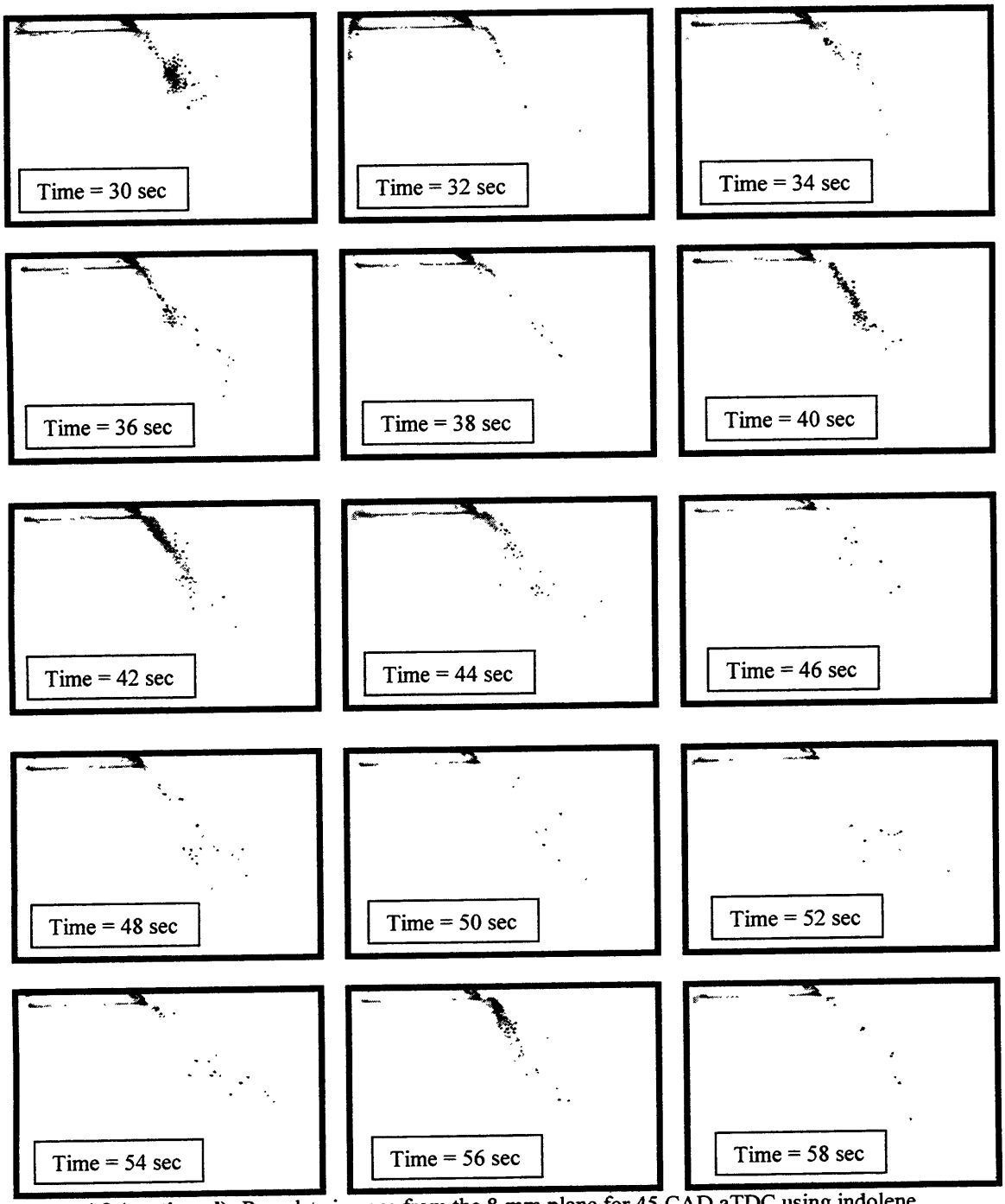

Figure 4.8 (continued): Raw data images from the 8-mm plane for 45 CAD aTDC using indolene

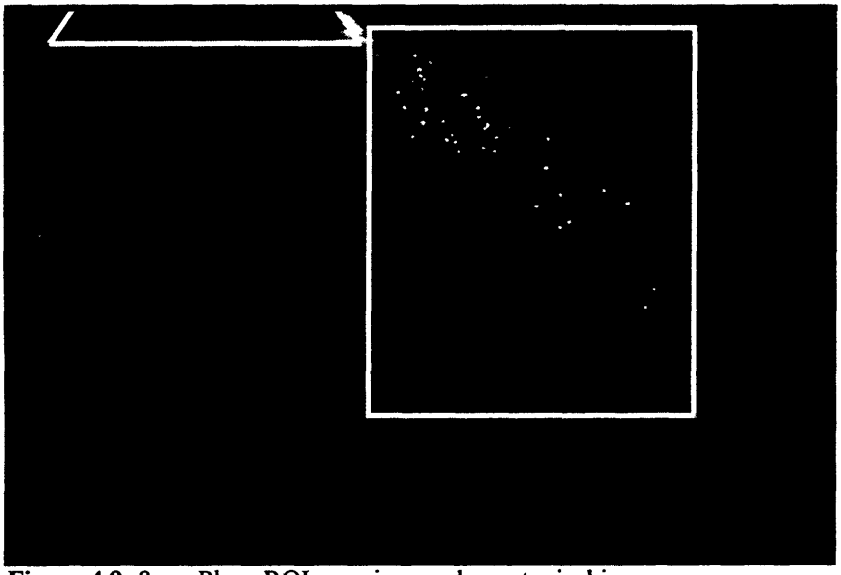

Figure 4.9: 8mm Plane ROI superimposed on a typical image

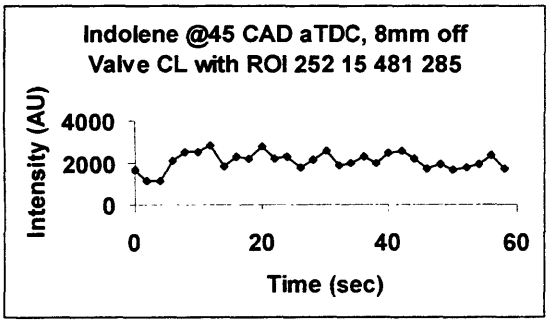

Figure 4.10 (a): Average pixel intensities with ROI (252, 15) – (481, 285), 8mm off valve centerline @ 45 CAD aTDC with indolene fuel

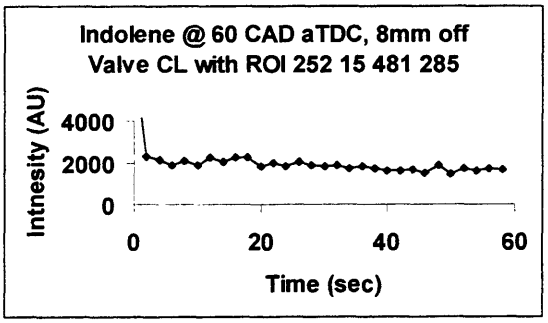

Figure 4.10 (b): Average pixel intensities with ROI (252, 15) – (481, 285), 8mm off valve centerline @ 60 CAD aTDC with indolene fuel

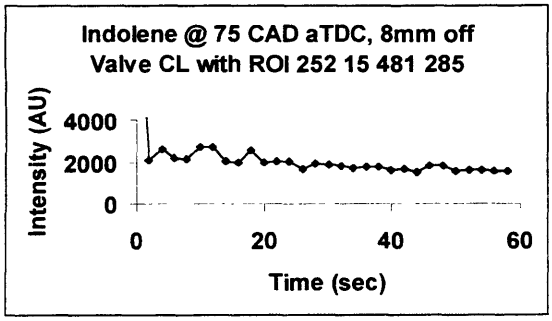

Figure 4.10 (c): Average pixel intensities with ROI (252, 15) – (481, 285), 8mm off valve centerline @ 75 CAD aTDC with indolene fuel

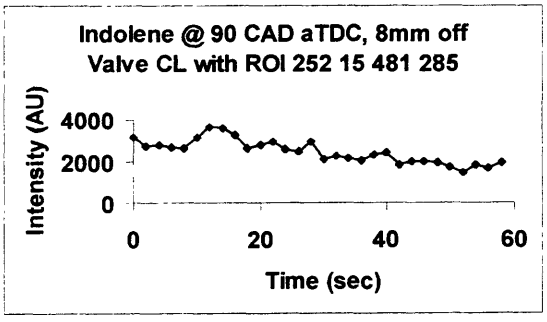

Figure 4.10 (d): Average pixel intensities with ROI (252, 15) – (481, 285), 8mm off valve Centerline @ 90 CAD aTDC with Indolene fuel

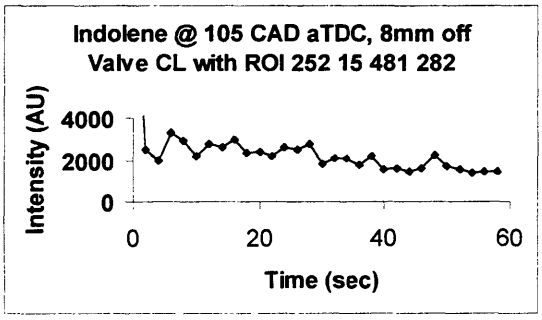

Figure 4.10 (e): Average pixel intensities with ROI (252, 15) – (481, 285), 8mm off valve centerline @ 105 CAD aTDC with indolene fuel

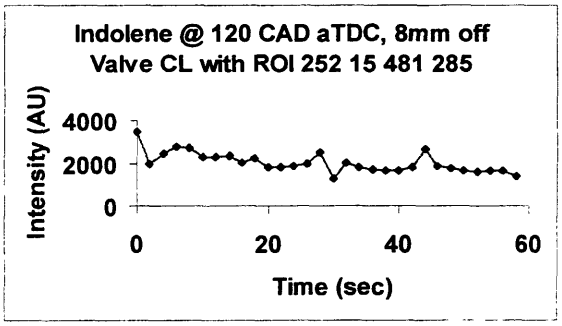

Figure 4.10 (f): Average pixel intensities with ROI (252, 15) – (481, 285), 8mm off valve centerline @ 120 CAD aTDC using indolene fuel

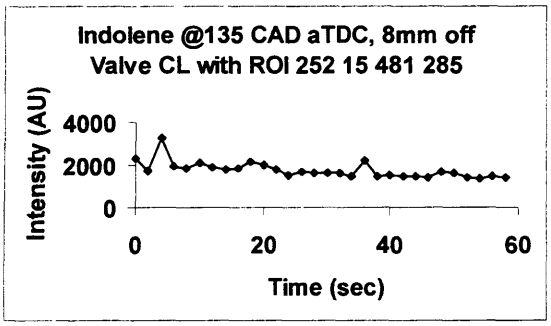

Figure 4.10 (g): Average pixel intensities with ROI (252, 15) – (481, 285), 8mm off valve centerline @ 135 CAD aTDC with indolene fuel

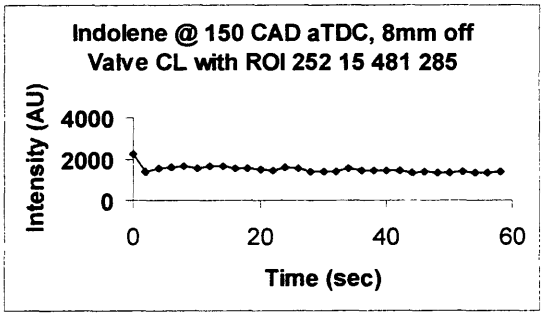

Figure 4.10 (h): Average pixel intensities with ROI (252, 15) – (481, 285), 8mm off valve centerline @ 150 CAD aTDC using indolene fuel

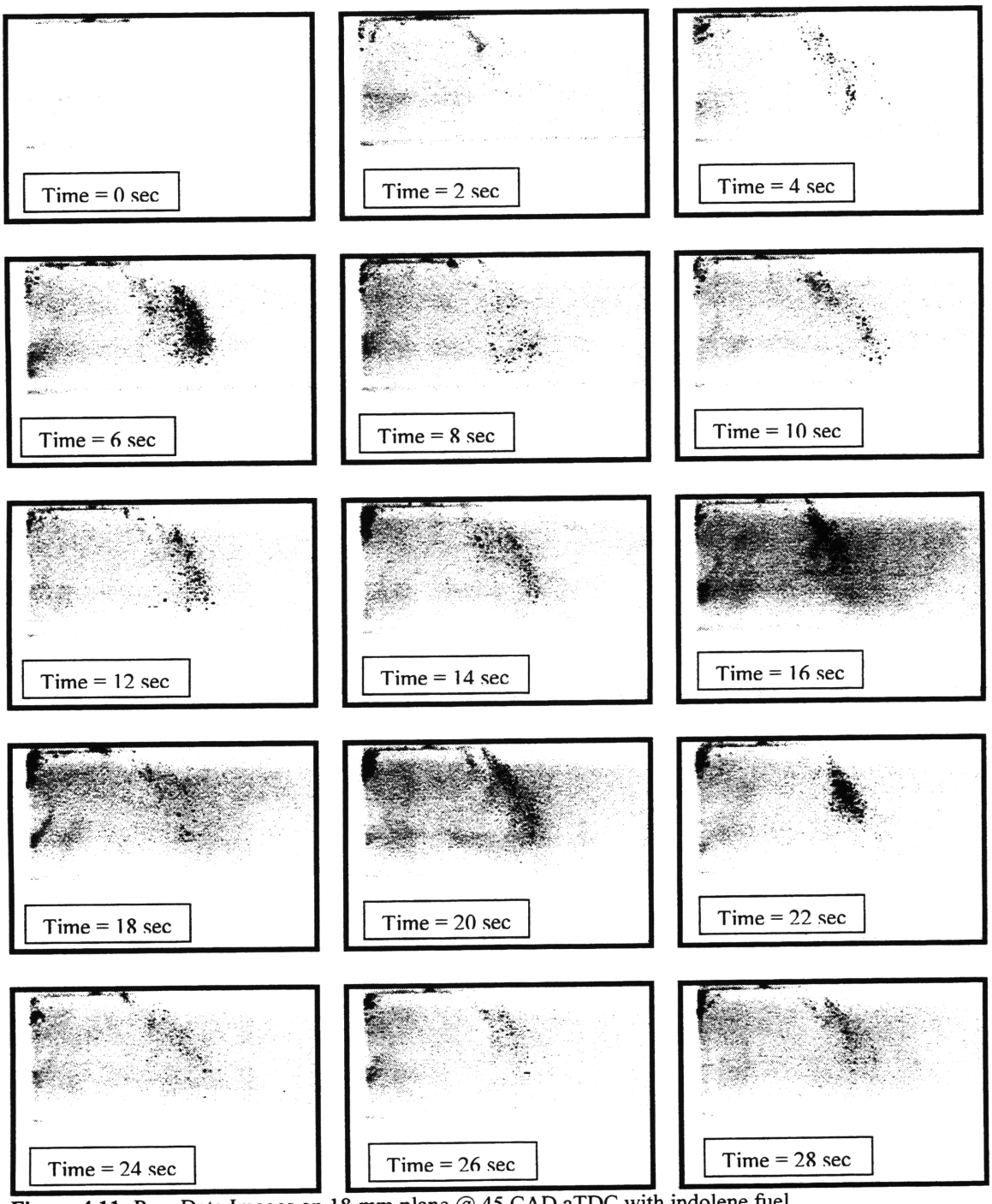

Figure 4.11: Raw Data Images on 18-mm plane @ 45 CAD aTDC with indolene fuel

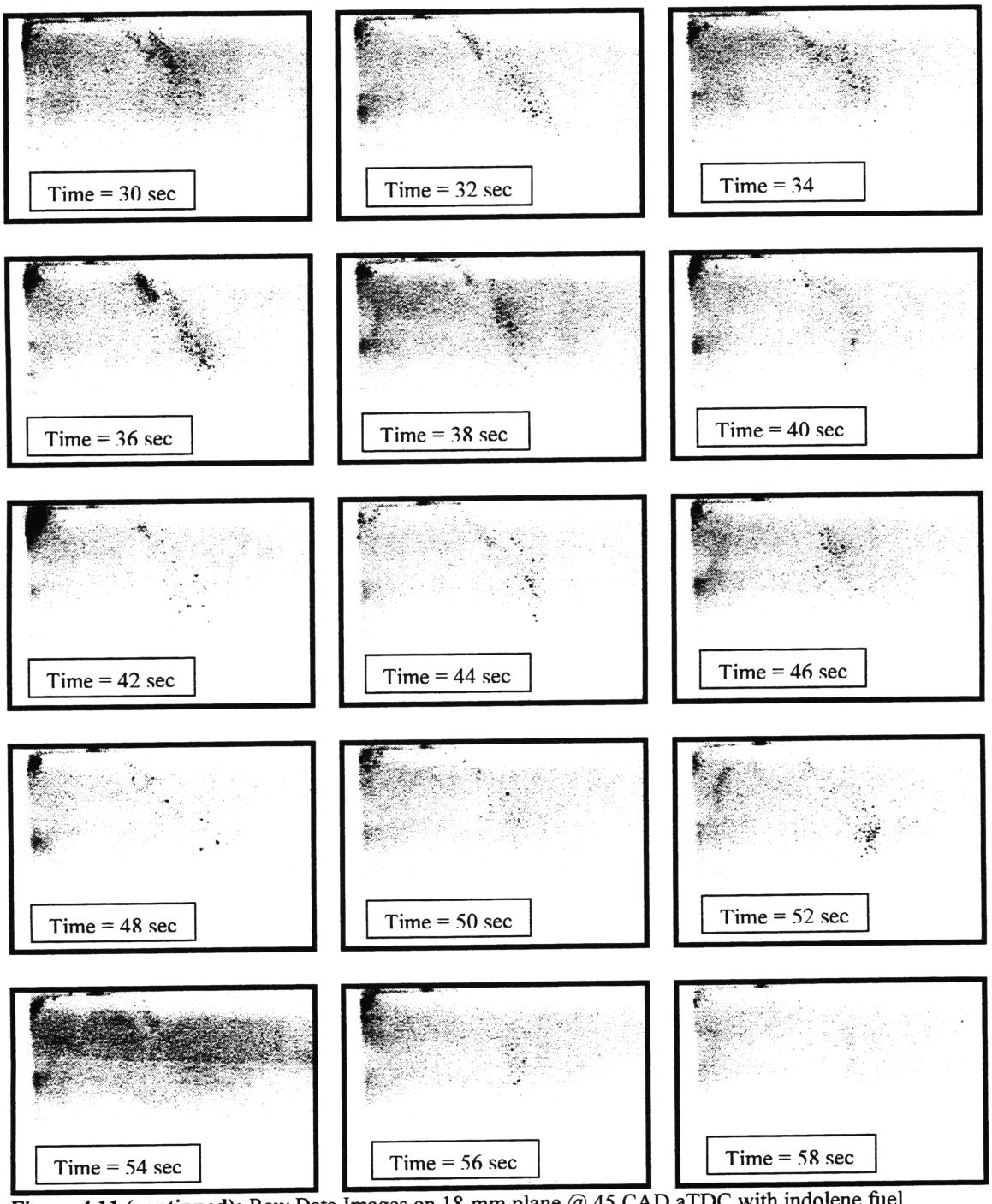

Figure 4.11 (continued): Raw Data Images on 18-mm plane @ 45 CAD aTDC with indolene fuel

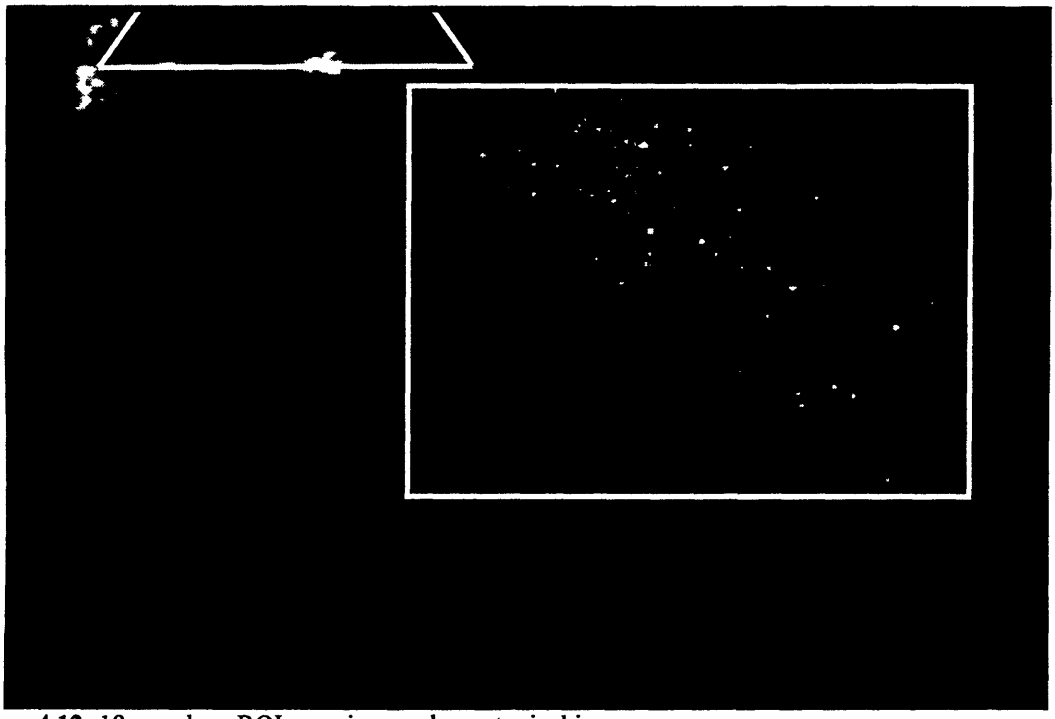

Figure 4.12: 18mm plane ROI superimposed on a typical image

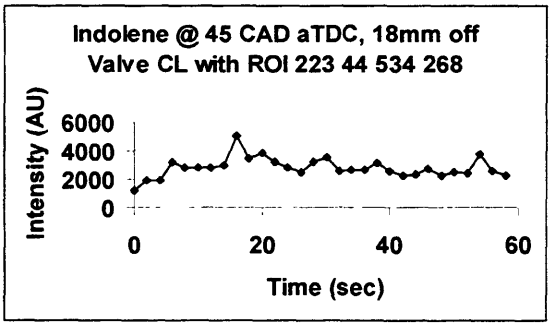

Figure 4.13 (a): Average pixel intensities with ROI (223, 44) – (534, 268), 18mm off valve centerline @ 45 CAD aTDC using indolene fuel

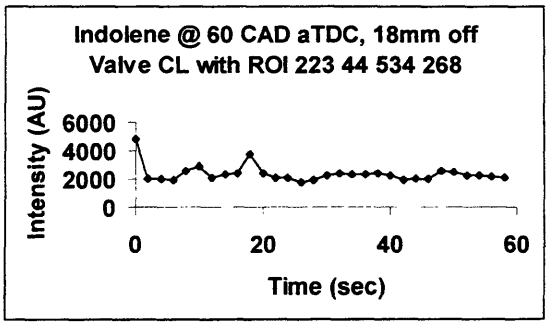

Figure 4.13 (b): Average pixel intensities with ROI (223, 44) – (534, 268), 18mm off valve centerline @ 60 CAD aTDC using indolene fuel

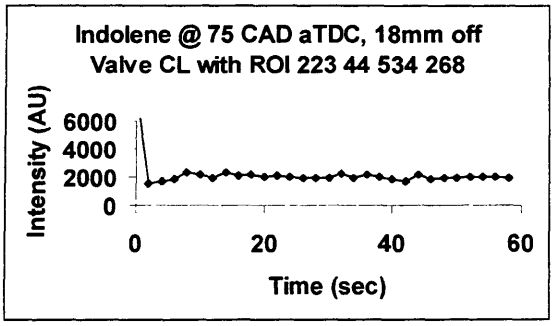

Figure 4.13 (c): Average pixel intensities with ROI (223, 44) – (534, 268), 18mm off valve centerline @ 75 CAD aTDC using indolene fuel

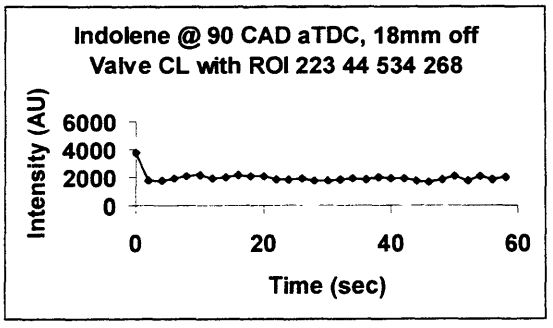

Figure 4.13 (d): Average pixel intensities with ROI (223, 44) – (534, 268), 18mm off valve centerline @ 90 CAD aTDC using indolene fuel

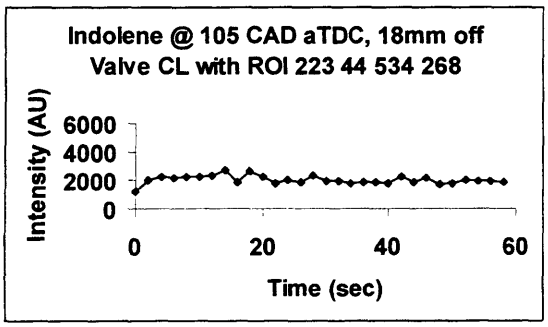

Figure 4.13 (e): Average pixel intensities with ROI (223, 44) – (534, 268), 18mm off valve centerline @ 105 CAD aTDC using indolene fuel

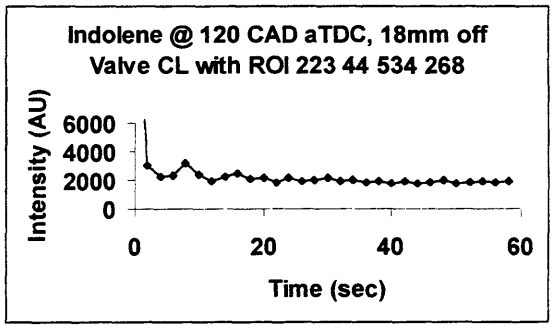

Figure 4.13 (f): Average pixel intensities with ROI (223, 44) – (534, 268), 18mm off valve centerline @ 120 CAD aTDC using indolene fuel

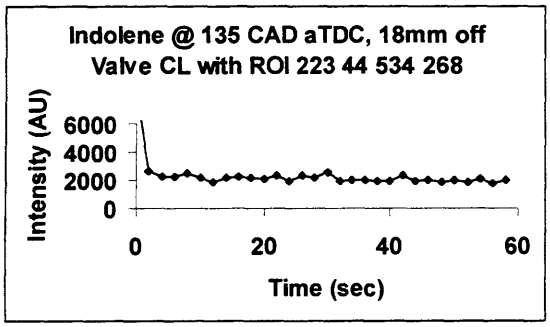

Figure 4.13 (g): Average pixel intensities with ROI (223, 44) – (534, 268), 18mm off valve centerline @ 135 CAD aTDC using indolene fuel

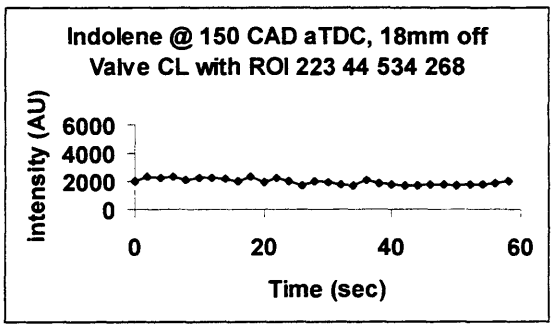

Figure 4.13 (h): Average pixel intensities with ROI (223, 44) – (534, 268), 18mm off valve centerline @ 150 CAD aTDC using indolene fuel

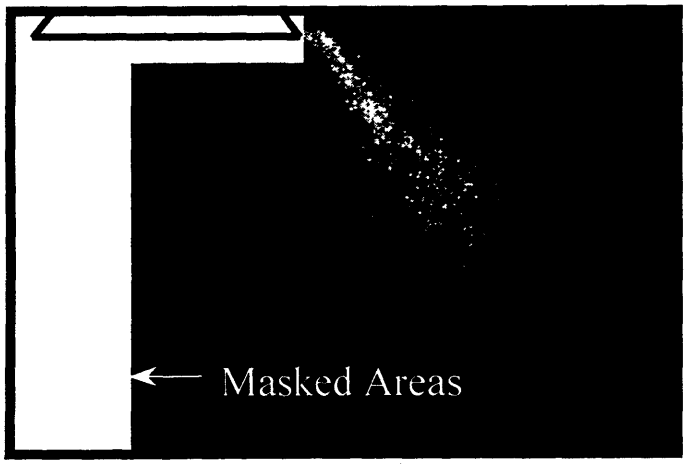

Figure 4.14: Raw Image with mask shown

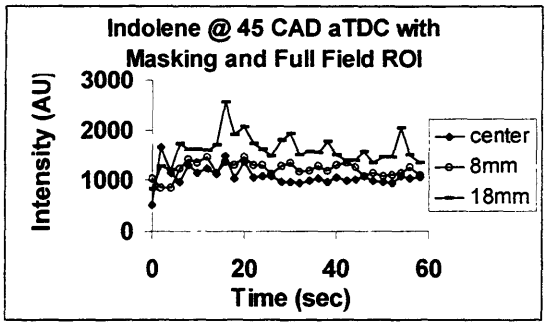

Figure 4.15 (a): Average pixel intensities with masking and full field ROI for centerline, 8-9mm and 18mm planes @ 45 CAD aTDC using indolene fuel

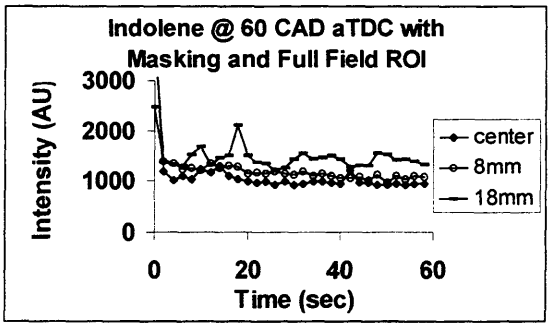

Figure 4.15 (b): Average pixel intensities with masking and full field ROI for centerline, 8-9mm and 18mm planes @ 60 CAD aTDC using indolene fuel

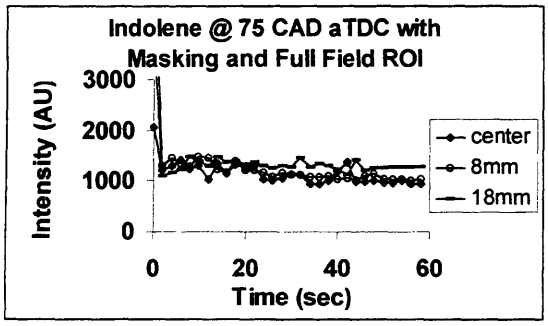

Figure 4.15 (c): Average pixel intensities with masking and full field ROI for centerline, 8-9mm and 18mm planes @ 75 CAD aTDC using indolene fuel

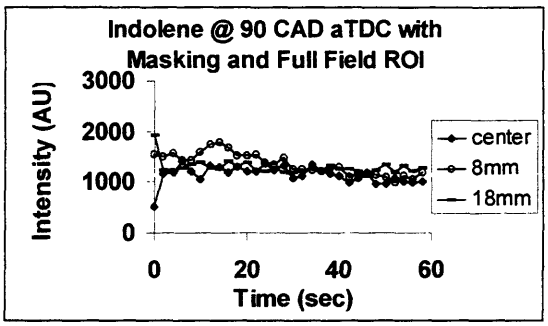

Figure 4.15 (d): Average pixel intensities with masking and full field ROI for centerline, 8-9mm and 18mm planes @ 90 CAD aTDC using indolene fuel

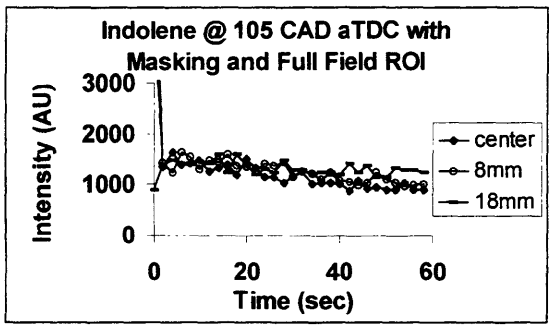

Figure 4.15 (e): Average pixel intensities with masking and full field ROI for centerline, 8-9mm and 18mm planes @ 105 CAD aTDC using indolene fuel

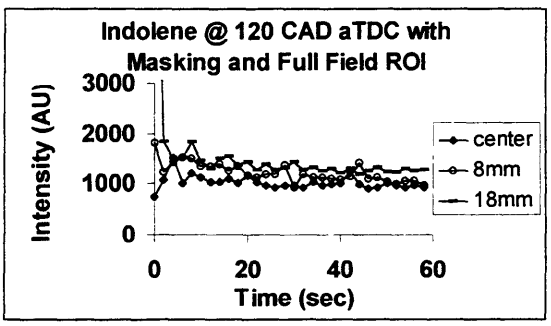

Figure 4.15 (f): Average pixel intensities with masking and full field ROI for centerline, 8-9mm and 18mm planes @ 120 CAD aTDC using indolene fuel

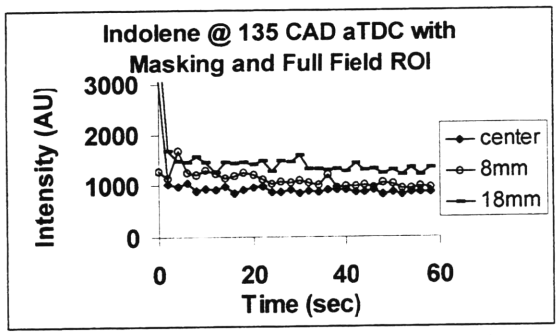

Figure 4.15 (g): Average pixel intensities with masking and full field ROI for centerline, 8-9mm and 18mm planes @ 135 CAD aTDC using indolene fuel

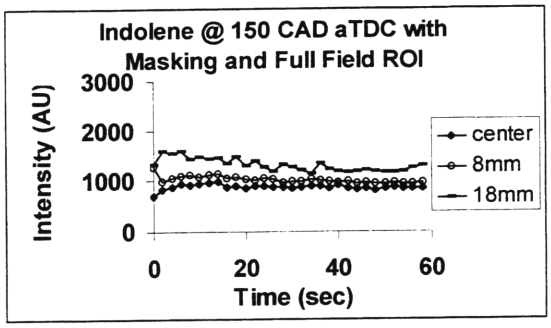

Figure 4.15 (h): Average pixel intensities with masking and full field ROI for centerline, 8-9mm and 18mm planes @ 75 CAD aTDC using indolene fuel

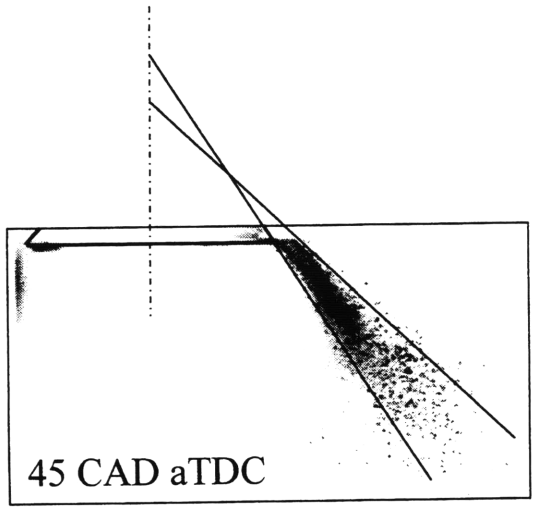

Figure 4.16 (a): Averaged Image with borders of fuel stream superimposed

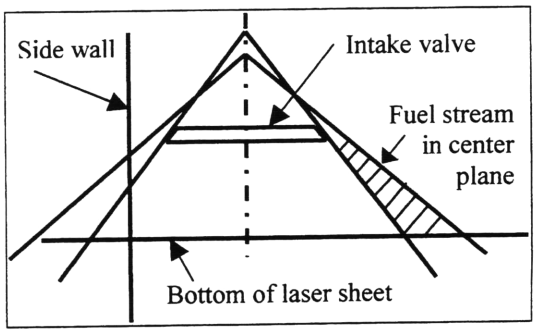

Figure 4.16 (b): Mirror of fuel borders to left side of valve

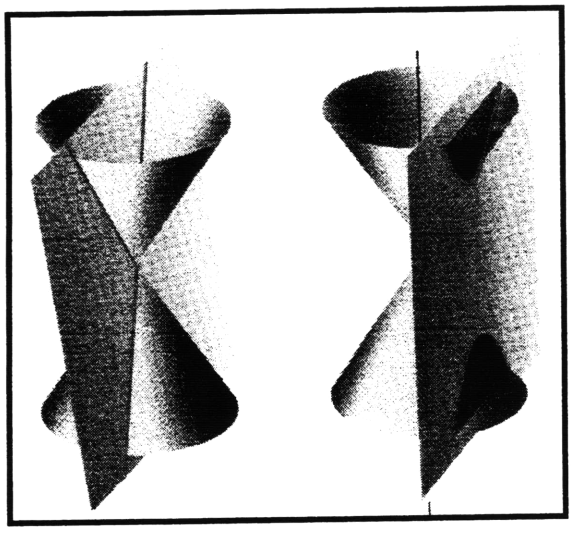

Figure 4.16 (c): Vertical planes intersecting hollow cones (Thomas and Finney)

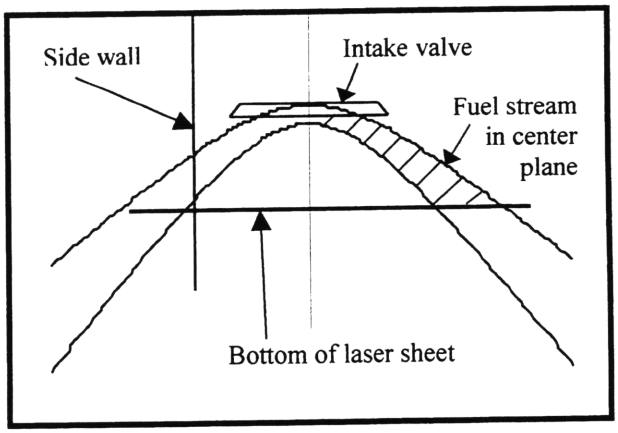

Figure 4.16 (d): Parabolas bordering fuel stream on 18mm plane

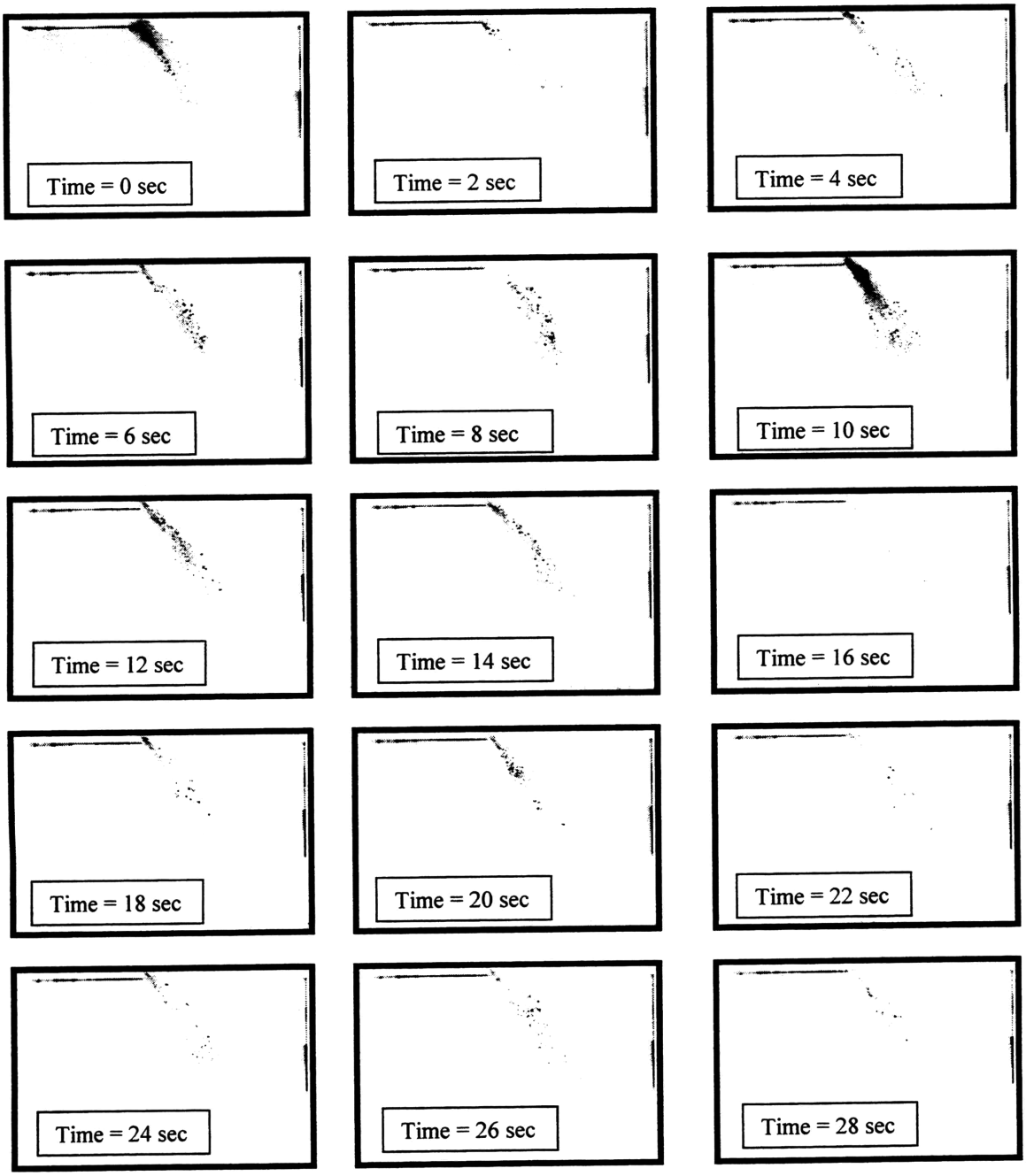

Figure 4.17: Raw data images for iso-octane acetone mixture @ 45 CA aTDC on centerline plane

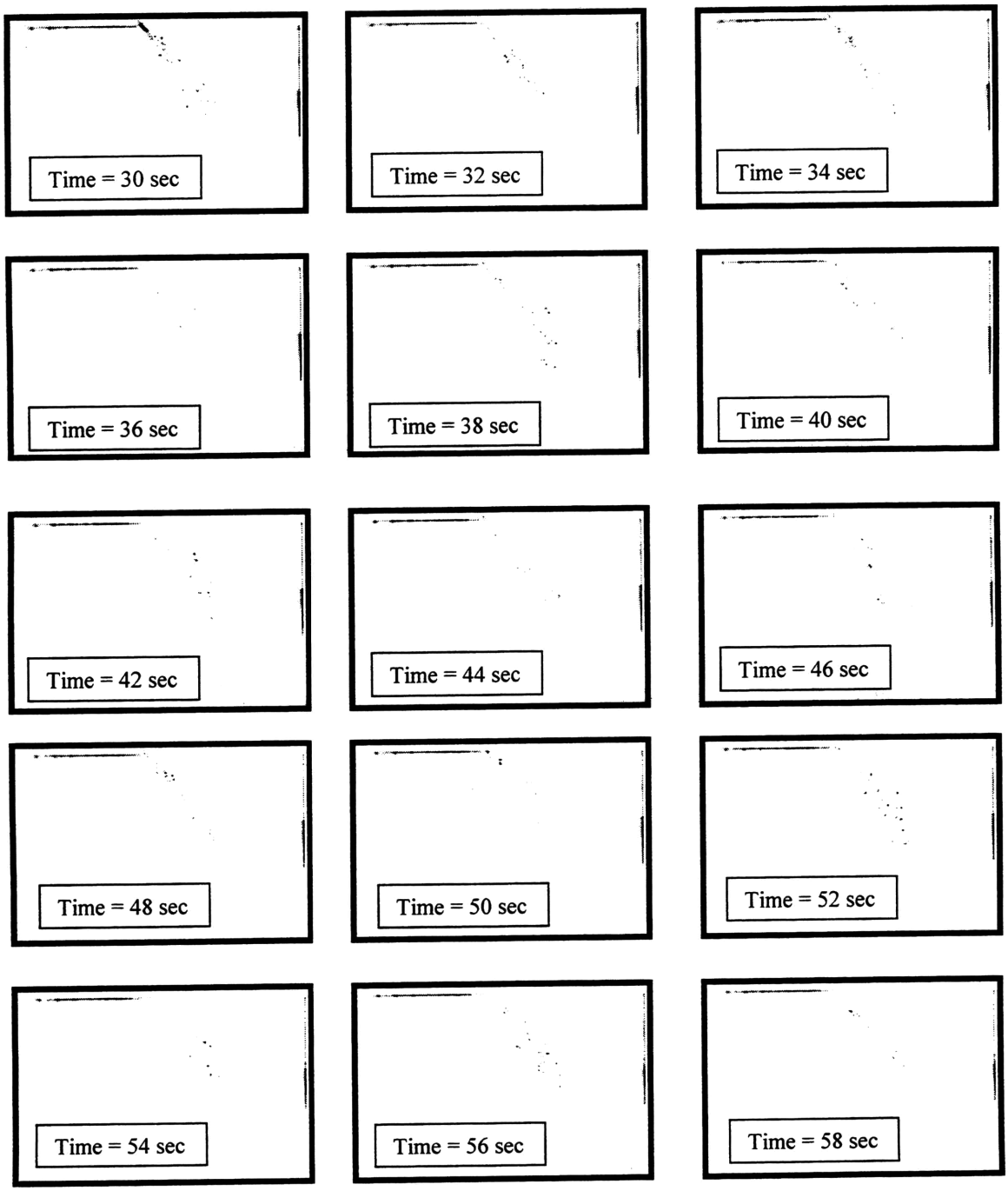

Figure 4.17 (continued): Raw data images for iso-octane acetone mixture @ 45 CA aTDC on centerline plane

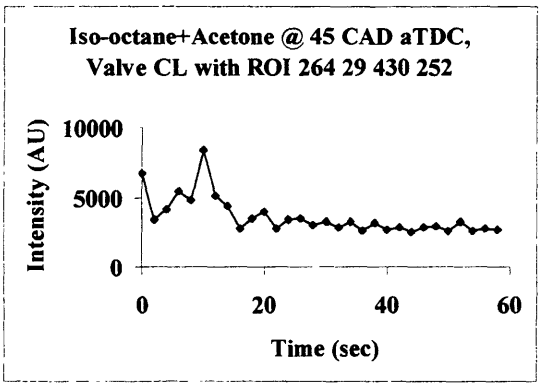

Figure 4.18 (a): Average pixel intensities with ROI (264, 29) – (430, 252) on the valve centerline @ 45 CAD aTDC using iso-octane, acetone fuel mixture

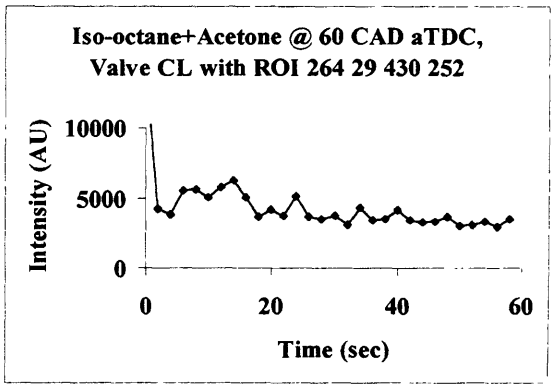

Figure 4.18 (b): Average pixel intensities with ROI (264, 29) – (430, 252) on the valve centerline @ 60 CAD aTDC using iso-octane, acetone fuel mixture

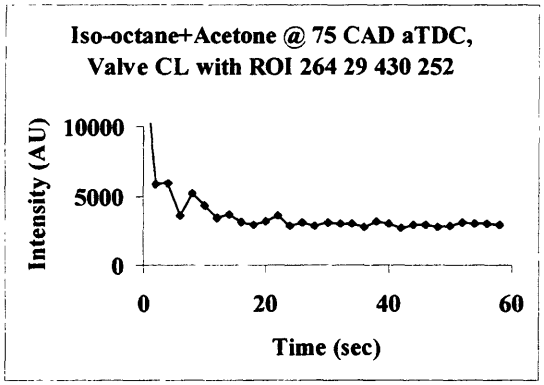

Figure 4.18 (c): Average pixel intensities with ROI (264, 29) – (430, 252) on the valve centerline @ 75 CAD aTDC using iso-octane, acetone fuel mixture

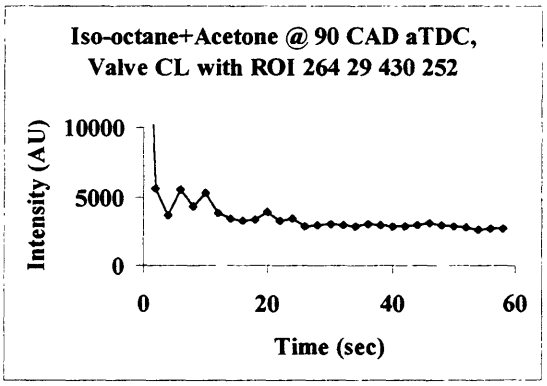

Figure 4.18 (d): Average pixel intensities with ROI (264, 29) – (430, 252) on the valve centerline @ 90 CAD aTDC using iso-octane, acetone fuel mixture

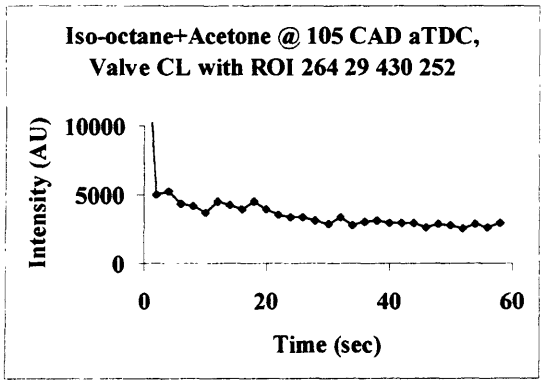

Figure 4.18 (e): Average pixel intensities with ROI (264, 29) – (430, 252) on the valve centerline @ 105 CAD aTDC using iso-octane, acetone fuel mixture

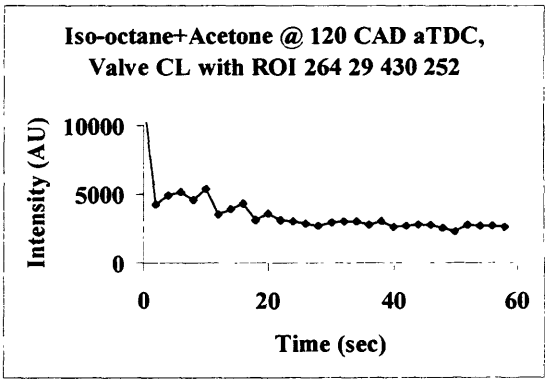

Figure 4.18 (f): Average pixel intensities with ROI (264, 29) – (430, 252) on the valve centerline @ 120 CAD aTDC using Iso-octane, acetone fuel mixture

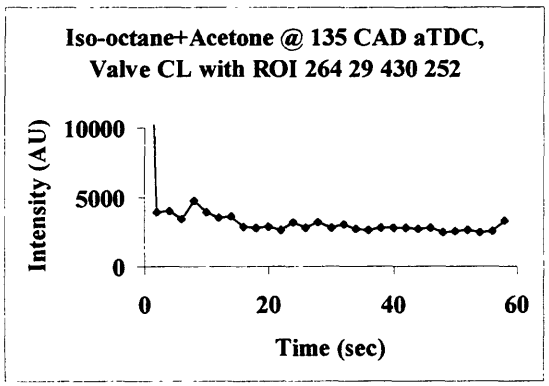

Figure 4.18 (g): Average pixel intensities with ROI (264, 29) – (430, 252) on the valve centerline @ 135 CAD aTDC using iso-octane, acetone fuel mixture

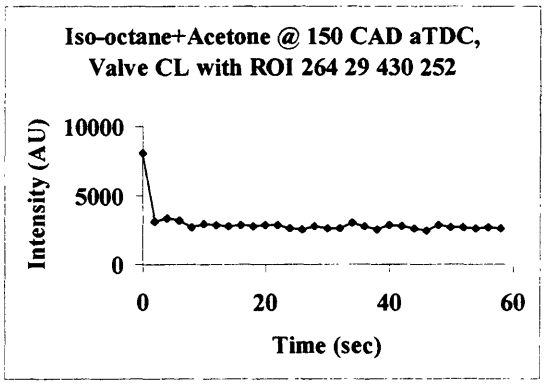

Figure 4.18 (h): Average pixel intensities with ROI (264, 29) – (430, 252) on the valve centerline @ 150 CAD aTDC using iso-octane, acetone fuel mixture

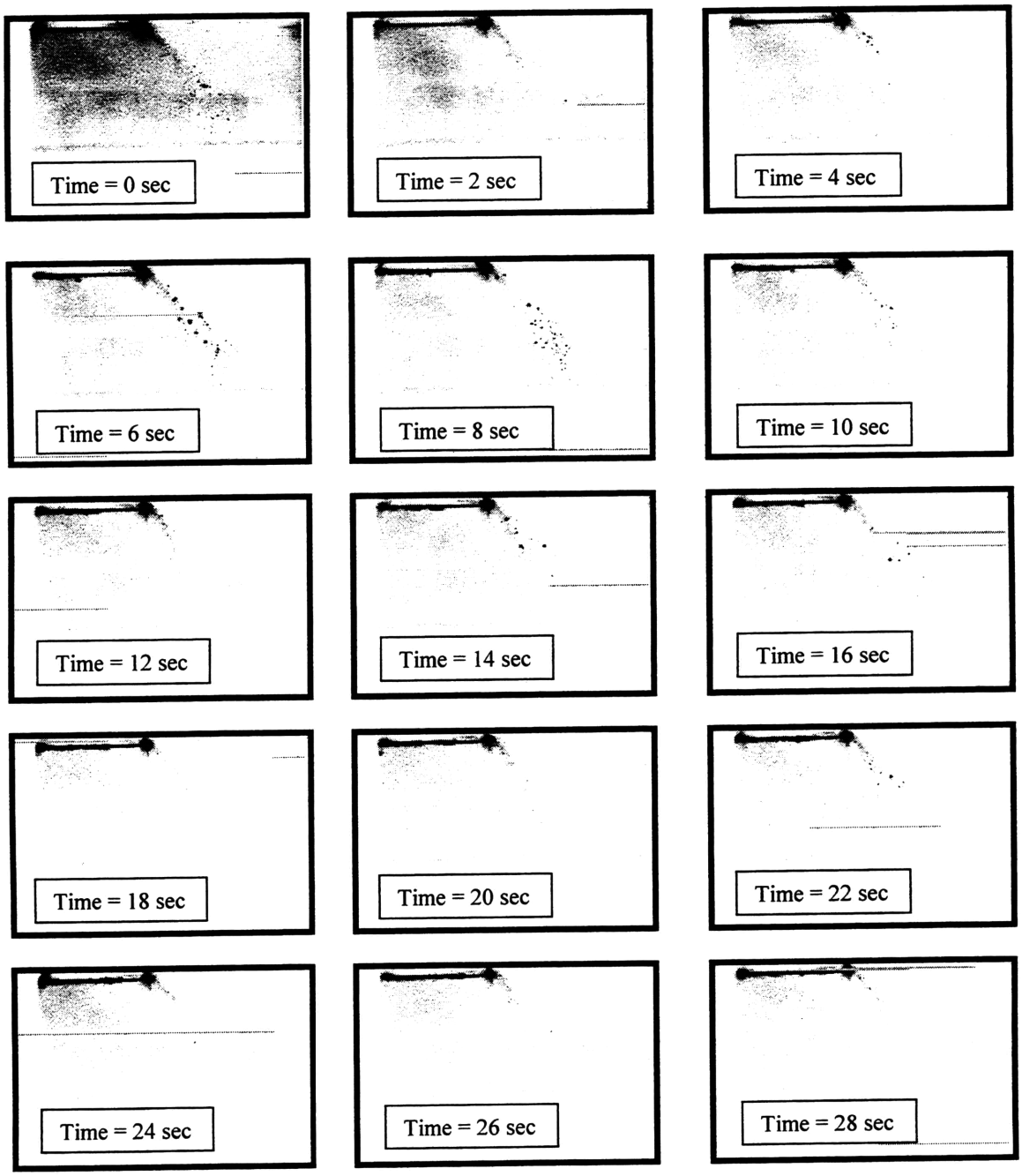

Figure 4.19: Raw images for iso-octane acetone fuel mixture @ 45 CAD aTDC on 8-mm plane

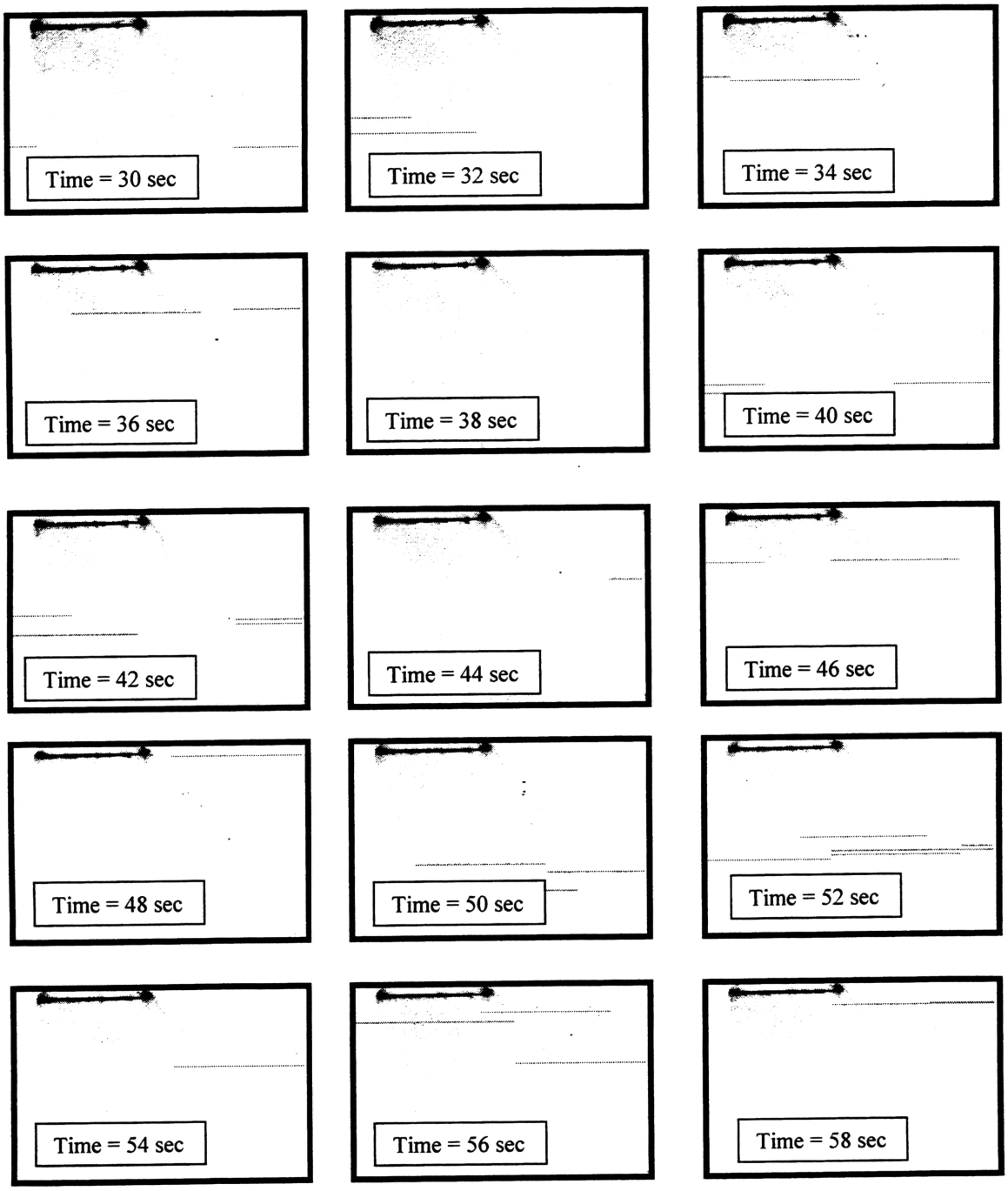

Figure 4.19 (continued): Raw images for iso-octane acetone fuel mixture @ 45 CAD aTDC on 8-mm plane

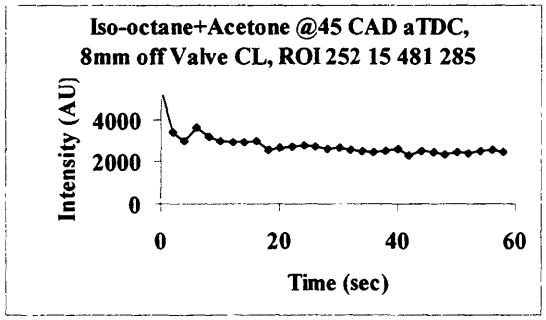

Figure 4.20 (a): Average pixel intensities with ROI (252, 15) – (481, 285), 8mm off valve centerline @ 45 CAD aTDC with iso-octane, acetone fuel mixture

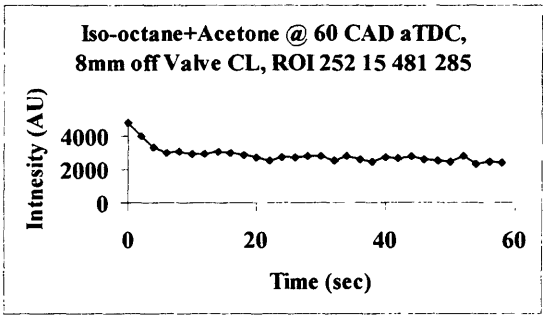

Figure 4.20 (b): Average pixel intensities with ROI (252, 15) – (481, 285), 8mm off valve centerline @ 60 CAD aTDC with iso-octane, acetone fuel mixture

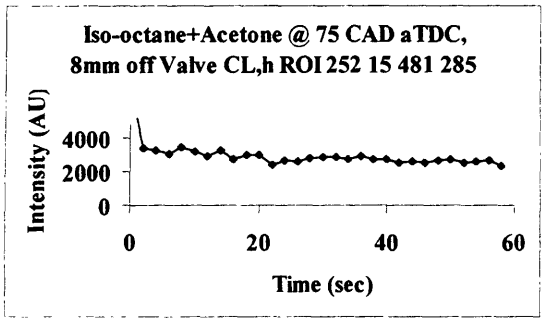

Figure 4.20 (c): Average pixel intensities with ROI (252, 15) – (481, 285), 8mm off valve centerline @ 75 CAD aTDC with iso-octane, acetone fuel mixture

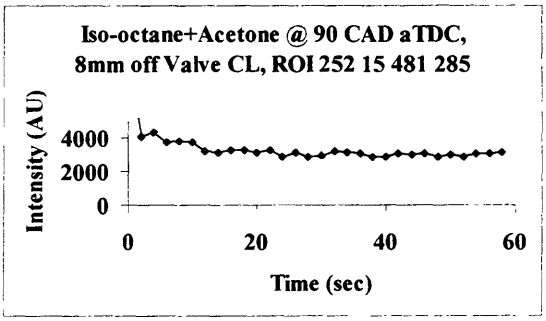

Figure 4.20 (d): Average pixel intensities with ROI (252, 15) – (481, 285), 8mm off valve centerline @ 90 CAD aTDC with iso-octane, acetone fuel mixture

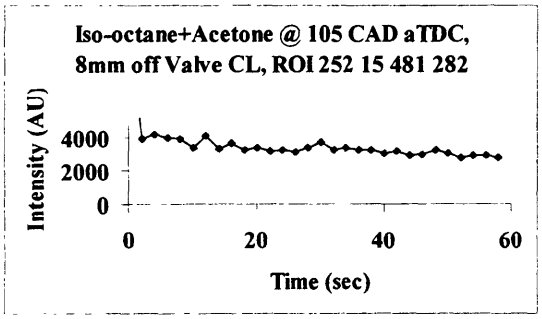

Figure 4.20 (e): Average pixel intensities with ROI (252, 15) – (481, 285), 8mm off valve centerline @ 105 CAD aTDC with iso-octane, acetone fuel mixture

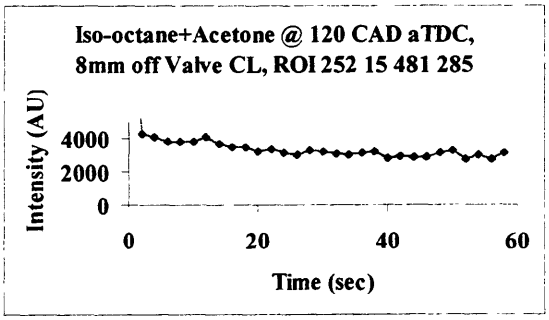

Figure 4.20 (f): Average pixel intensities with ROI (252, 15) – (481, 285), 8mm off valve centerline @ 120 CAD aTDC with iso-octane, acetone fuel mixture

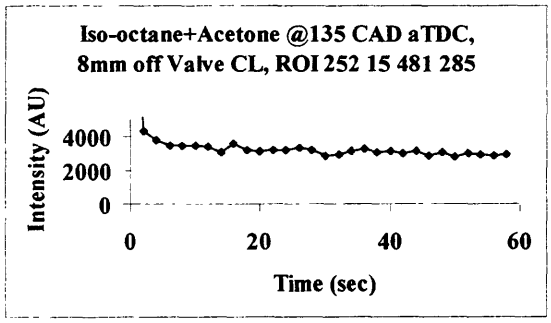

Figure 4.20 (g): Average pixel intensities with ROI (252, 15) – (481, 285), 8mm off valve centerline @ 135 CAD aTDC with iso-octane, acetone fuel mixture

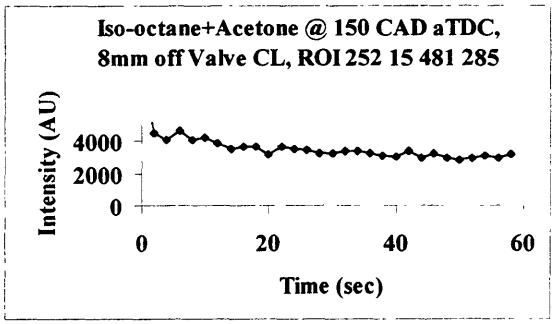

Figure 4.20 (h): Average pixel intensities with ROI (252, 15) – (481, 285), 8mm off valve centerline @ 150 CAD aTDC with iso-octane, acetone fuel mixture

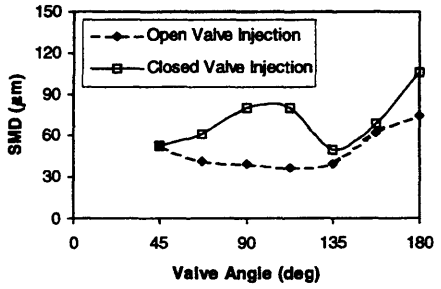

Figure 4.21 (a): Droplet diameter distribution around the valve circumference

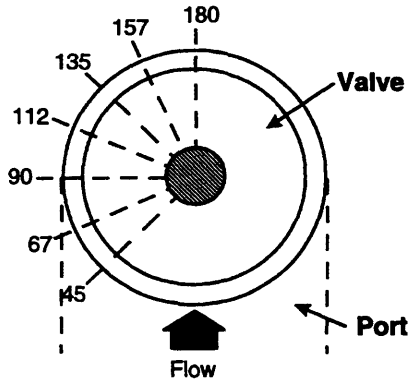

Figure 4.21 (b): Schematic of valve angles used in Figure 4.21 (a)

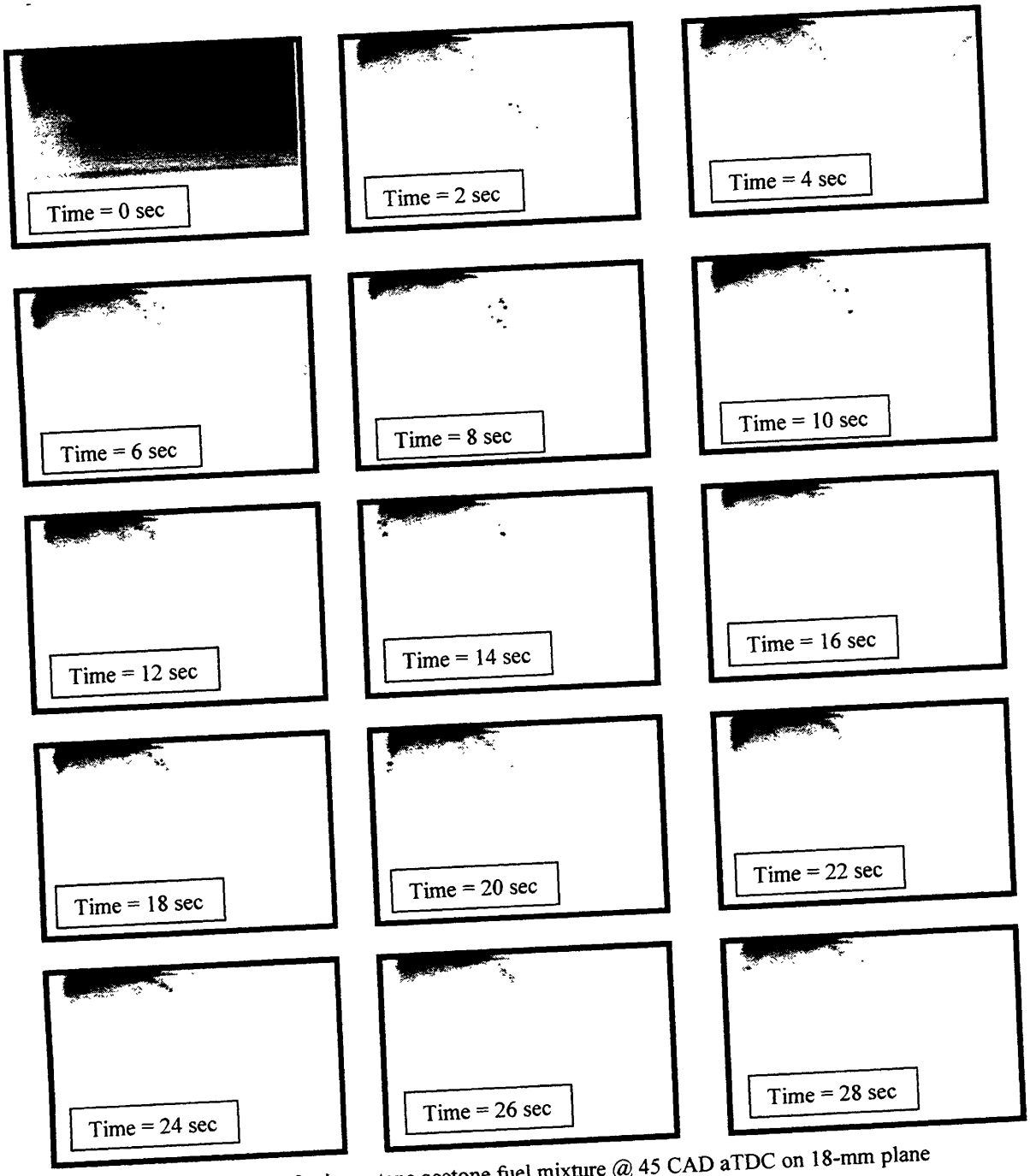

Figure 4.22: Raw images for iso-octane acetone fuel mixture @ 45 CAD aTDC on 18-mm plane

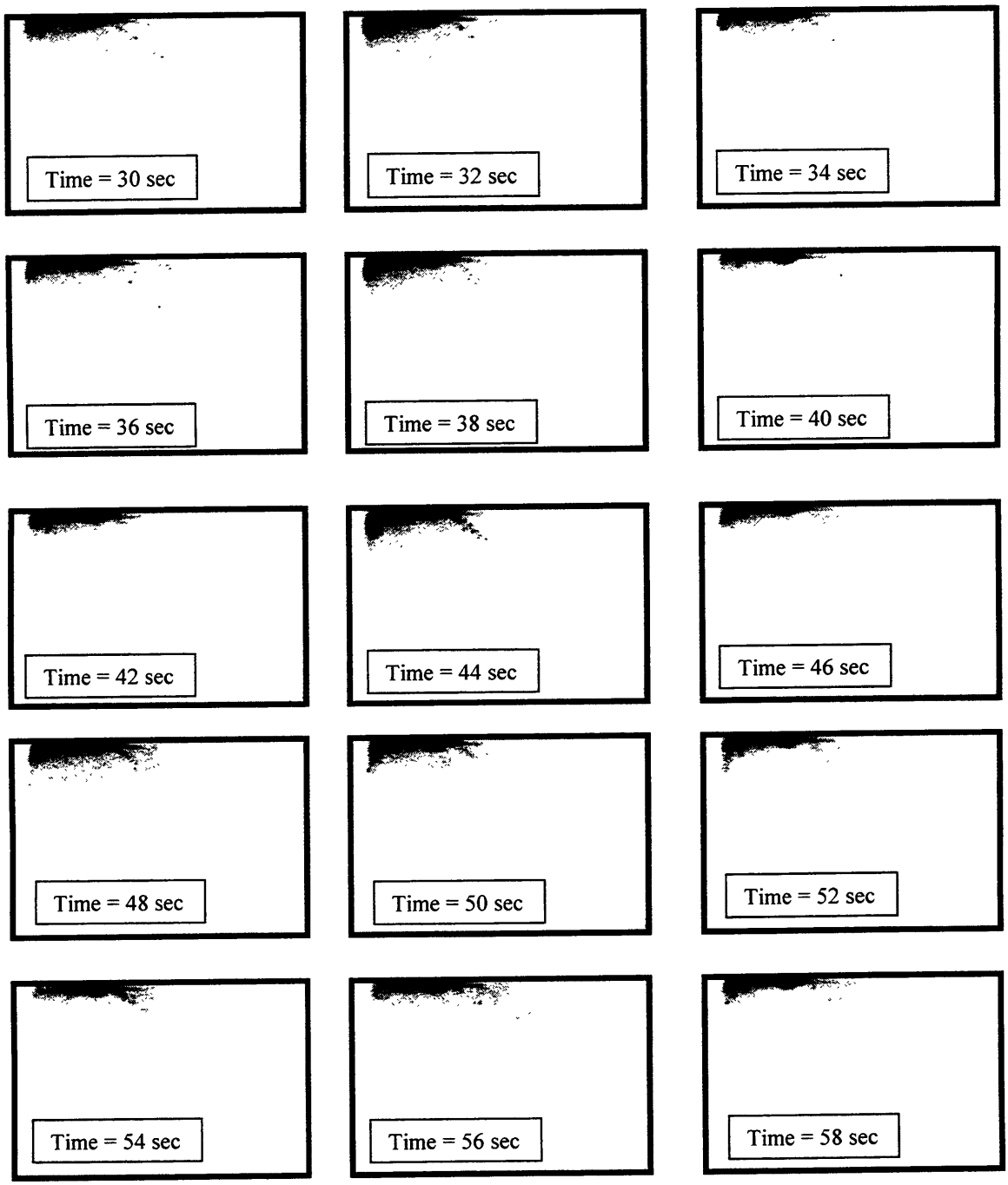

Figure 4.22 (continued): Raw images for iso-octane acetone fuel mixture @ 45 CAD aTDC on 18-mm plane

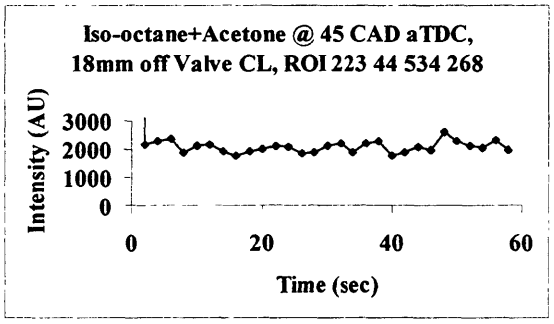

Figure 4.23 (a): Average pixel intensities with ROI (223, 44) – (534, 268), 18mm off valve centerline @ 45 CAD aTDC using iso-octane, acetone fuel mixture

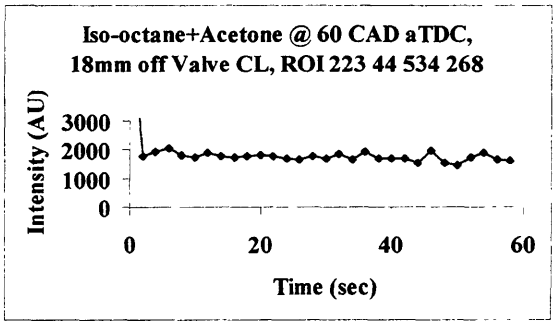

Figure 4.23 (b): Average pixel intensities with ROI (223, 44) – (534, 268), 18mm off valve centerline @ 60 CAD aTDC using iso-octane, acetone fuel mixture

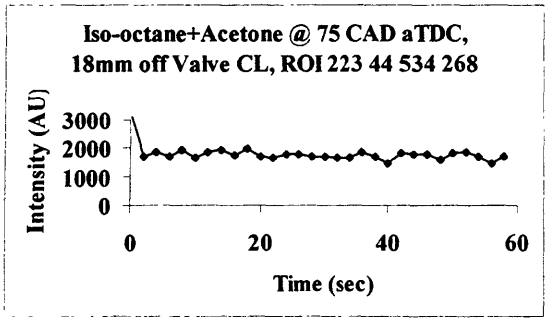

Figure 4.23 (c): Average pixel intensities with ROI (223, 44) – (534, 268), 18mm off valve centerline @ 75 CAD aTDC using iso-octane, acetone fuel mixture

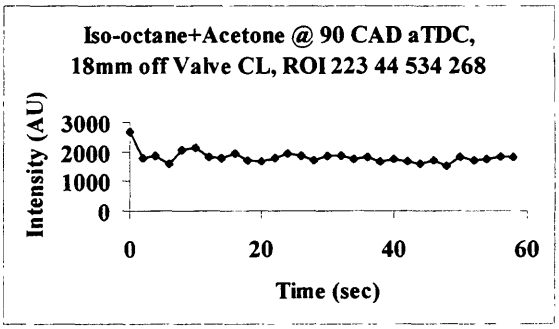

Figure 4.23 (d): Average pixel intensities with ROI (223, 44) – (534, 268), 18mm off valve centerline @ 90 CAD aTDC using iso-octane, acetone fuel mixture

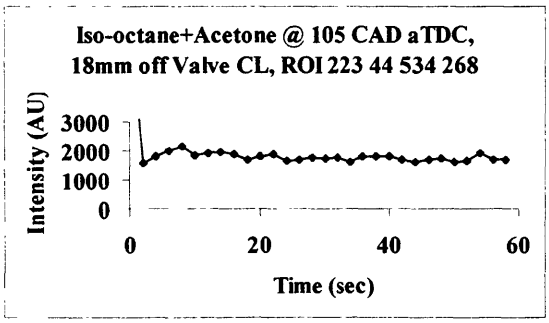

Figure 4.23 (e): Average pixel intensities with ROI (223, 44) – (534, 268), 18mm off valve Centerline @ 105 CAD aTDC using iso-octane, acetone fuel mixture

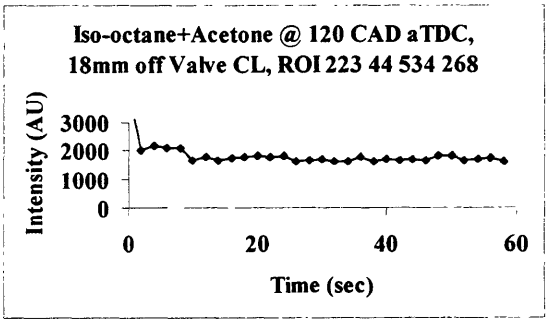

Figure 4.23 (f): Average pixel intensities with ROI (223, 44) – (534, 268), 18mm off valve centerline @ 120 CAD aTDC using iso-octane, acetone fuel mixture

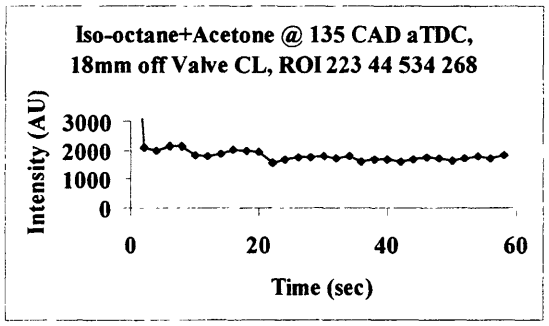

Figure 4.23 (g): Average pixel intensities with ROI (223, 44) – (534, 268), 18mm off valve centerline @ 135 CAD aTDC using iso-octane, acetone fuel mixture

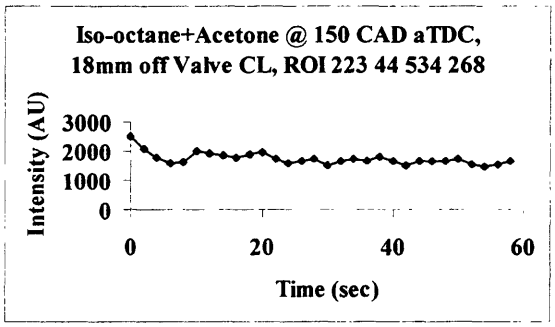

Figure 4.23 (h): Average pixel intensities with ROI (223, 44) – (534, 268), 18mm off valve centerline @ 45 CAD aTDC using iso-octane, acetone fuel mixture

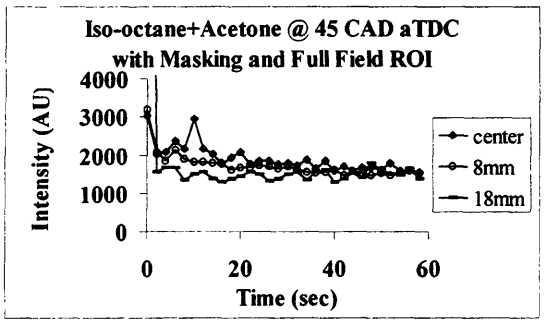

Figure 4.24 (a): Average pixel intensities with masking and full field ROI for centerline, 8-9mm and 18mm planes @ 45 CAD aTDC using iso-octane, acetone fuel mixture

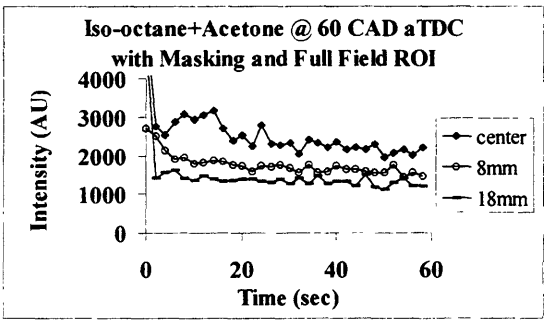

Figure 4.24 (b): Average pixel intensities with masking and full field ROI for centerline, 8-9mm and 18mm planes @ 60 CAD aTDC using iso-octane, acetone fuel mixture

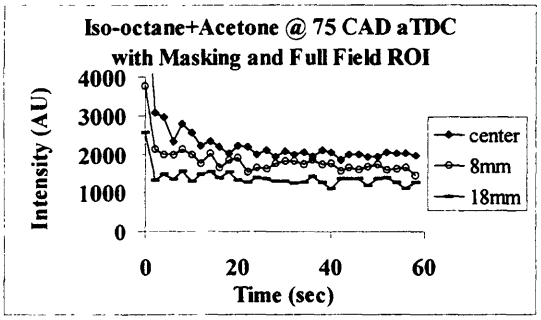

Figure 4.24 (c): Average pixel intensities with masking and full field ROI for centerline, 8-9mm and 18mm planes @ 75 CAD aTDC using iso-octane, acetone fuel mixture

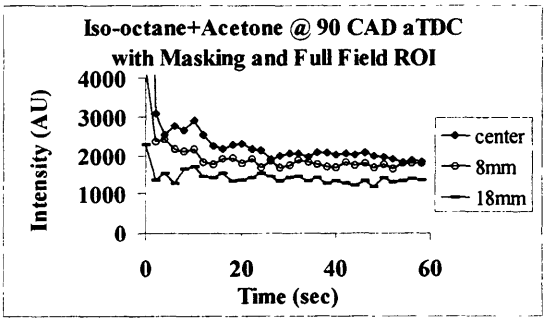

Figure 4.24 (d): Average pixel intensities with masking and full field ROI for centerline, 8-9mm and 18mm planes @ 90 CAD aTDC using iso-octane, acetone fuel mixture

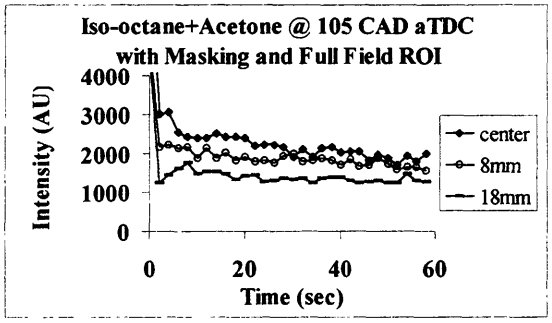

Figure 4.24 (e): Average Pixel Intensities with masking and full field ROI for centerline, 8-9mm and 18mm planes @ 105 CAD aTDC using Iso-octane, Acetone Fuel Mixture

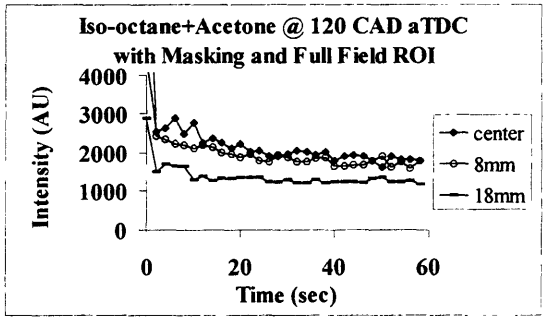

Figure 4.24 (f): Average Pixel Intensities with masking and full field ROI for centerline, 8-9mm and 18mm planes @ 120 CAD aTDC using Iso-octane, Acetone Fuel Mixture

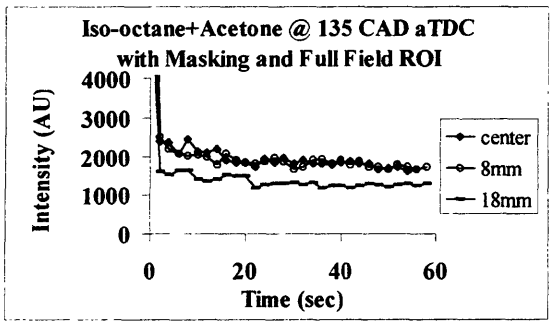

Figure 4.24 (g): Average Pixel Intensities with masking and full field ROI for centerline, 8-9mm and 18mm planes @ 135 CAD aTDC using Iso-octane, Acetone Fuel Mixture

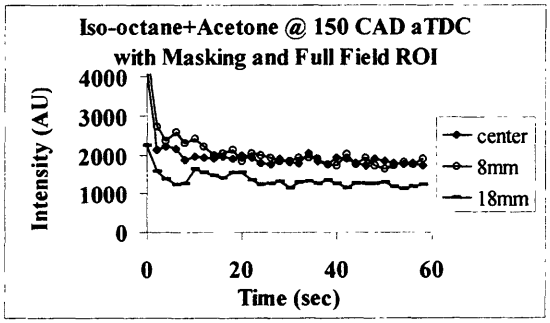

Figure 4.24 (h): Average Pixel Intensities with masking and full field ROI for centerline, 8-9mm and 18mm planes @ 150 CAD aTDC using Iso-octane, Acetone Fuel Mixture

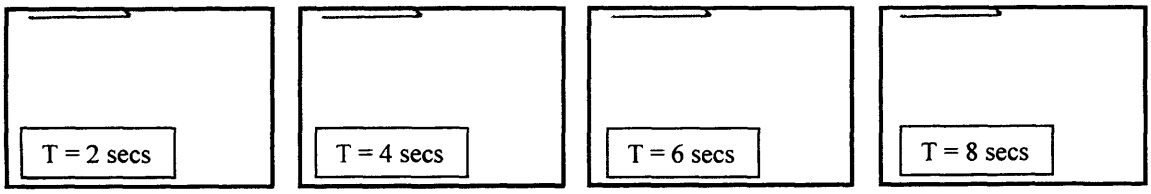

Figure 4.25 - Consecutive images on 8mm plane with iso-octane, 3-pentanone fuel mixture

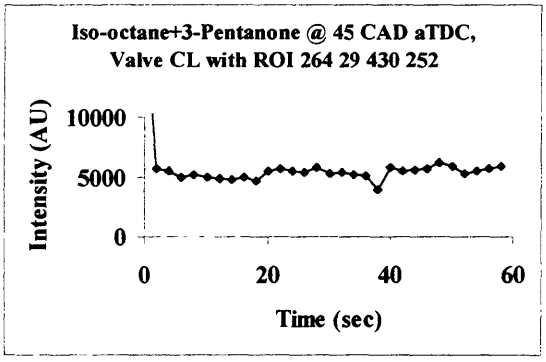

Figure 4.26 (a): Average pixel intensities with ROI (264, 29) – (430, 252) on the valve centerline @ 45 CAD aTDC using iso-octane, 3-pentanone fuel mixture

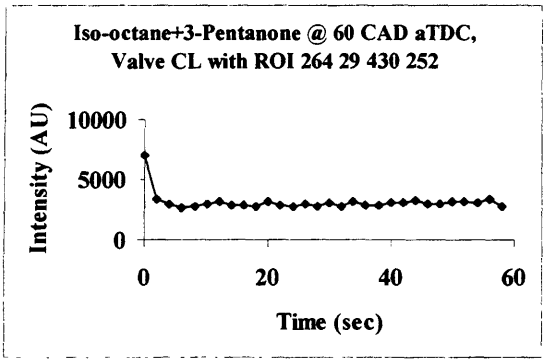

Figure 4.26 (b): Average pixel intensities with ROI (264, 29) – (430, 252) on the valve centerline @ 60 CAD aTDC using iso-octane, 3-pentanone fuel mixture

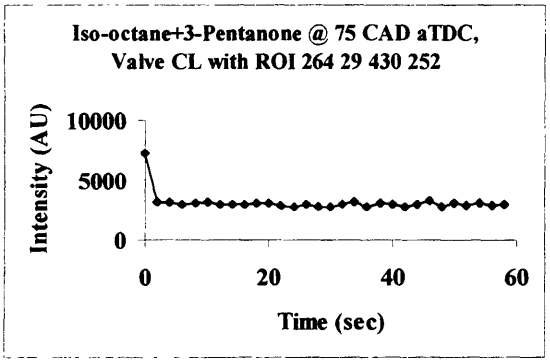

Figure 4.26 (c): Average pixel intensities with ROI (264, 29) – (430, 252) on the valve centerline @ 75 CAD aTDC using iso-octane, 3-pentanone fuel mixture

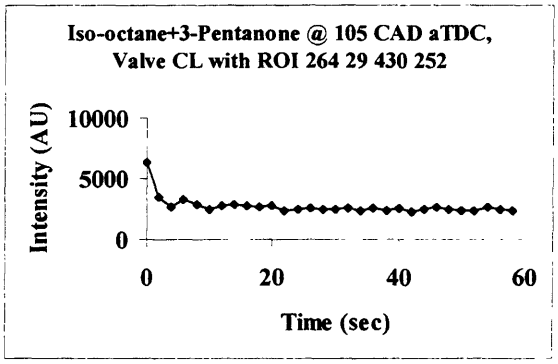

Figure 4.26 (e): Average pixel intensities with ROI (264, 29) – (430, 252) on the valve centerline @ 105 CAD aTDC using iso-octane, 3-pentanone fuel mixture

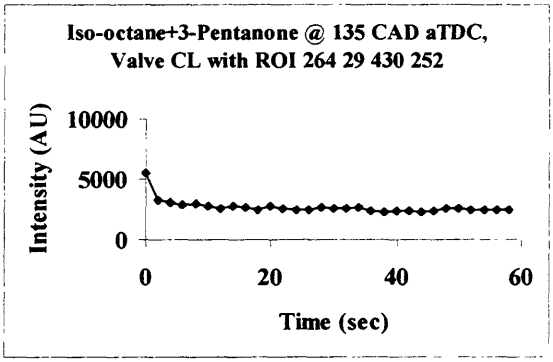

Figure 4.26 (g): Average pixel intensities with ROI (264, 29) – (430, 252) on the valve centerline @ 135 CAD aTDC using iso-octane, 3-pentanone fuel mixture

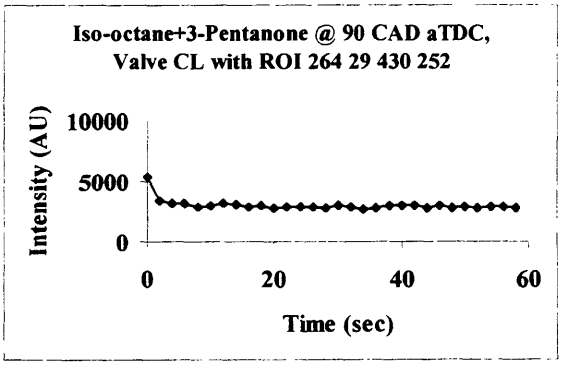

Figure 4.26 (d): Average pixel intensities with ROI (264, 29) – (430, 252) on the valve centerline @ 90 CAD aTDC using iso-octane, 3-pentanone fuel mixture

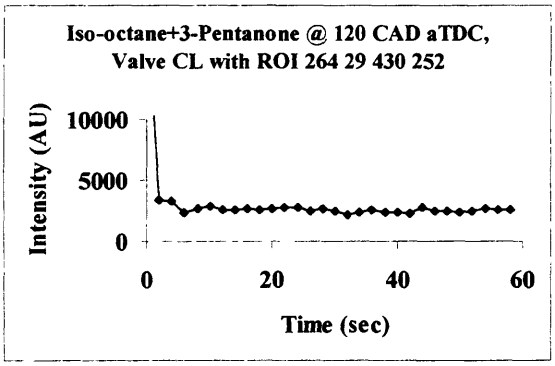

Figure 4.26(f): Average pixel intensities with ROI (264, 29) – (430, 252) on the valve centerline @ 120 CAD aTDC using iso-octane, 3-pentanone fuel mixture

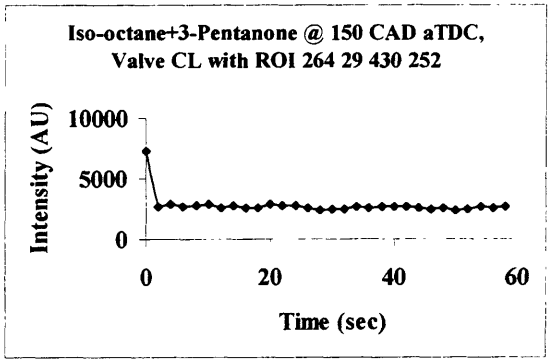

Figure 4.26 (h): Average pixel intensities with ROI (264, 29) – (430, 252) on the valve centerline @ 150 CAD aTDC using iso-octane, 3-pentanone fuel mixture

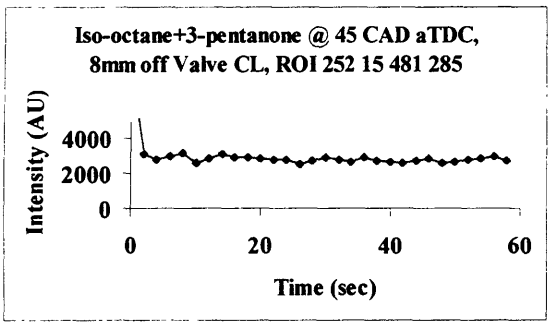

Figure 4.27 (a): Average Pixel Intensities with ROI (252, 15) – (481, 285), 8mm off Valve Centerline @ 45 CAD aTDC with Iso-octane, 3-pentanone Fuel Mixture

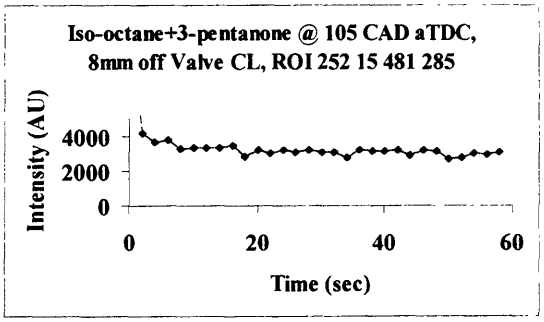

Figure 4.27 (e): Average Pixel Intensities with ROI (252, 15) – (481, 285), 8mm off Valve Centerline @ 105 CAD aTDC with Iso-octane, 3-pentanone Fuel Mixture

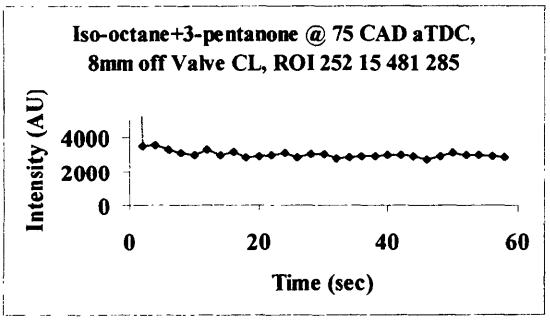

Figure 4.27 (c): Average Pixel Intensities with ROI (252, 15) – (481, 285), 8mm off Valve Centerline @ 75 CAD aTDC with Iso-octane, 3-pentanone Fuel Mixture

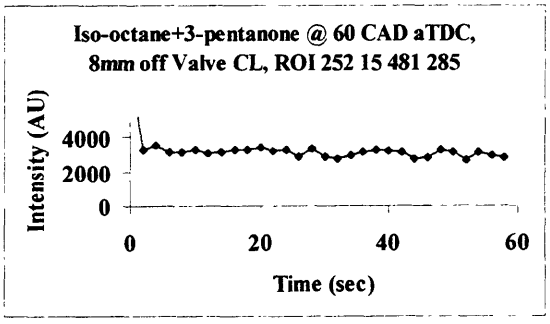

Figure 4.27 (b): Average Pixel Intensities with ROI (252, 15) – (481, 285), 8mm off Valve Centerline @ 60 CAD aTDC with Iso-octane, 3-pentanone Fuel Mixture

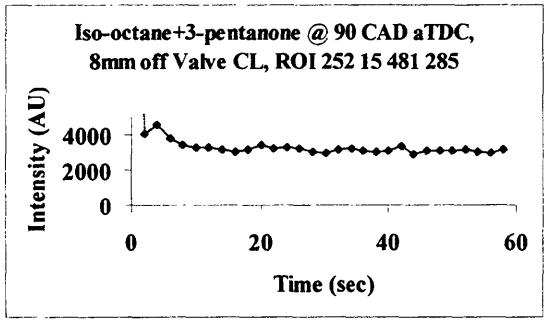

Figure 4.27 (d): Average Pixel Intensities with ROI (252, 15) – (481, 285), 8mm off Valve Centerline @ 90 CAD aTDC with Iso-octane, 3-pentanone Fuel Mixture

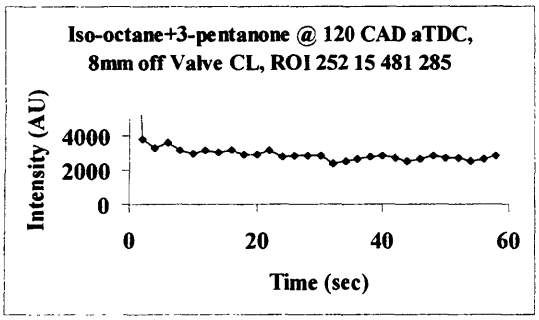

Figure 4.27 (f): Average Pixel Intensities with ROI (252, 15) – (481, 285), 8mm off Valve Centerline @ 120 CAD aTDC with Iso-octane, 3-pentanone Fuel Mixture

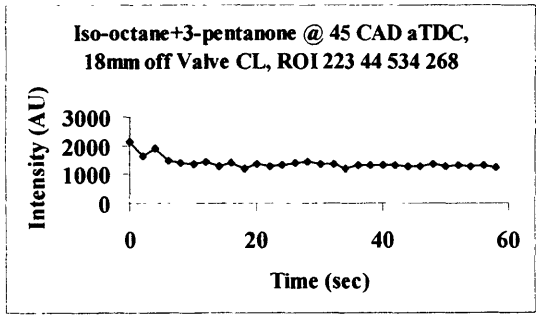

Figure 4.28 (a): Average Pixel Intensities with ROI (223, 44) – (534, 268), 18mm off Valve Centerline @ 45 CAD aTDC using Iso-octane, 3-pentanone Fuel Mixture

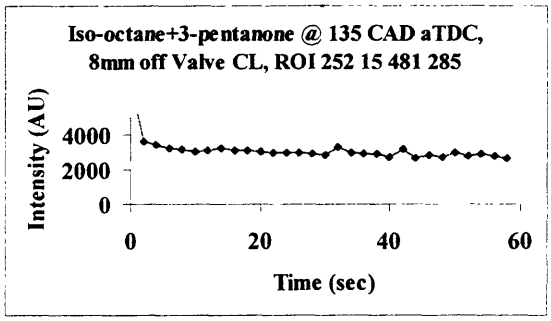

Figure 4.27 (g): Average Pixel Intensities with ROI (252, 15) – (481, 285), 8mm off Valve Centerline @ 135 CAD aTDC with Iso-octane, 3-pentanone Fuel Mixture

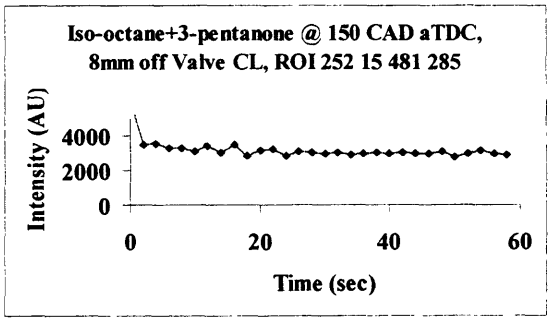

Figure 4.27 (h): Average Pixel Intensities with ROI (252, 15) – (481, 285), 8mm off Valve Centerline @ 150 CAD aTDC with Iso-octane, 3-pentanone Fuel Mixture

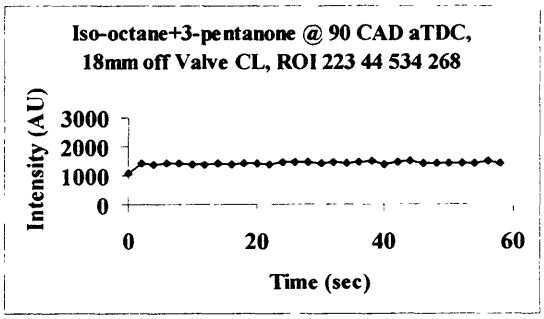

Figure 4.28 (c): Average Pixel Intensities with ROI (223, 44) – (534, 268), 18mm off Valve Centerline @ 90 CAD aTDC using Iso-octane, 3-pentanone Fuel Mixture

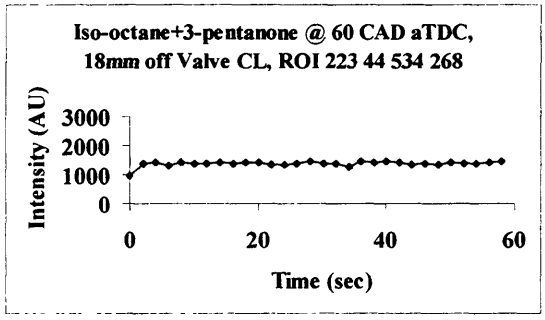

Figure 4.28 (b): Average Pixel Intensities with ROI (223, 44) – (534, 268), 18mm off Valve Centerline @ 60 CAD aTDC using Iso-octane, 3-pentanone Fuel Mixture

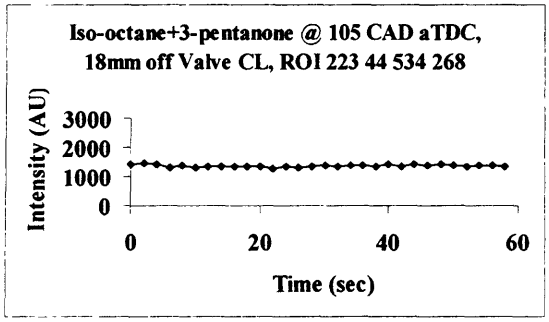

Figure 4.28 (d): Average Pixel Intensities with ROI (223, 44) – (534, 268), 18mm off Valve Centerline @ 105 CAD aTDC using Iso-octane, 3-pentanone Fuel Mixture

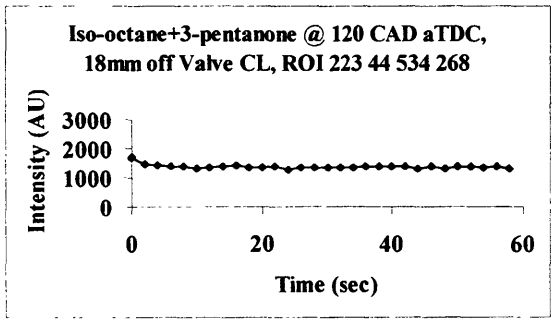

Figure 4.28 (e): Average Pixel Intensities with ROI (223, 44) – (534, 268), 18mm off Valve Centerline @ 120 CAD aTDC using Iso-octane, 3-pentanone Fuel Mixture

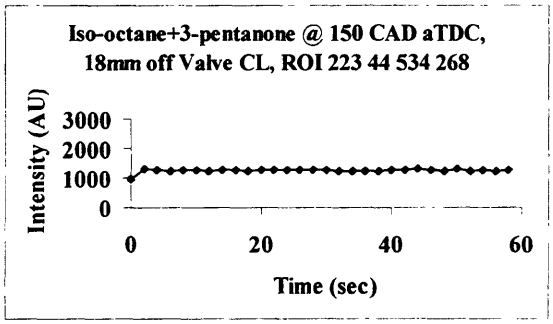

Figure 4.28 (g): Average Pixel Intensities with ROI (223, 44) – (534, 268), 18mm off Valve Centerline @ 135 CAD aTDC using Iso-octane, 3-pentanone Fuel Mixture

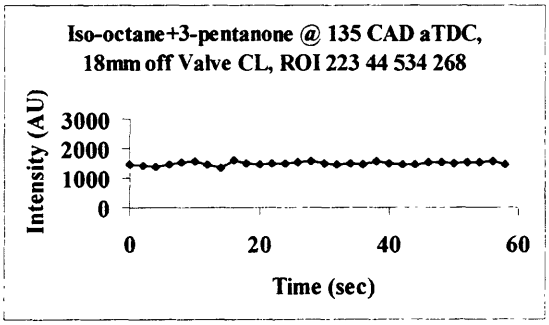

Figure 4.28 (f): Average Pixel Intensities with ROI (223, 44) – (534, 268), 18mm off Valve Centerline @ 135 CAD aTDC using Iso-octane, 3-pentanone Fuel Mixture

5 EXPERIMENTAL RESULTS – ANALYSIS OF SPATIAL BEHAVIOR

In this chapter the development of liquid fuel in the cylinder on a CA basis is analyzed and the images are related to engine events of maximum piston speed and max valve lift. To analyze the acquired images on a CA basis it is necessary to eliminate the effect of any cyclic variations. Although this eliminates the ability of discerning variations due to transients associated with cold start, the procedure allows identification of the average fuel distribution. This is achieved through the averaging of a set of thirty images taken at a single CA position. This procedure has been automated through the use of the second Winview® macro, described in Appendix 1. The procedure involved in averaging the images was discussed in Chapter 3.

5.1 Centerline Plane

Figure 5.1 shows single-shot pictures of indolene fuel as a function of CAD. The fuel is first seen at approximately 45 CA degrees aTDC intake, where the valve gap area is small and the fuel is coming from both the valve seat and the cylinder head. As the valve gap widens, a spray develops from the head side, with little or no fuel coming from the valve seat. At the time close to maximum valve lift, 105 CA aTDC, liquid fuel emerges from the valve seat. This can be seen more clearly using averaged images. Thirty images, corresponding to 0 through 60 seconds after start of injection, were averaged over the starting period at each CA position, and the resulting images used to relate development to engine events.

Figure 5.2 shows averaged images for the centerline plane related to piston speed and valve lift. Examination of these images shows the origin of the liquid fuel entering the cylinder. At 45 CAD aTDC, when the valve gap is small, the fuel is stripped from both the valve back and from the cylinder head. At 60 CA degrees aTDC the majority of the fuel comes from the port wall. This is also the case for the 75, 90, 120, 135 and 150 CA degree positions. However, at the 105 CA degree position a significant amount of liquid fuel comes also from the back of the intake valve. At this position in the intake stroke the valve is almost all the way open. A possible reason for the appearance of the additional fuel at this time is the effect of inertia of the fuel as the valve reaches maximum valve lift and decelerates. At the same point the piston has just passed its point of maximum speed, which means the speed of the air in the intake, port is close to its maximum as well. This results in enhanced strip atomization of any liquid fuel in the vicinity of the edge of the intake valve.

5.2 8 mm Plane

Figure 5.3 shows overlaid images for the plane 8-9 mm off the valve centerline. It is harder to interpret the source of the fuel in theses images than in the centerline case. The reason for this is that there is an overlap of the two fuel streams, i.e. the stream coming from the valve seat on the intake port appears to be partially

in front of the stream coming from the back of the intake valve. However, it is still possible to discern slightly more fuel coming from the valve back in the 105 CAD aTDC case than in the other CA positions.

5.3 18 mm Plane

Figure 5.4 shows overlaid images for the plane 18-mm off the valve centerline. In this case there is no clear source of the fuel. This is most probably due to the fact that the laser is not cutting the stream in a plane normal to the direction of flow, as was the case in the centerline. This results in more overlap in the images, with any fuel coming from the port wall positioned almost completely in front of the stream coming off the back of the intake valve, making it harder to interpret.

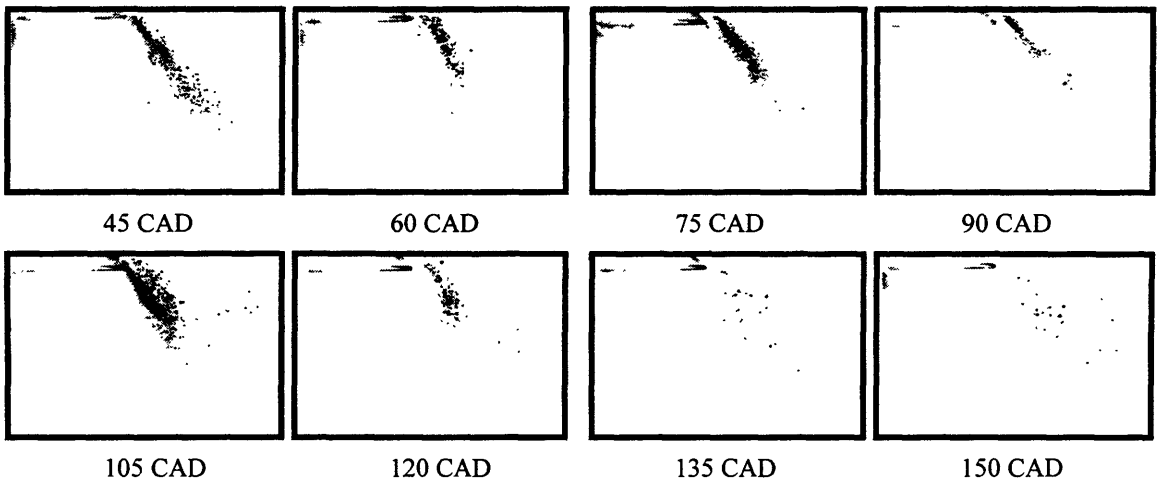

Figure 5.1: Single shot images of indolene as a function of crank angle (Images shown without background subtraction or masking)

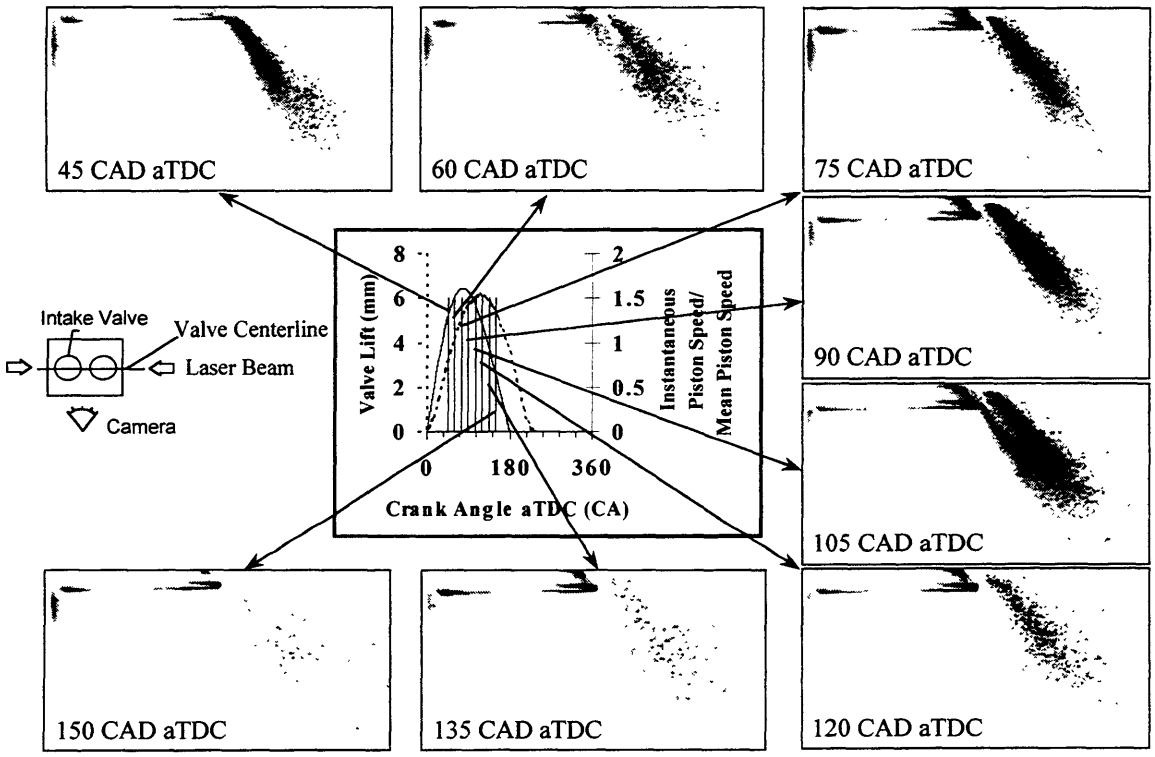

Figure 5.2: Averaged Images for the centerline plane related to valve lift and piston speed

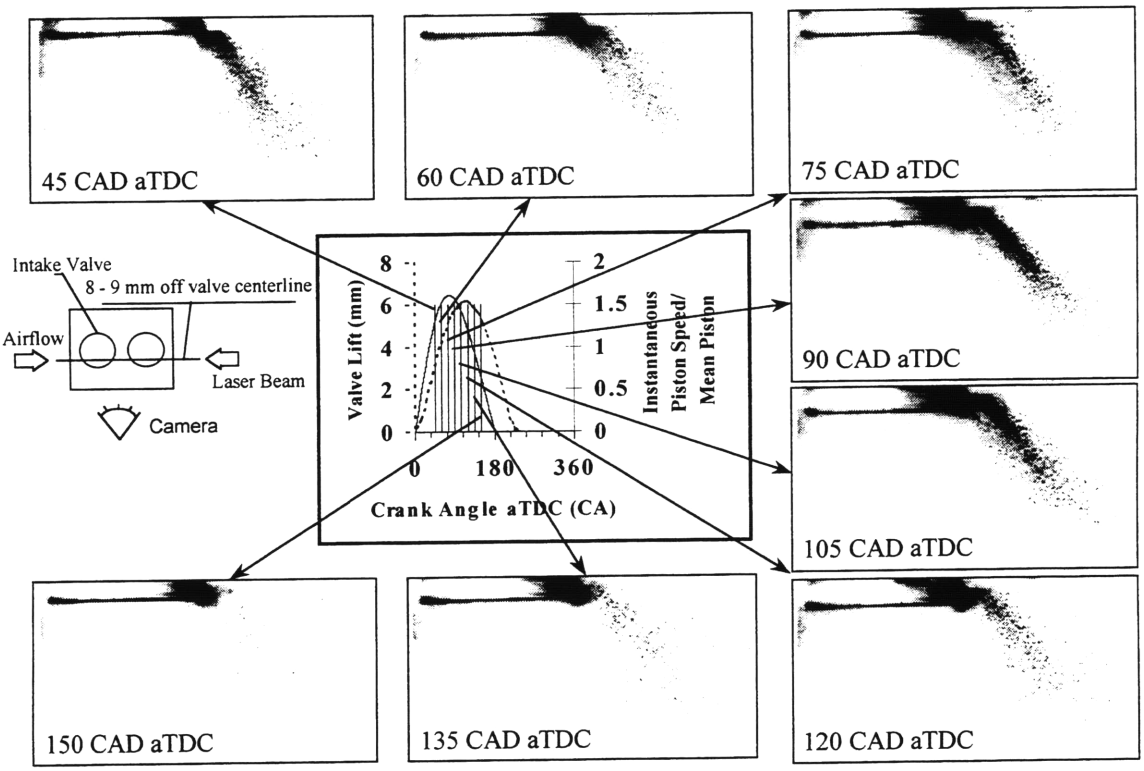

Figure 5.3: Averaged Images for the plane 8-9 mm off the valve centerline related to valve lift and piston speed

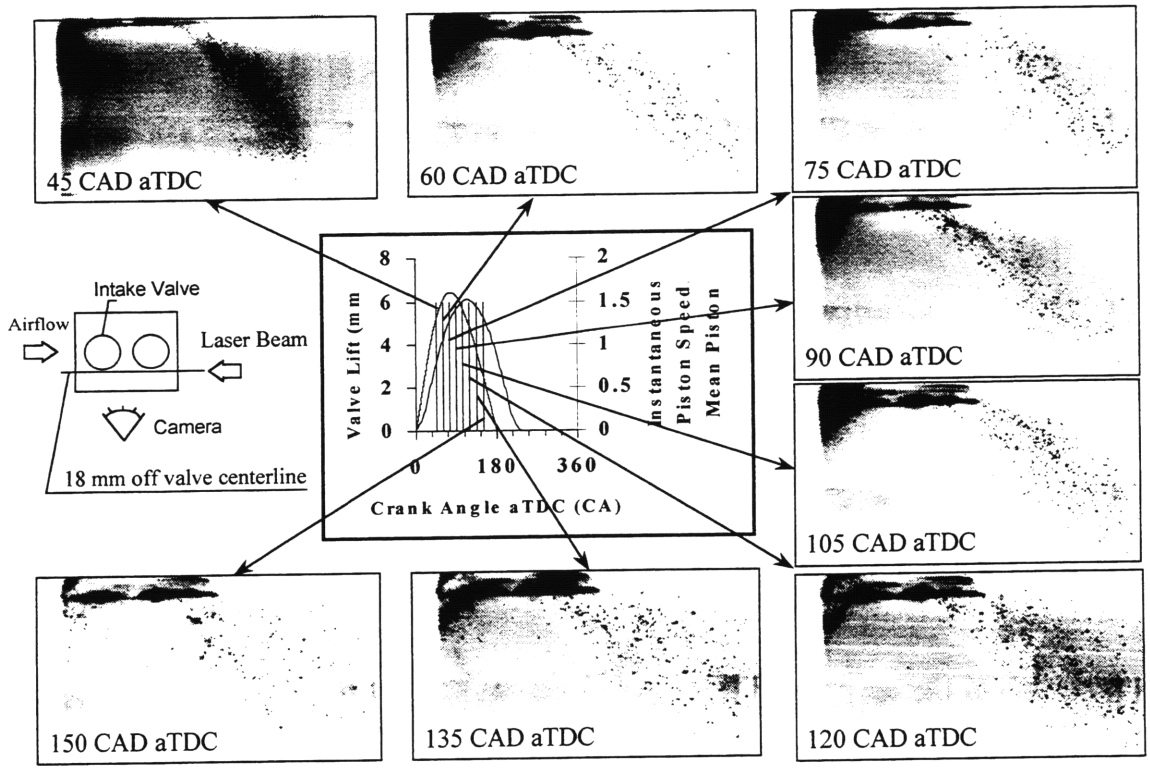

Figure 5.4: Averaged Images for the plane 18 mm off the valve centerline related to valve lift and piston speed

6 CONCLUSIONS AND SUMMARY

This project used a laser induced fluorescence installation to examine the liquid fuel present in the cylinder of a firing port-fuel injected spark ignition engine. Volatility effects were investigated through the use of three different fuel/fuel dopant mixtures; indolene, to represent the low volatility compounds present in indolene, iso-octane/acetone to represent the high volatility components of indolene, and iso-octane/3-pentanone to represent the medium range compounds present in indolene. These mixtures were investigated on three different planes through the cylinder; on a plane through the centerline of the intake valve, a plane offset 8 mm from the centerline of the valve, and a plane offset 18 mm from the centerline of the valve. The different combinations of fuels and planes were analyzed on both a temporal and spatial basis.

Images were collected every two seconds for the first sixty seconds of the warm-up period, at various different crank angle positions. A closed valve injection strategy was used with the injector aimed such that the majority of the fuel landed on the back of the intake valve. The results from these studies are summarized below.

Results for indolene show three peaks in liquid fuel quantity present in the cylinder. These correspond to:

1. An initial peak in the first cycle of operation, caused by the six times stoichiometric enrichment strategy used on the first injected cycle.
2. A second peak at anywhere from 12- to 20-seconds, corresponding to the period of maximum liquid fuel inflow into the cylinder.
3. A final peak occurring at approximately 40-second. This peak coincides with the peak in the mass of liquid fuel present in the intake port as documented by other investigators.

The results for the iso-octane/acetone mixture reach steady state much quicker and show a significantly less pronounced peak at 40-seconds than in the case of indolene. Both volatility differences and the distribution of droplets entering the cylinder around the intake valve explain this difference.

When comparing the relative intensity values of the different planes for each fuel/fuel dopant mixture it is seen that for indolene, the centerline plane has the lowest concentration, and the 18-mm plane has the highest concentration. In the case of the iso-octane, acetone fuel mixture this trend is reversed, with the highest intensity occurring in the centerline plane, and the lowest intensity occurring in the 18-mm plane. This effect can be attributed to a combination of factors. In the case of the centerline plane there is a shadowing effect by the valve stem which acts to reduce the amount of liquid fuel present in this plane. Accentuating this effect is the fact that the smaller droplets on the 18 mm plane will have a higher concentration of the fluorescing, low volatility components, leading to a higher fluorescent signal, and hence the interpretation that there is more liquid fuel present on the 18 mm plane. This uncertainty in the

concentration of the fluorescing compounds in the droplets makes it very difficult to quantify LIF signals or even to compare them on a relative basis. The reversal in the order of planes for the iso-octane/acetone fuel mixture is explained by the fact that the concentration of the high volatility, fluorescing, acetone is most likely lower in the smaller droplets of the 18 mm plane.

The spatial development of liquid fuel in the cylinder shows where the liquid fuel originates from for the different crank angle positions analyzed. At the position closest to maximum valve lift and maximum piston speed there is significantly more liquid fuel originating from the valve back than in any other crank angle position. At this crank angle the airflow past the valve will be close to its maximum, since air velocity scales well with piston speed. The liquid fuel is at the edge of the intake valve, due to its own inertia and the fact that the valve is decelerating to a stop. These combined effects result in more liquid fuel being stripped off the back of the intake valve at this position compared with the other positions.

Laser induced fluorescence is a valuable technique for analysis of the mechanisms by which fuel enters the cylinder, but one must be careful in making any quantitative inferences from the fluorescence signal. The technique is restricted by the uncertainty in the concentration of fluorescing compounds in evaporating droplets and by cyclic variability. Considerably more work has to be performed on issues regarding signal calibration before the technique can be reliably used for quantitative analysis.

References

1. Cheng, W.K., Hamrin, D., Heywood, J.B., Hochgreb, S. Min, K.D., and Norris, M., "An Overview of Hydrocarbon Emissions Mechanisms in Spark-Ignition Engines", *SAE Transactions*, v. 102, p.1207-1220 (1993).
2. Hochgreb, S., "Combustion-Related Emissions in SI Engines," Chapter 6, pp. 118-170, in Handbook of Air Pollution from Internal Combustion Engines, edited by Sher, E., Academic Press, (1998)
3. Takeda, K., Yaegashi, T., Sekiguchi, K., Saito, K., an Imatake, N., "Mixture Preparation and HC Emissions of a 4-Valve Engine with Port Fuel Injection During Cold Starting and Warm-up", *SAE Paper* 950074 (1995)
4. Schurov, S. M. and Collings, N., "An Experimental Investigation of Fuel Transport in a Port Injected Engine", *SAE Paper* 952485 (1995)
5. Fujikawa, T., Hattori, Y., Akihama, K., "Quantitative 2-D Fuel Distribution Measurements in an SI Engine Using Laser-Induced Fluorescence with Suitable Combination of Fluorescence Tracer and Excitation Wavelength", *SAE Paper* 972944, (1997)
6. Johnen, T. and Haug, M., "Spray Formation Observation and Fuel Film Development Measurements in the Intake of a Spark Ignition Engine", *SAE Paper* 950511, (1995).
7. Felton, P.G., Kyritsis, D.C., and Fulcher, S.K., "LIF Visualization of Liquid Fuel in the Intake Manifold During Cold Start", *SAE Paper* 952464, (1995).
8. Knapp, M., Luczak, A., Beushausen, V., Hentschel, W., and Andresen, P., "Vapor/Liquid Visualization with Laser-Induced Exciplex Fluorescence in an SI-Engine for Different Fuel Injection Timings", *SAE Paper* 961122, (1996).
9. Witze, P.O. and Green, R.M., "LIF and Flame-Emission Imaging of Liquid Fuel Films and Pool Fires in an SI Engine During a Simulated Cold Start", *SAE Paper* 970866, (1997)
10. Kelly-Zion, P.L., Styron, J.P., Lee, C.-F., Lucht, R.P., Peters, J.E., and White, R.A., "In-Cylinder Measurements of Liquid Fuel During the Intake Stroke of a port-Injected Spark Ignition Engine", *SAE Paper* 972945, (1997).
11. Schuenemann, Muench and Leipertz "Interaction of Airflow and Injected Fuel Spray Inside the Intake Port of a Six Cylinder Four Valve SI Engine", *SAE Paper* 972984 (1997)
12. Posylkin, M., Taylor, A.M.K.P., Vannobel, F., and Whitelaw, J.H., "Fuel Droplets Inside a Firing Spark-Ignition Engine", *SAE Paper* 941989, (1994).
13. Cousyn, B., Posylkin, M., Vannobel, F., and Whitelaw, J.H., "Droplet Characteristics in Two Cylinders of a Firing Spark Ignition Engine", *SAE Paper* 952466, (1995).
14. Hardalupas, Y., Taylor, A.M.K.P., Whitelaw, J.H., Ishii, K., Miyano, H., and Urata, Y., "Influence of Injection Timing on In-Cylinder Fuel Distribution in a Honda VTEC-E Engine", *SAE Paper* 950507, (1995).

15. Meyer, R., Yilmaz, E., Heywood, J.B., "Liquid Fuel Flow Phenomena in the Vicinity of the Intake Valve of a Firing Port Injected SI Engine", submitted to the SAE Fuels and Lubricants Conference, 1998.
16. Meyer, R., Heywood, J.B., Liquid Fuel Transport Mechanisms into the Cylinder of a Firing Port-Injected SI Engine During Start Up", *SAE Paper* 970865, (1997).
17. Whelan, D.E., Kelly-Zion, P.L., Lee, C.F., Peters, J.E., White, R.A., "Back-Flow Atomization in the Intake Port of Spark Ignition Engines", *SAE Paper* 972988, 1997
18. Eckbreth, A.C., Laser Diagnostics for Combustion Temperature and Species, Abacus Press, 1988.
19. Namazian, M., Hansen, S., Lyford-Pike, E., Sanchez-Brasse, J., Heywood, J.B., and Rife, J., "Schlieren Visualization of the Flow and Density Fields in the Cylinder of a Spark-Ignition Engine", *SAE Paper* 800044, (1980).
20. Shelby M., VanDerWege, B., Hochgreb, S., "Early Spray Development in Gasoline Direct-Injected Spark Ignition Engines", *SAE Paper* 980160, (1998).
21. Le Coz, J.F., Catalano, C., Baritaud, T., "Application of laser induced fluorescence for measuring the thickness of liquid films on transparent walls", Proc. 7th Int. Symposium on Applications of Laser Techniques to Fluid Dynamics, Adrian, R.J. (editor), Lisbon (1994) 29.3.1 –29.3.8
22. Hansen, D., Lee, E., "Radiative and Nonradiative transitions in the First Excited Singlet State of Symmetrical Methyl-substituted acetones", *The Journal of Chemical Physics*, Vol. 62, No. 1 (1975)
23. Witze and Green
24. Thomas G. B., and Finney, R. L., Calculus and Analytic Geometry, Addison Wesley 1992.

APPENDIX 1

Macro basic, the macro language associated with the Winview software, is an interpretive language which can be used to automate tasks in data acquisition and data processing. The language is modeled after the standard language "Basic", but has been changed to suit the needs of most Winview users. The biggest change is that the language supports operations on arrays as an elemental data type. For the purposes of this work two macros have been written and are described briefly here:

A2.1 Intensity Calculation Macro Description:

This macro, named "intenscal.cmd" automates the task of performing the winview statistics command for each frame in an image file and will even analyze multiple frames. The inputs and outputs for the file are explained in the initial comments of the program itself, which is included in the next few pages.

A2.2 Overlay Macro Description:

The second macro, called "overlay.cmd" automates the task of overlaying the frames of an image file. This macro will also take multiple files as inputs and for each one will add the intensity values at each pixel position for all of the frames in the image file and output the resulting frame to a single frame file. Again the inputs and outputs are described in detail in the text of the program, which is also included.

The biggest problem encountered while using Macro Basic was understanding the significance of the Mathpointer variables. In nearly all programs associated with macro basic the functions DOWNLOADMATHOPERATION, DOWNLOADMATHARG, DOWNLOADMATHRESULT and RUNMATH are used. These functions are all associated with a mathpointer variable. The mathpointer is assigned a function using the DOWNLOADMATHOPERATION command, for example

```
Mathpointer Math
```

```
let Math = DOWNLOADMATHOPERATION( 1, 2, 0 )
```

The first of these two lines declares a variable called "Math" as type "Mathpointer". The second line assigns it an operation indicated by the first parameter in the argument of the DOWNLOADMATHOPERATION command, in this case a "1", which stands for addition, i.e. Math is an addition operation. Unfortunately the Macro Basic manual does not contain a list of the assignments associated with this parameter. However, by recording a macro and performing the tasks to be automated, the required value for the parameter can be determined.

The next stage is to associate arguments with the Math operation. The DOWNLOADMATHARG command does this. For example

```
let tmp = DOWNLOADMATHARG( Math, 1, "c:\winview\data\moon.spe", 1, 1,
                                                    1, 1, 384, 1, 1, 576, 0 )
let tmp = DOWNLOADMATHARG( Math, 2, "c:\winview\data\moon.spe", 2, 2,
                                                    1, 1, 384, 1, 1, 576, 0 )
```

These two lines assign two arguments to the mathpointer indicated by parameter one. Parameter two denotes the number argument being defined. Parameter three the file which contains the desired argument. Parameters four and five are the start and stop frames which the argument will consist of. The remainder of the parameters are do not usually change much and their meaning is explained well enough in the manual.

The third stage of this process is to define an output file which will hold the resultant image. This is done using the DOWNLOADMATHRESULT command.

```
let tmp = DOWNLOADMATHRESULT( Math, c:\winview\data\result.spe", 1,
                                                    1, 1, 1, 384, 1, 1, 576, 1, 0, 2 )
```

This second parameter assigns an output file for the mathoperation defined in the first parameter. The third and fourth parameters are the start and end frames for the output file. Again the remainder of the parameters are not varied much, with the exception of the last parameter which defines whether or not the result file should be overwritten (parameter is set to 2), appended to (parameter is set to 3), created as temporary (parameter is set to 1), incremented (parameter is set to 4) or prompted for (parameter is set to 5).

A2.3 Intensity Macro Code

```
rem             ********* MACRO OBJECTIVE **********

rem     The purpose of the macro is to take a list of files to be processed and
rem     their corresponding background files as input and to write out the

rem     total and average intensity values of a user defined region of interest
rem     (ROI) to user named files.


rem             ********* MACRO INPUTS *********

rem     This macro is takes as input a text file which holds a list of names of rem     data files to be
processed followed by the name of the file containing
rem     a background image for this data file. The layout of this text file is
rem     as follows, where the first line is the number of data files to be
rem     processed:


rem       2

rem       c:\winview\macro\datafile.spe c:\winview\macro\bckgrnd.spe
rem       c:\windows\users\joe\datafle2.spe c:\windows\users\joe\bckgrnd2.spe


rem     As well as this text file the macro requires one other text file as
rem     input. This second file should hold the coordinates of the rectangular
rem     region of interest to be analyzed. The coordinates should be of the

rem     form x1 y1 x2 y2 as shown below


rem       1 1 576 384

rem     The user will be prompted for these text files whenever the macro is
rem     run



rem             ********* MACRO OUTPUTS *********



rem     There will also be a space in the prompt box to input the names of the
rem     files which will hold the results of the processing . Here two file
rem     names will be required, one to hold the information on average
rem     intensity values integrated over the region of interest after
rem     background subtraction. The second output file will hold the
rem     information on total intensity values integrated over the region of
rem     interest after background subtraction. The output will be in a separate
rem     column for each file processed. Columns are separated by spaces. There
```

```
rem     will be thirty rows*



rem     * Authors Note: This file is designed to work with image files
rem       containing thirty frames, this may be changed by changing the value
rem       of numofframes on line 113



rem Author: Mark Dawson
rem Sloan Automotive Lab
rem MIT
rem December 20 1997
rem Variable Declaration

let VALID = 1  rem ROI set to valid
let INVALID = -1 rem ROI set to invalid
let FOINPUTFNUM = 6
let TOTINTRESULTFILENUM = 5    rem ROI result file handle
let AVGINTRESULTFILENUM = 4    rem ROI result file handle
let ROIFILENUM = 3     rem ROI template file handle
let RECTANGLE = 1   rem rectangle is 1
let fillflag = 0      rem if set to 1, this flag will fill roi with constant.

MATHPOINTER Math

FLOAT StdDev, AveInt, TotalInt, MinIntensity, MaxIntensity
FLOAT TotalPixels, CenterMassX, CenterMassY
LONG x1, y1, x2, y2, MinLocX, MinLocY, MaxLocX, MaxLocY
INT roiX1, roiY1, roiX2, roiY2, subX1, subX2, subY1, subY2

int roidata(1, 4)       rem array to hold data on region of interest
int subdata(1, 4)

string avgresultfile     rem name of file to which results are to be written
let avgresultfile = "c:\user\mark\avgint"

string totresultfile     rem name of file to which results are to be written
let totresultfile = "c:\user\mark\totint"

string roifile    rem name of file containing information on region of interest
let roifile = "c:\winview\Roidata"

string fileofinputfiles   rem name of text file containing names of files to be
                    rem processed

let fileofinputfiles = "c:\winview\inputint"

input " Enter Average Intensity Result file name ", avgresultfile,
" Enter Total Intensity Result file name ", totresultfile,
" Enter Template file name ", roifile,
```

```
" Enter the name of the file containing input file names ", fileofinputfiles

open roifile for user text input as ROIFILENUM     rem -- v2.05 or up
open fileofinputfiles for user text input as FOINPUTFNUM

read ROIFILENUM, roidata(1, 1), roidata(1, 2), roidata(1, 3), roidata(1, 4)

let roiY1 = roidata(1, 2)
let roiY2 = roidata(1, 4)
let roiX1 = roidata(1, 1)
let roiX2 = roidata(1, 3)

int numoffiles        rem number of input files
int cntoffiles        rem counter for input files
int numoffframes      rem number of frames per file
int cntoffframes      rem counter for frames
string filename       rem name of file being processed
string bckgrndname    rem name of background file for file being processed
float avgbckint       rem Average intensity of background file
float totbckint       rem Total intensity of background

read FOINPUTFNUM, numoffiles
let numoffframes = 30
float AVGINT(numoffiles, numoffframes)
float TOTINT(numoffiles, numoffframes)
float AVGINTTEMP(numoffiles, 1)
float TOTINTTEMP(numoffiles, 1)

open avgresultfile for user text output as AVGINTRESULTFILENUM
open totresultfile for user text output as TOTINTRESULTFILENUM
let tmp = CLEARPRINTWINDOW
let cntoffiles = 0

rem *****                                    *****
rem *****   MAIN LOOP FOR PROCESSING FILES AUTOMATICALLY   *****
rem *****                                    *****

while cntoffiles < numoffiles

   let cntoffiles = cntoffiles + 1

   read FOINPUTFNUM, filename, bckgrndname

   print "processing file ", cntoffiles, 1
   print cntoffiles
   print " of "
   print numoffiles
   read ROIFILENUM, subdata(1, 1), subdata(1, 2), subdata(1, 3), subdata(1, 4)
   let subX1 = subdata(1, 1)
   let subY1 = subdata(1, 2)
   let subX2 = subdata(1, 3)
   let subY2 = subdata(1, 4)
   let Math = DOWNLOADMATHOPERATION(
              56,  rem math operator --> ROI RECT
              2,  rem ID -- DO NOT MODIFY
```

```
            0 ) rem Constant Value

let tmp = DOWNLOADMATHARG(
            Math,
            1, rem Math Argument 1
            bckgrndname, rem Input Image
            1, rem Start Frame
            2, rem End Frame
            1, rem Skip Frame
            roiY1, rem Start Strip
            roiY2, rem End Strip
            1, rem Skip Strip
            roiX1, rem Start Pixel
            roiX2, rem End Pixel
            0 )  rem File Type

let tmp = SETROIFILEACCESS(
            Math,
            2 ) rem ROI File Access Result



let tmp = DOWNLOADMATHRESULT(
          Math,
          "temp", rem Result Image
          1, rem Start Frame
          1, rem End Frame
          1, rem Skip Frame
          roiY1, rem Start Strip
          roiY2, rem End Strip
          1, rem Skip Strip
          roiX1, rem Start Pixel
          roiX2, rem End Pixel
          -1, rem Valuetype
          0, rem Filetype
          2) rem File Access

let tmp = ROIRECTSTATS( Math, StdDev, AveInt, TotalInt,
            MinIntensity, MaxIntensity, TotalPixels,
            x1, y1, x2, y2, MinLocX, MinLocY, MaxLocX,
            MaxLocY, CenterMassX, CenterMassY, fillflag)
let avgbckint = AveInt
let totbckint = TotalInt

let cntoffframes = 0

rem *****                                  *****
rem ***** SUB-LOOP FOR PROCEESING FILES FRAME BY FRAME *****
rem *****                                  *****

while cntoffframes < numoffframes

          let cntoffframes = cntoffframes + 1

          let Math = DOWNLOADMATHOPERATION(
```

```
                    56,  rem math operator --> ROI RECT
                    2,  rem ID -- DO NOT MODIFY
                    0 ) rem Constant Value

            let tmp = DOWNLOADMATHARG(
                    Math,
                    1,  rem Math Argument 1
                    filename,  rem Input Image
                    cntoffframes,  rem Start Frame
                    cntoffframes + 1,  rem End Frame
                    1,  rem Skip Frame
                    roiY1,  rem Start Strip
                    roiY2,  rem End Strip
                    1,  rem Skip Strip
                    roiX1,  rem Start Pixel
                    roiX2,  rem End Pixel
                    0 )  rem File Type

            let tmp = SETROIFILEACCESS(
                    Math,
                    2 ) rem ROI File Access Result



            let tmp = DOWNLOADMATHRESULT(
                    Math,
                    "temp",  rem Result Image
                    cntoffframes,  rem Start Frame
                    cntoffframes,  rem End Frame
                    1,  rem Skip Frame
                    roiY1,  rem Start Strip
                    roiY2,  rem End Strip
                    1,  rem Skip Strip
                    roiX1,  rem Start Pixel
                    roiX2,  rem End Pixel
                    -1,  rem Valuetype
                    0, rem Filetype
                    2) rem File Access

            let tmp = ROIRECTSTATS( Math, StdDev, AveInt, TotalInt,
                    MinIntensity, MaxIntensity, TotalPixels,
                    x1, y1, x2, y2, MinLocX, MinLocY, MaxLocX,
                    MaxLocY, CenterMassX, CenterMassY,
                    fillflag)

            let AVGINT(cntoffiles, cntoffframes) = AveInt rem - avgbckint
            let TOTINT(cntoffiles, cntoffframes) = TotalInt rem - totbckint

    wend  rem end of sub-loop

wend   rem end of main loop

rem      ************              ************
rem      ************  Write to File  ************
rem      ************              ************
```

```
let cntoffframes = 0
while cntoffframes < numoffframes
    let cntoffframes = cntoffframes + 1
    let cntoffiles = 0
    while cntoffiles < numoffiles
        let cntoffiles = cntoffiles + 1
        let AVGINTTEMP(cntoffiles, 1) = AVGINT(cntoffiles, cntoffframes)
        let TOTINTTEMP( cntoffiles, 1) = TOTINT(cntoffiles, cntoffframes)
    wend
    write AVGINTRESULTFILENUM, AVGINTTEMP
    write TOTINTRESULTFILENUM, TOTINTTEMP
wend

close ROIFILENUM
close AVGINTRESULTFILENUM
close TOTINTRESULTFILENUM
close FOINPUTFNUM
print "Macro Finished ", numoffiles + 1, 1      rem End of Macro
```

A2.4 Overlay Macro Code

```
rem             ********* MACRO OBJECTIVE **********

rem     The purpose of the macro is to take a list of files to be processed and
rem     their corresponding background files as input and to write out the

rem     total and average intensity values of a user defined region of interest
rem     (ROI) to user named files.


rem             ********* MACRO INPUTS *********

rem     This macro is takes as input a text file which holds a list of names of rem     data files to be
processed followed by the name of the file containing
rem     a background image for this data file. The layout of this text file is
rem     as follows, where the first line is the number of data files to be
rem     processed:


rem       2

rem       c:\winview\macro\datafile.spe c:\winview\macro\bckgrnd.spe
rem       c:\windows\users\joe\datafle2.spe c:\windows\users\joe\bckgrnd2.spe


rem     As well as this text file the macro requires one other text file as
rem     input. This second file should hold the coordinates of the rectangular
rem     region of interest to be analyzed. The coordinates should be of the

rem     form x1 y1 x2 y2 as shown below
```

```
rem      1 1 576 384

rem    The user will be prompted for these text files whenever the macro is
rem    run

rem              ********* MACRO OUTPUTS *********

rem    There will also be a space in the prompt box to input the names of the
rem    files which will hold the results of the processing . Here two file
rem    names will be required, one to hold the information on average
rem    intensity values integrated over the region of interest after
rem    background subtraction. The second output file will hold the
rem    information on total intensity values integrated over the region of
rem    interest after background subtraction. The output will be in a separate
rem    column for each file processed. Columns are separated by spaces. There
rem    will be thirty rows*

rem    * Authors Note: This file is designed to work with image files
rem      containing thirty frames, this may be changed by changing the value
rem      of numofframes on line 113

rem Author: Mark Dawson
rem Sloan Automotive Lab
rem MIT
rem December 20 1997
rem Variable Declaration

let VALID = 1  rem ROI set to valid
let INVALID = -1 rem ROI set to invalid
let FOINPUTFNUM = 6
let TOTINTRESULTFILENUM = 5    rem ROI result file handle
let AVGINTRESULTFILENUM = 4    rem ROI result file handle
let ROIFILENUM = 3     rem ROI template file handle
let RECTANGLE = 1   rem rectangle is 1
let fillflag = 0      rem if set to 1, this flag will fill roi with constant.

MATHPOINTER Math

FLOAT StdDev, AveInt, TotalInt, MinIntensity, MaxIntensity
FLOAT TotalPixels, CenterMassX, CenterMassY
LONG x1, y1, x2, y2, MinLocX, MinLocY, MaxLocX, MaxLocY
INT roiX1, roiY1, roiX2, roiY2, subX1, subX2, subY1, subY2
```

```
int roidata(1, 4)       rem array to hold data on region of interest
int subdata(1, 4)

string avgresultfile     rem name of file to which results are to be written
let avgresultfile = "c:\user\mark\avgint"

string totresultfile     rem name of file to which results are to be written
let totresultfile = "c:\user\mark\totint"

string roifile    rem name of file containing information on region of interest
let roifile = "c:\winview\Roidata"

string fileofinputfiles   rem name of text file containing names of files to be
                    rem processed

let fileofinputfiles = "c:\winview\inputint"

input " Enter Average Intensity Result file name ", avgresultfile,
" Enter Total Intensity Result file name ", totresultfile,
" Enter Template file name ", roifile,
" Enter the name of the file containing input file names ", fileofinputfiles

open roifile for user text input as ROIFILENUM     rem -- v2.05 or up
open fileofinputfiles for user text input as FOINPUTFNUM

read ROIFILENUM, roidata(1, 1), roidata(1, 2), roidata(1, 3), roidata(1, 4)

let roiY1 = roidata(1, 2)
let roiY2 = roidata(1, 4)
let roiX1 = roidata(1, 1)
let roiX2 = roidata(1, 3)

int numoffiles        rem number of input files
int cntoffiles        rem counter for input files
int numoffframes      rem number of frames per file
int cntoffframes      rem counter for frames
string filename       rem name of file being processed
string bckgrndname    rem name of background file for file being processed
float avgbckint       rem Average intensity of background file
float totbckint       rem Total intensity of background

read FOINPUTFNUM, numoffiles
let numoffframes = 30
float AVGINT(numoffiles, numoffframes)
float TOTINT(numoffiles, numoffframes)
float AVGINTTEMP(numoffiles, 1)
float TOTINTTEMP(numoffiles, 1)

open avgresultfile for user text output as AVGINTRESULTFILENUM
open totresultfile for user text output as TOTINTRESULTFILENUM
let tmp = CLEARPRINTWINDOW
let cntoffiles = 0

rem *****                                                    *****
```

```
rem *****   MAIN LOOP FOR PROCESSING FILES AUTOMATICALLY   *****
rem *****                                  *****

while cntoffiles < numoffiles

   let cntoffiles = cntoffiles + 1

   read FOINPUTFNUM, filename, bckgrndname

   print "processing file ", cntoffiles, 1
   print cntoffiles
   print " of "
   print numoffiles
   read ROIFILENUM, subdata(1, 1), subdata(1, 2), subdata(1, 3), subdata(1, 4)
   let subX1 = subdata(1, 1)
   let subY1 = subdata(1, 2)
   let subX2 = subdata(1, 3)
   let subY2 = subdata(1, 4)
   let Math = DOWNLOADMATHOPERATION(
              56,  rem math operator --> ROI RECT
              2,  rem ID -- DO NOT MODIFY
              0 ) rem Constant Value

   let tmp = DOWNLOADMATHARG(
              Math,
              1,  rem Math Argument 1
              bckgrndname,  rem Input Image
              1,  rem Start Frame
              2,  rem End Frame
              1,  rem Skip Frame
              roiY1,  rem Start Strip
              roiY2,  rem End Strip
              1,  rem Skip Strip
              roiX1,  rem Start Pixel
              roiX2,  rem End Pixel
              0 )   rem File Type

   let tmp = SETROIFILEACCESS(
              Math,
              2 ) rem ROI File Access Result



   let tmp = DOWNLOADMATHRESULT(
             Math,
             "temp",  rem Result Image
             1,  rem Start Frame
             1,  rem End Frame
             1,  rem Skip Frame
             roiY1,  rem Start Strip
             roiY2,  rem End Strip
             1,  rem Skip Strip
             roiX1,  rem Start Pixel
             roiX2,  rem End Pixel
             -1,  rem Valuetype
```

```
        0, rem Filetype
        2) rem File Access

let tmp = ROIRECTSTATS( Math, StdDev, AveInt, TotalInt,
          MinIntensity, MaxIntensity, TotalPixels,
          x1, y1, x2, y2, MinLocX, MinLocY, MaxLocX,
          MaxLocY, CenterMassX, CenterMassY, fillflag)
let avgbckint = AveInt
let totbckint = TotalInt

let cntoffframes = 0

rem *****                                *****
rem ***** SUB-LOOP FOR PROCEESING FILES FRAME BY FRAME *****
rem *****                                *****

while cntoffframes < numoffframes

        let cntoffframes = cntoffframes + 1

        let Math = DOWNLOADMATHOPERATION(
                   56,  rem math operator --> ROI RECT
                   2,  rem ID -- DO NOT MODIFY
                   0 ) rem Constant Value

        let tmp = DOWNLOADMATHARG(
                   Math,
                   1,  rem Math Argument 1
                   filename,  rem Input Image
                   cntoffframes,  rem Start Frame
                   cntoffframes + 1,  rem End Frame
                   1,  rem Skip Frame
                   roiY1,  rem Start Strip
                   roiY2,  rem End Strip
                   1,  rem Skip Strip
                   roiX1,  rem Start Pixel
                   roiX2,  rem End Pixel
                   0 )  rem File Type

        let tmp = SETROIFILEACCESS(
                   Math,
                   2 ) rem ROI File Access Result



        let tmp = DOWNLOADMATHRESULT(
                   Math,
                   "temp",  rem Result Image
                   cntoffframes,  rem Start Frame
                   cntoffframes,  rem End Frame
                   1,  rem Skip Frame
                   roiY1,  rem Start Strip
                   roiY2,  rem End Strip
                   1,  rem Skip Strip
                   roiX1,  rem Start Pixel
```

```
                    roiX2,  rem End Pixel
                    -1,  rem Valuetype
                    0, rem Filetype
                    2) rem File Access

        let tmp = ROIRECTSTATS( Math, StdDev, AveInt, TotalInt,
                    MinIntensity, MaxIntensity, TotalPixels,
                    x1, y1, x2, y2, MinLocX, MinLocY, MaxLocX,
                    MaxLocY, CenterMassX, CenterMassY,
                    fillflag)

        let AVGINT(cntoffiles, cntofframes) = AveInt rem - avgbckint
        let TOTINT(cntoffiles, cntofframes) = TotalInt rem - totbckint

   wend  rem end of sub-loop

wend   rem end of main loop

rem      ************              ************
rem      ************  Write to File  ************
rem      ************              ************

let cntofframes = 0
while cntofframes < numofframes
    let cntofframes = cntofframes + 1
    let cntoffiles = 0
    while cntoffiles < numoffiles
        let cntoffiles = cntoffiles + 1
        let AVGINTTEMP(cntoffiles, 1) = AVGINT(cntoffiles, cntofframes)
        let TOTINTTEMP( cntoffiles, 1) = TOTINT(cntoffiles, cntofframes)
    wend
    write AVGINTRESULTFILENUM, AVGINTTEMP
    write TOTINTRESULTFILENUM, TOTINTTEMP
wend

close ROIFILENUM
close AVGINTRESULTFILENUM
close TOTINTRESULTFILENUM
close FOINPUTFNUM
print "Macro Finished ", numoffiles + 1, 1      rem End of Macro
```

APPENDIX 2

The data acquisition programs for the square piston engine are written in LabView®, and are used in conjunction with a National Instruments data acquisition board. LabView® is a graphical software package, whose programs are called virtual instruments (VI's). There is a large library of VI's shipped with LabView®, which has proved very useful. Included in this library are a number of VI's on how to both acquire and subsequently view the data. These examples are the basis for the VI's used for data acquisition with the square piston engine, and the user is advised to review these examples.

LabView® VI's include a front panel, which acts as the interface to the user and insulates the user from the actual program. The source code for the VI is contained in the block diagram which is written in G. G is a modular, graphical programming language and all subroutines in the VI are represented as icons on the block diagram. Color-coded wires interconnect the various subroutines and LabView® function icons.

A2.1 Equipment:

The data acquisition system consists of a 120 MHz personal computer with 16 megabytes of memory. The data acquisition board is a National Instruments Lab-PC-1200 with a 50 pin I/O connector block. Programs were written in LabView® version 4.0.1. A National Instruments PC-TIO-10 is used for controlling the engine spark and injection signals.

Data AcQuisition (DAQ) Board Description:
The Lab-PC-1200 DAQ board includes 8 analog I/O channels, with 12 bit resolution, and two groups of timers: one group having two 16 bit timers, A0 and A1, is used exclusively for internal data acquisition timing and one group consisting of 3, TTL compatible, 16 bit timers, B0, B1 , and B2, is used for general purpose. As well as being general purpose counters/timers, counters B0 and B1 could also be used for internal data acquisition timing, or B1 could be used for analog input timing. B2 is reserved for external use as a general-purpose timer/counter. Each counter has a clock (CLK) input pin, a gate (GATE) input pin, and an out (OUT) pin.

The board can acquire data in one of three modes: controlled acquisition mode, freerun acquisition mode and interval-scanning mode. In this case we use the freerun acquisition mode. In freerun mode the pulses to signal a A/D conversion can either come internally from counter A0 or externally, as is the case in the square piston test cell, via the EXTCONV (signal is TTL active low) pin on the board. The software keeps tack of the number of conversions that have occurred and, in the case of internal acquisition timing, turns off counter A0 either after the required number of conversions has been obtained or after some other user defined criterion has been met.

The board is capable of single- and multiple-channel acquisition[1]. With single channel acquisition, the board executes a A/D conversion on a specified analog input channel every sample interval. The board executes a multiple channel acquisition operation by repeatedly scanning a sequence of analog input channels in decreasing consecutive order every sample interval . The highest numbered channel being the start channel. For example, if channel 2 is specified as the start channel, the scan sequence is as follows:

ch 3, ch 2, ch 1, ch 0, ch 3, ch 2, ch 1, ch 0, ch 3, ch 2, ch 1, ch 0, ...

The sample interval is the amount of time that elapses between successive A/D conversions, which is controlled either by counter A0 or, as is the case here the EXTCONV pin. The engines crank angle signal is connected to the EXTCONV pin, giving 720 scans of each channel per cycle.

The 50 pin I/O connector block acts as an interface between the DAQ board and the external signals.

A2.2 Data Acquisition Program:

Figure A2.1 shows the user interface for the data acquisition program which is named "Cont Acq to File (binary).vi". This interface is called the front panel and everything which appears on it is represented This program will write a user defined number of scans to a binary file, the name of which the user will be prompted for. The data that is being acquired will also be displayed in the charts on the front panel. The acquisition will start either when the specifications for the trigger have been met or, in the case of no triggering, when the "Enter" button is hit on the prompt screen for the filename. The setup can acquire up to seven channels ending with channel 0. The channels should be entered on the front panel in descending order separated by a comma, for example 3,2,1,0. On the front panel there is a section for a user-supplied header which will be included at the beginning of the binary file. There should never be any need to change the hardware settings.

This program uses circular buffering to perform data acquisition. Circular buffering is where the DAQ device is continuously acquiring data to a buffer in the background while LabView® retrieves the acquired data. When the buffer has been filled, the new data overwrites the old data at the beginning of the buffer, i.e. it goes back to the beginning. This means data can read continuously into memory but only a defined amount of memory is used. In order to prevent unread data from being overwritten the vi has to retrieve data from the buffer. This is where problems can arise. If the buffer is too small or the VI is not reading enough data from it then unread data will be overwritten. On the front panel there are three displays which helps the user monitor the buffering; the buffer size, the number of scans to write to disk at a time, and the scan backlog. The buffer size is given in scans and is set to 1000 by default, the number of scans to write to disk each time (i.e. the number of scans to read from the buffer each time) is set to 500 by default, and can never

exceed the buffer size. The scan backlog indicates the number of scans that remain in the buffer after each read and should not be allowed go above about 100. If the scan backlog begins to get too high then the user should either increase the size of the buffer or increase the number of scans written to disk each time.

At the completion of data acquisition the VI will display the size of the binary file and also show the total number of scans written to file, which can be any number less than the maximum number of scans which the user defined. As mentioned above one scan is performed every crank angle degree and so 720 scans occur every cycle this is equivalent to 6000 scans every second at an engine speed of 1000 rpm. The default value for the maximum number of scans is 700000, which is equivalent to approximately 116 secs of operation or about two minutes. The file size works out at approximately 725 kilobytes per channel per minute, which can result in very large files, particularly for multi-channel acquisition.

Source Code Explanation:
Figure A2.2, Frame 0:
This frame is the first of a sequence of three. First the user is prompted for a file name using the file open command. The user defined header is written to the file, included in which is a space for the number of scans in the file, which will be added at the end of acquisition. This frame then configures the hardware for analog input and begins the acquisition either immediately or based on a trigger. After this the VI enters a while loop which continuously acquires data until either the maximum number of scans is reached or the stop button is pressed on the front panel.

Figure A2.3, Frame 1:
The second frame rewrites the user-supplied header to the beginning of the binary file, this time including the number of scans in the file.

Figure A2.4, Frame 2:
The third and final frame of the sequence displays the size of the binary file on the front panel

A2.3 Data Viewer Program:

Once the data has been acquired, it can be viewed using the file "Graph two Acquired Files (binary).vi". Figure A2.5 shows the front panel for this program. On the front panel there is both a header viewer and a data viewer. The header viewer will display the user-supplied header present in a binary file. The data viewer will display the channels the user would like to view, which may come from one or two files.

Source Code Explanation

Figure A2.6, Main While Loop

This main loop will keep the viewing program running until the stop button is pressed. Reading the loop from left to right there is a sub-while loop included in the main loop. The program will stay in this loop until either the data view button, the header view button, or the stop button on the front panel is pressed. If the stop button is pressed the program will exit. If the header view or data view button is pressed, control will transfer to the case structure above the while loop. Depending on which button is pressed a different number will be passed to the main case statement, which takes up most of the main while loop. If the header view button was pressed, a zero will be passed to the case statement and the 0'th case, which is displayed in figure A2.6, will be executed. This zero case causes a user supplied filename to be passed to a sub-VI which will pop-up a new front panel and show all header associated with the file. If no filename is supplied then the user will be prompted for one.

Figure A2.7

If the data view button was pressed then a one will be passed to the main case statement. The length of the string containing the channels to be viewed from file two will be compared to zero, if it equals zero then control enters the true case of another case statement. This true case will display the data from one file. This case prompts the user for a filename, reads the size of the binary header reads the binary header, processes the header into its different sections. From this header the 'number of scans contained in the file' determines how many scans to read from the file, and the channel settings are used to determine the polarity and scale properties for the graph axes. The scans are then read from the file and passed to a for loop, which cuts out the data for the channels of interest to the user. These scans are then graphed in the upper plot on the front panel. This case will clear the front panel display and exit if one of either the stop, clear, data view or header view buttons is pressed.

Figure A2.8

If the length of the string containing the channels to be viewed from file two was not equal to zero then control enters the false case. This case contains a sequence structure, which will execute frame by frame. The first frame of three, frame zero, shown in figure A2.8, will read the data from the first file and prepare it for plotting, as described for the true case above. The second frame, frame one, shown in figure A2.9, will do the same for the data from the second file. The third and final frame, frame two, shown in figure A2.10, will pass the data from both frames to their respective plots on the front panel. This third frame will clear the graphs and exit if one of either the stop, clear, data view or header view buttons is pressed.

Figure A2.11

Finally, the third case of the main case statement does nothing and is entered if the stop button was pressed.

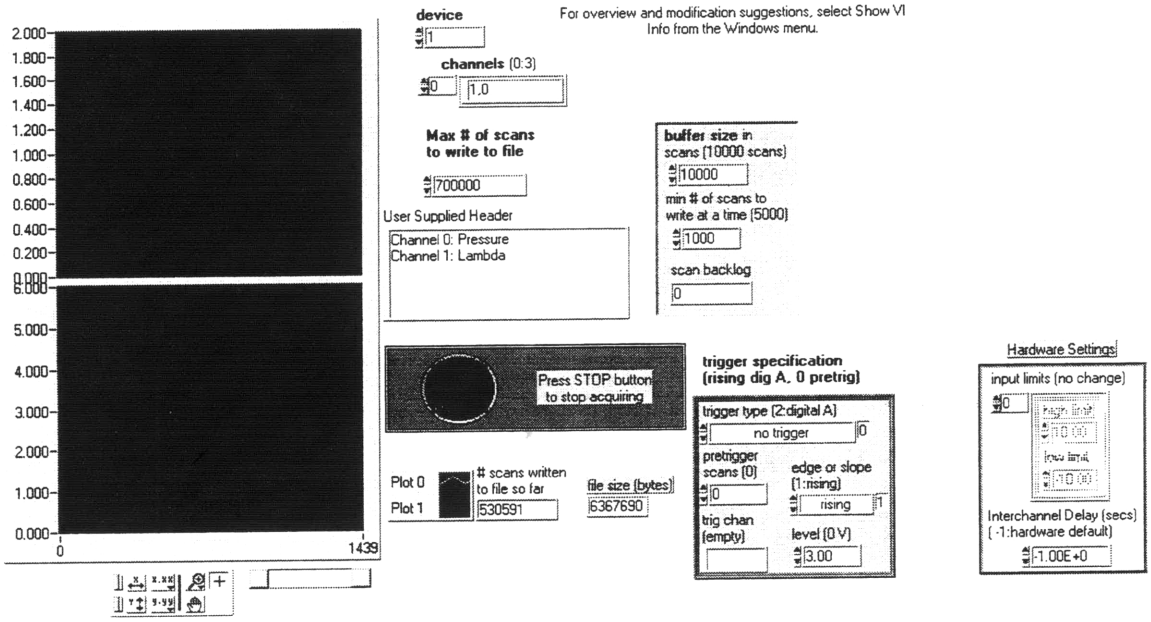

Figure A2.1: Data acquisition program user interface

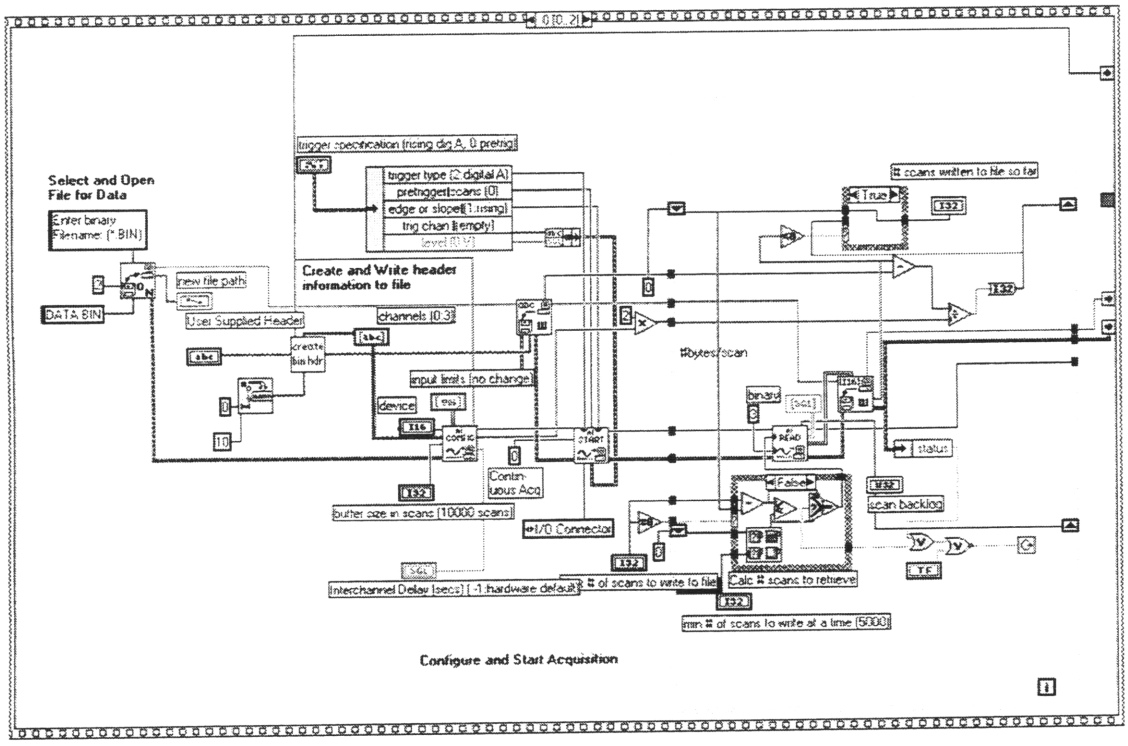

Figure A2.2: Frame 0

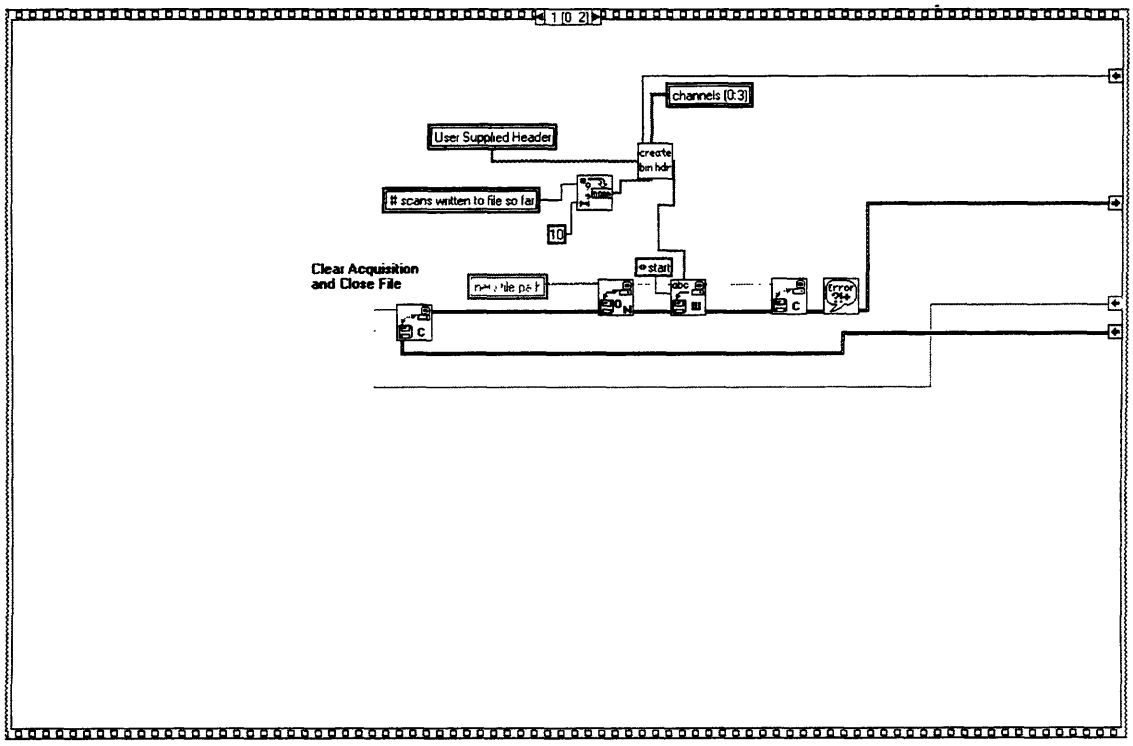

Figure A2.3: Frame 1

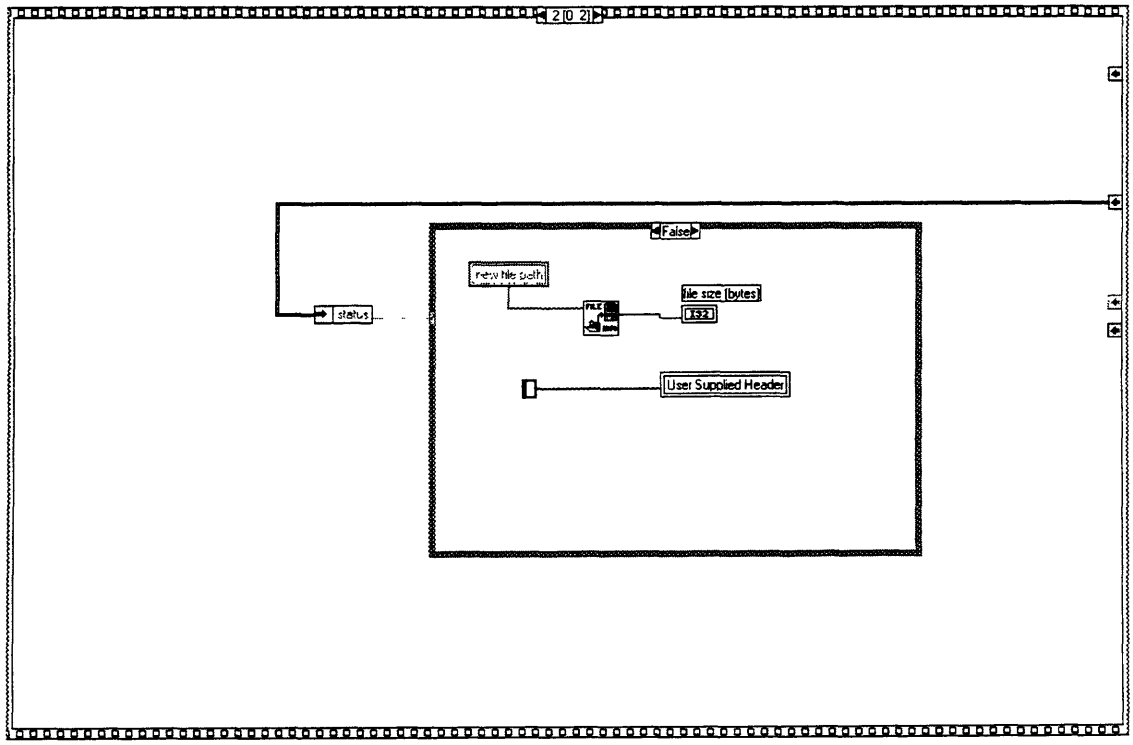

Figure A2.4: Frame 2

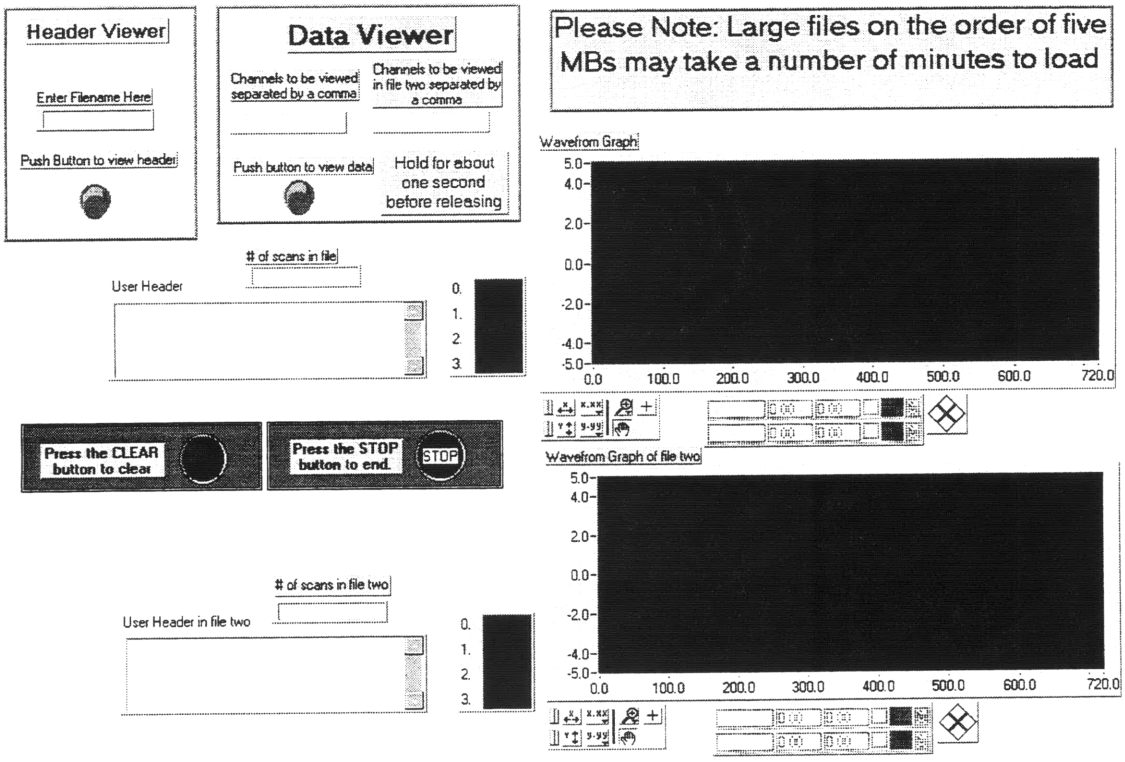

Figure A2.5: Data viewer program user interface

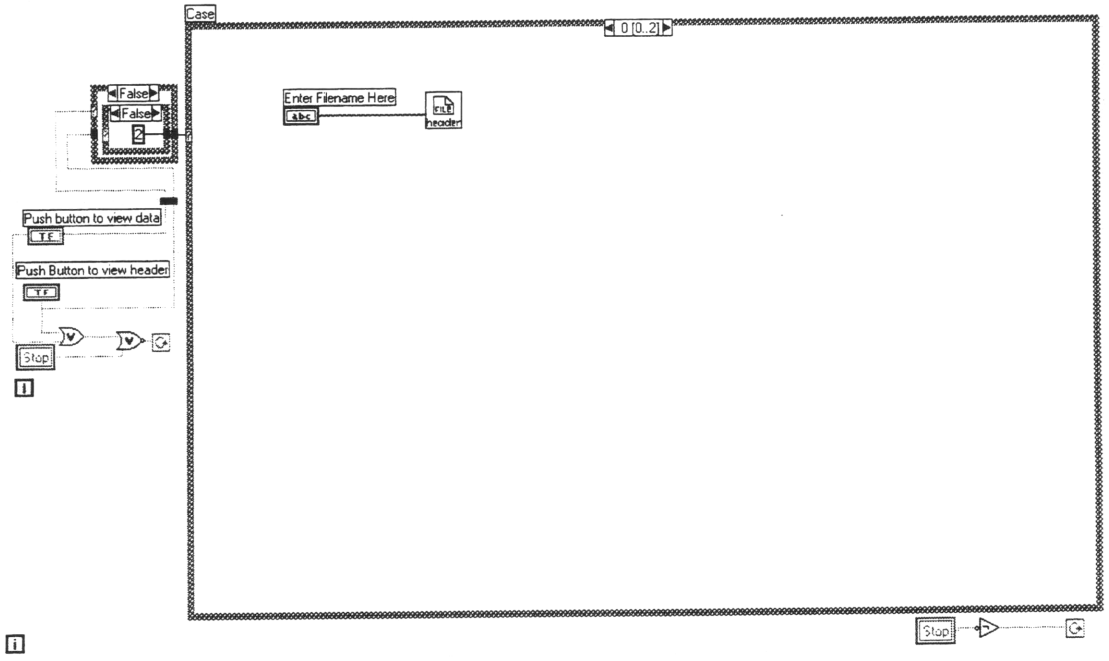

Figure A2.6: Case 0

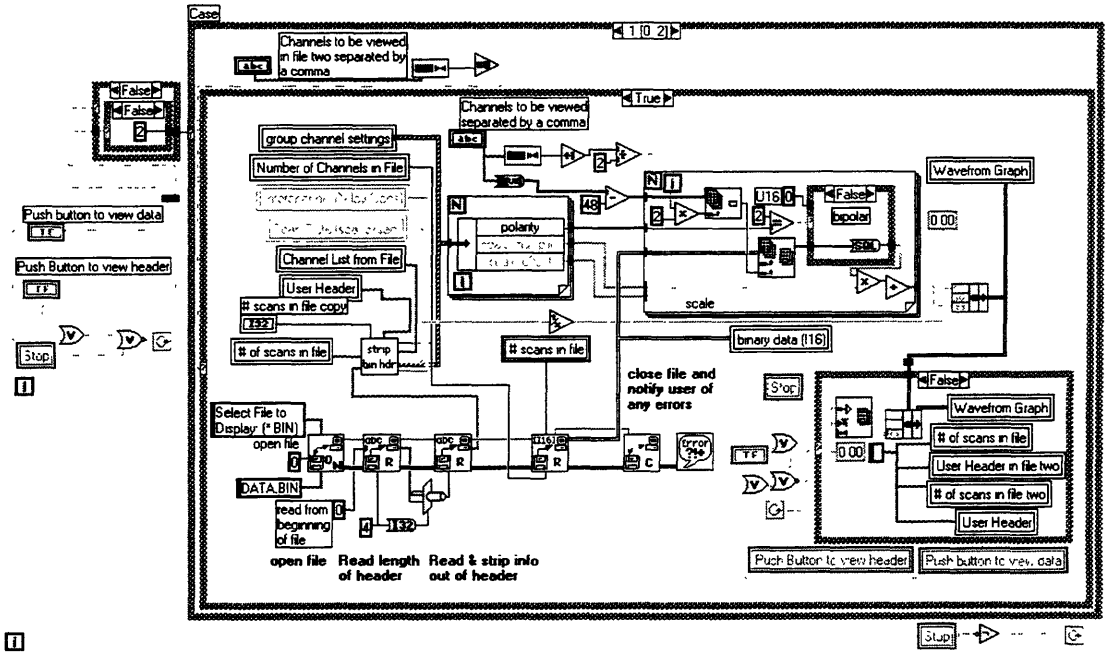

Figure A2.7: Case 1, true

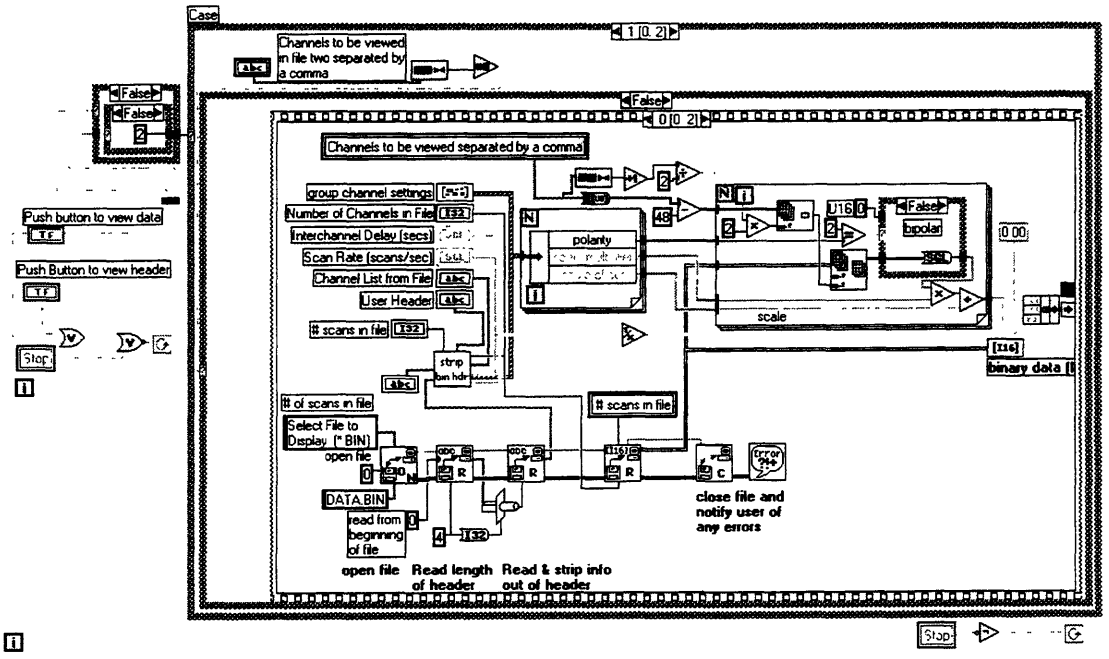

Figure A2.8: Case 1, false, frame 0

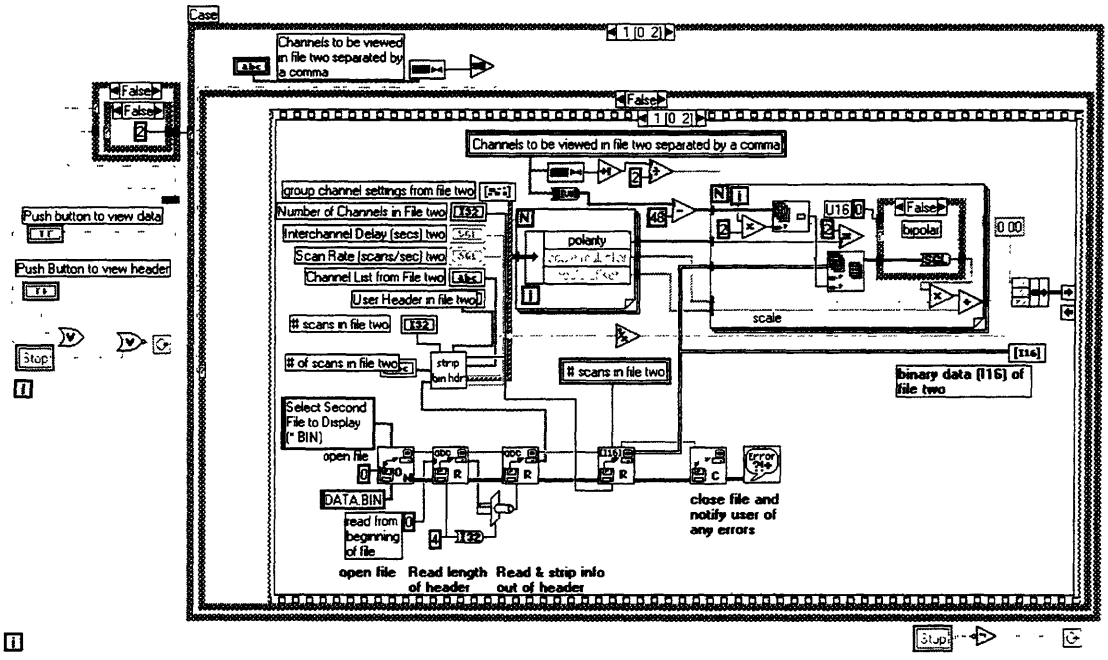

Figure A2.9: Case 1, false, frame 1

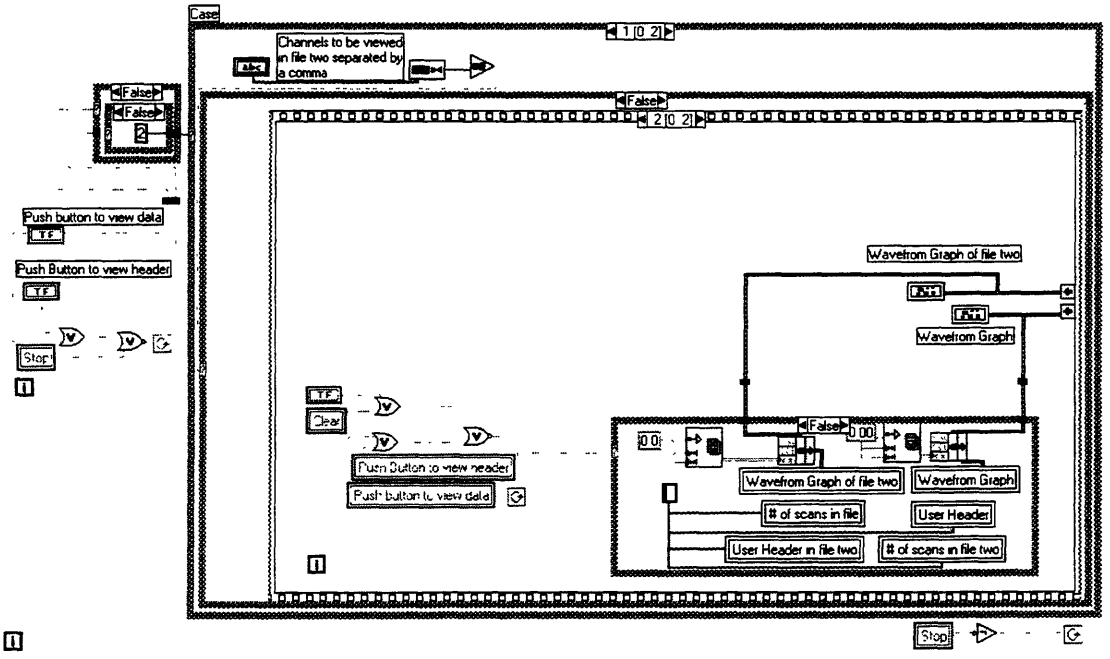

Figure A2.10: Case 1, false, frame 2

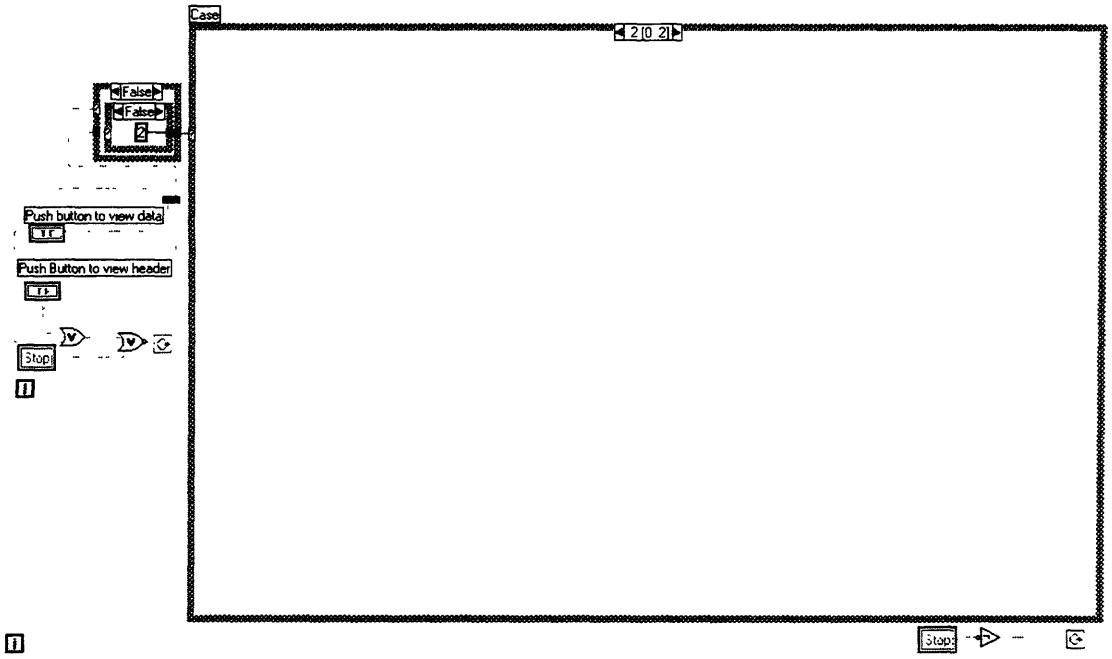

Figure A2.11: Case 2

Appendix 3

- Lens cap removed
- Camera gate width at correct setting
- Camera trigger set to external
- Laser High Voltage/Energy set correctly
- Laser trigger set to external
- Engine controller turned on
- Injection timing set correctly
- DCI box pulse generator set to correct CA position
- Laser door open
- Conditions of experiment recorded for future reference
- Winview® software Autostore setting turned on
- Fuel pump turned on
- Oil pump turned on
- Motor set to correct speed

Once all of these points have been checked the equipment is prepared for an experiment. The next list details the steps involved in performing a complete experiment:

- Turn on motor and let engine reach required speed
- Turn on spark signal on engine controller
- Turn on injection signal on engine controller
- Start data acquisition program to acquire pressure data, etc.
- Enable injection using first pulse enrichment box
- Simultaneously start image acquisition on Winview® software
- Once acquisition is complete, disable injection using first pulse enrichment box
- Turn off motor
- Turn off engine controller and data acquisition system